Crystal growth, magnetism, transport and superconductivity of two dimensional sodium cobalt oxide single crystals

Dapeng Chen
University of Wollongong

Crystal Growth, Magnetism, Transport and Superconductivity of Two Dimensional Sodium Cobalt Oxide Single Crystals

A thesis submitted in fulfillment of the requirements for the award of the degree of

DOCTOR OF PHILOSOPHY

from

UNIVERSITY OF WOLLONGONG

by

Dapeng Chen (B.C., M.E.)

Institute for Superconducting and Electronic Materials

2008

DECLARATION

This is to certify that the work presented in this thesis was carried out by the candidate in the laboratories of the Institute for Superconducting and Electronic Materials (ISEM), at the University of Wollongong, NSW, Australia, and has not been submitted for a degree to any other institution of higher education.

Dapeng Chen

2008

ACKNOWLEDGMENTS

I would like to express my sincere appreciate and gratitude to my supervisors, Prof. Xiaolin Wang, Prof. S. X. Dou, and Prof. Chengtian Lin, for their continuous academic guidance, encouragement, and support during my three years of PhD study in the Institute for Superconducting and Electronic Materials at the University of Wollongong.

I would also like to express my gratitude to Dr. T. Silver, Dr. J. Horvat, Dr. Alex Pan, Dr. Aihua Li, and Mr. Xun Xu, for their contributions in measurements, useful discussions, and suggestions.

This work would not have been completed without the help of Dr. J. Stempfer, G. Götz, K.-H. Bender, and C. Bush from the Max Planck Institute for Solid State Research, Germany; Prof. Guoqing Zheng and K. Matamo from Okayama University; J. Laverock and S. B. Dugdale from the University of Bristol; R. L. Meng and Prof. C. W. Chu from the University of Houston; J. A. Duffy, J. Wooldridge, G. Balakrishnan, and M. R. Lees from the University of Warwick; A. Andrejczuk, M. Itou, and Y. Sakurai from the Japan Synchrotron Radiation Research Institute; and Hui Zhang from Kunming University of Science and Technology. I would like to sincerely thank all of them for their great collaboration.

My special thanks to all my colleagues at ISEM, and all the members and technicians at the Faculty of Engineering for their friendly help and assistance in using the facilities.

I would also like to acknowledge the University of Wollongong for providing me with two scholarships – an International Postgraduate Research Scholarship (IPRS) and a University Postgraduate Award (UPA) with top-up award.

Finally I wish to thank my family members and my friends for their patience and support.

Table of Contents

List of Figures

List of Tables

ABSTRACT

The objective of this work was to study the single crystal growth of Na_xCoO_2 by the optical floating zone technique and the intrinsic properties of the high quality single crystal samples thus produced. The properties of the superconductors derived from it will also be reported.

This thesis, after a literature review on the Na_xCoO_2 family and the superconductors derived from it, reports a systematic study on growing Na_xCoO_2 (x = 0.32–1.00) and $Na_xCoO_2 \cdot yH_2O$ (x = 0.22–0.47, y = 1.3). The experiments demonstrate that nearly pure α- (x = 0.90–1.00) and ά- (x = 0.75) phases of Na_xCoO_2 crystals could be obtained using the optical floating zone method, while other phases with lower sodium content, x < 0.70 (β-phase with x = 0.55, 0.60 and γ-phase with x = 0.65 and 0.70, respectively), are observed always to contain Na_2O, Co_3O_4, and Na-poor phases. There is experimental evidence that the dependence of the superconducting transition temperature on Na content is much weaker than reported earlier. Implications of the Na effect for understanding of the structure, thermoelectricity, and superconducting phase diagram are discussed.

Na-extraction and hydration were carried out on the α- and ά-samples to obtain the superconducting phase. Hydrated single crystals exhibit cracked layers perpendicular to the *c*-axis, due to a large expansion when the water is inserted into the structure. A study of intercalation/de-intercalation was performed to determine the stability of the hydrated phase and the effects of hydration on the structure of the compound. X-ray diffraction and thermogravimetric experiments were used to monitor the processes of accommodation of water molecules and their removal from the crystal lattice. The initial intercalation process takes place with two water molecules (corresponding to y = 0.6) inserted in a formula unit, followed by a group of four (y = 1.3) to form a $Na(H_2O)_4$ cluster. Thermogravimetric analysis suggests that de-intercalation occurs with the removal of the water molecules one by one from the hydrated cluster at elevated temperatures of approximately 50, 100, 200, and 300^{o}C. My investigations reveal that the hydration process is dynamic and that water molecule intercalation and de-intercalation follow different reaction paths in an irreversible way.

This thesis also contains intensive studies on the cobalt oxide superconductors $Na_xCoO_2 \cdot 1.3H_2O$ based on ^{59}Co nuclear magnetic resonance (NMR) and nuclear quadrupole resonance (NQR) measurements. For the sample with x = 0.26 and critical temperature T_c = 4.6 K, it was found that the spin–lattice relaxation rate, $1/T_1$, shows a T^3 variation below T_c and down to very low temperatures, which indicates the presence of line nodes in the superconducting (SC) gap function. The spin susceptibility below T_c for these samples was also studied via Knight shift measurements. The spin part of the Knight

shift decreases below T_c in both the *a*- and *c*- directions, indicating a singlet spin state of the Cooper pairs. The results strongly suggest that the superconducting state is a d-wave state. Based on bulk measurements of the electron momentum distribution, using the technique of x-ray Compton scattering, the evidence that small, elliptically shaped pockets do indeed exist in the Fermi surface of cobalt oxide superconductors was presented.

The magnetic properties of two-layer Na_xCoO_2 (x = 0.42, 0.82, and 0.87) were studied. The magnetic susceptibility measurements revealed considerable anisotropy along H//*ab* and H//*c* for the as-grown single crystals. It was found that an antiferromagnetic transition with Néel temperature, T_N = 21 K, occurred for the x = 0.82 sample, and there was a paramagnetic phase for the x = 0.87 sample over a wide temperature range from 2 to 300 K, while the sample with x = 0.42 showed a monotonic increase of χ with increasing temperature above ~100 K. In addition, the x = 0.82 sample had the largest derived anisotropic g-factor ratio ($g_{ab}/g_c \approx 1.30$), whereas the sample with x = 0.42 was nearly isotropic ($g_{ab}/g_c \approx 0.96$).

Magnetic susceptibility measurements on three-layer α-Na_xCoO_2 (x = 0.91, 0.92, and 0.93) showed that the magnetic properties depend strongly on x. The compound was found to be antiferromagnetic at $T_N \approx 20$ K for x = 0.91 and x = 0.92, and paramagnetic for x = 0.93. In-plane and out-of-plane anisotropy were observed for the x = 0.91 crystals. In addition, the anisotropic g-factor ratio (g_{ab}/g_c) derived from the anisotropic

susceptibility along H//*ab* and H//*c* decreased significantly as the sodium composition increased from x = 0.91 to x = 0.93.

A systematic study was also carried out on the conduction mechanism and the anisotropy of the electrical transport properties of the α-$Na_{0.91}CoO_2$ single crystals. The resistivity was found to show a large anisotropy along the *ab* plane and the *c* axis. The resistivity below the metal-to-insulator transition temperature (20 K) can be well fitted by the variable-range hopping model. The high temperature range can be fitted well by $\rho(T) = \rho_0 + A\omega_s/\sinh^2(\hbar\omega_s/2k_BT) + BT^{7/2}$, both for the in-plane and the out-of-plane behaviours. Such behaviour provides evidence for small polaron and spin-wave scattering metallic conduction in heavily Na-doped sodium cobaltate.

Chapter 1 Introduction

1.1. Introduction

The discovery of high-temperature superconductors (HTSCs) [21] in layered copper oxides has encouraged scientists to investigate for unknown materials for more than two decades. Many new materials and spectacular phenomena of great scientific interest and/or technological importance have been discovered [2], but the behaviors of these materials are very complex, and there is still no widespread agreement on the origin of the superconductivity [3].

A_xMX_2 type compounds (A = alkaline metal, M = transition metal, X = O, S, Se) have attracted much attention as cathode materials for many years [4]. These compounds have a layered structure, and among them, there is an extensive group of oxides involving 3*d* transition-metals that have been investigated as a reference for HTSCs. In 1997, I. Terasaki et al. discovered the coexistence of a large in-plane thermoelectric (TE) power (~100 μV/K) and low resistivity (200 μΩ) at room temperature in $NaCo_2O_4$ (or $Na_{0.5}CoO_2$), which made the sodium cobaltate an attractive material for thermoelectric applications [5]. Recently, enhancement of the figure of merit Z has been found in poorly explored, heavily doped Na_xCoO_2 ($x > 0.75$), and a 40-fold enhancement of Z

was realized at the critical doping $x_p \approx 0.85$ (at 80 K), which greatly improves the prospects for TE applications [6].

$NaCo_2O_4$ belongs to a family of bronze-type compounds expressed as A_xMO_2 ($0.5 < x < 1$), which was first identified by Jansen and Hoppe [7]. An important similarity to HTSCs is that $NaCo_2O_4$ is a layered transition-metal oxide, where Na sites are ~ 50 % occupied and CoO_2 units are alternately stacked along the *c* axis. Thus, the physical properties are expected to be highly two dimensional (2D). However, the CoO_2 layer is different in structure from the CuO_2 layer of HTSCs: the former is a 2D triangular lattice, and the latter is a 2D square lattice. Early investigation by Tanaka, Nakamura, and Iida [8] has shown that polycrystalline $NaCo_2O_4$ is a good metal down to 12 K, although it shows Curie-Weiss-like susceptibility instead of the Pauli paramagnetism. According to their results, $NaCo_2O_4$ can be regarded as a doped 2D triangular spin lattice, which is worth comparing with the CuO_2 layer HTSCs.

The recently discovered superconductor $Na_{0.35}CoO_2 \cdot 1.3H_2O$ has attracted considerable attention as being the first layered superconductor to replace copper with cobalt and as evidence that important electronic correlations exist [9]. Its superconducting transition temperature of maximum $T_c < 5$ K exhibits composition dependence, with T_c decreasing for both under-doped and over-doped materials, as observed in the cuprates. Despite the major differences in their geometry and bond filling, there is the intriguing similarity that the cobalt superconductor has low spin Co^{4+} with S = ½, just as cuprate

superconductors have Cu^{2+} with S = 1/2. The similarities and discrepancies are shown in Fig. 1.1.

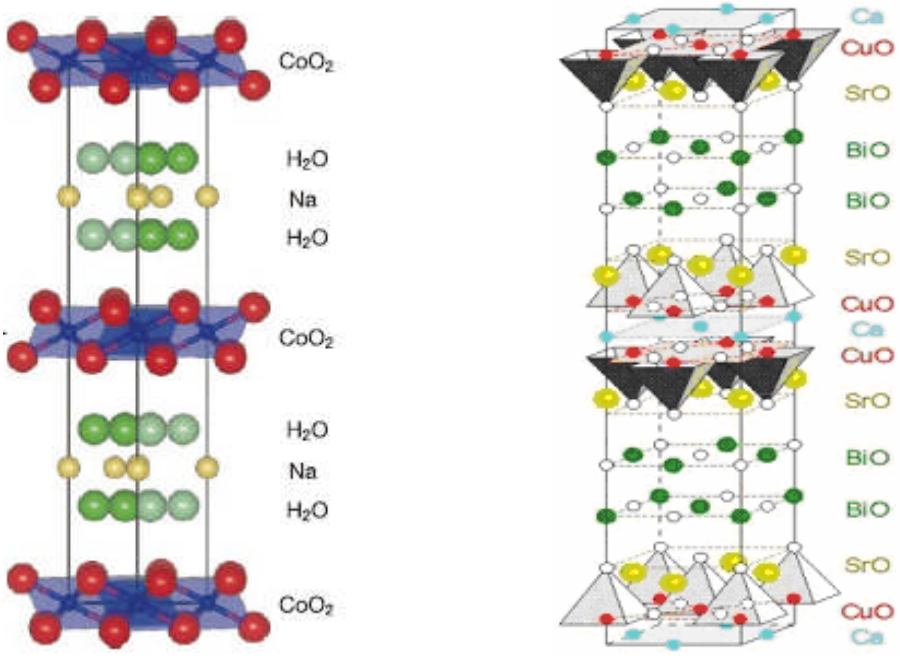

Cobaltate	Cuprate
Layered structure	Layered structure
Transitional metal oxides	Transitional metal oxides
2D CoO_2 layers	2D CuO_2 layers
Low spin (S=1/2) Co^{4+}	Low spin (S=1/2) Cu^{2+}
Octahedral CoO_6	Octahedral CuO_2
Triangular Co-lattice	Square Cu-lattice
Tc in narrow band filling	Tc in broad band filling

Fig. 1.1. The similarities and discrepancies between cobaltates and cuprates. The crystal structure of $Na_{0.35}CoO_2 \cdot 1.3H_2O$ [9] is on the left, and the crystal structure of Bi2212 is on the right.

However, the transport and magnetic properties of Na_xCoO_2 are strongly dependent on the Na content. It has been found that as x increases from 0.3, the ground state of these compounds goes from a paramagnetic metal through a charge ordered insulator (at x =

0.5) to a ‘Curie-Weiss metal’ (around x = 0.70), and finally to a weak-moment magnetically ordered state (x > 0.75) [10]. Muon spin rotation (μSR) and nuclear magnetic resonance (NMR) measurements have identified the stoichiometric three-layer Na_1CoO_2 phase to be a non-magnetic insulator [11, 12]. Thus the phase diagram of Na_xCoO_2 is different from that of cuprates. The superconducting ‘dome’ of Na_xCoO_2 is closer to Co^{3+} (S = 0) rather than Co^{4+} (S = 1/2) [13-15], and Na_xCoO_2 even shows magnetic ordering at $x \geq 0.75$, except for a special one at x = 0.5 [10, 16]. These interesting behaviours clearly indicate that the origin and functionality of strong correlations in these two materials are very different.

Whatever the relationship between these two types of superconductor may be, the cobalt superconductor at least could provide insight into the relationship between dimensionality and superconductivity. This suggests that a detailed characterization of the electronic and magnetic behavior of this new family of materials and their interplay with structural peculiarities may contribute to a more fundamental understanding of the high T_c superconductivity in cuprates and even lead to thermoelectronic applications.

Single crystals with high purity and perfection are in demand for every branch of research concerned with the solid state. The reason is easy to find, for the single crystals have strong characteristics of symmetry, structural simplicity, and purity, which endow the crystals with unique physical and chemical properties. With the crystal growth techniques that have been developed, more and more single crystals are used by

physicists, chemists, biologists, and material scientist to investigate their delicate structure, anisotropic properties, radiation damage, superconductivity, and nuclear and electron resonances. Extensive investigations have indicated that the intrinsic properties of a material cannot be ascertained until single crystals with sufficiently high purity and perfection can be prepared.

Na_xCoO_2 has a layered structure, so high quality single crystals with well defined stoichiometry are essential for the study of the intrinsic properties of this family of compounds, especially for anisotropic properties and neutron diffraction measurements.

Crystal growth methods may be divided into growth from the melt, from the vapour, from supersaturated solutions, and by other methods. Most of the studies on layered structure materials have reported using crystals grown from the melt [17, 18]. The flux method is used when materials decompose below the melting point or when they have high vapour pressure upon melting. The main disadvantage of this method is the possible introduction of flux into the crystals, as well as contamination from crucibles. As one of the crucible-free methods, the floating zone method allows such impurities to be avoided; it has been successfully used for high-T_c superconductor single crystal growth [19]. The theory of the floating zone method has long since been reported [20]. Here, the author will give a brief presentation of the travelling solvent zone method (TSZM), which has been widely chosen for the growth of large bulk high-T_c superconductor single crystals [19], as well as for the growth of layered Na_xCoO_2 for

fundamental research.

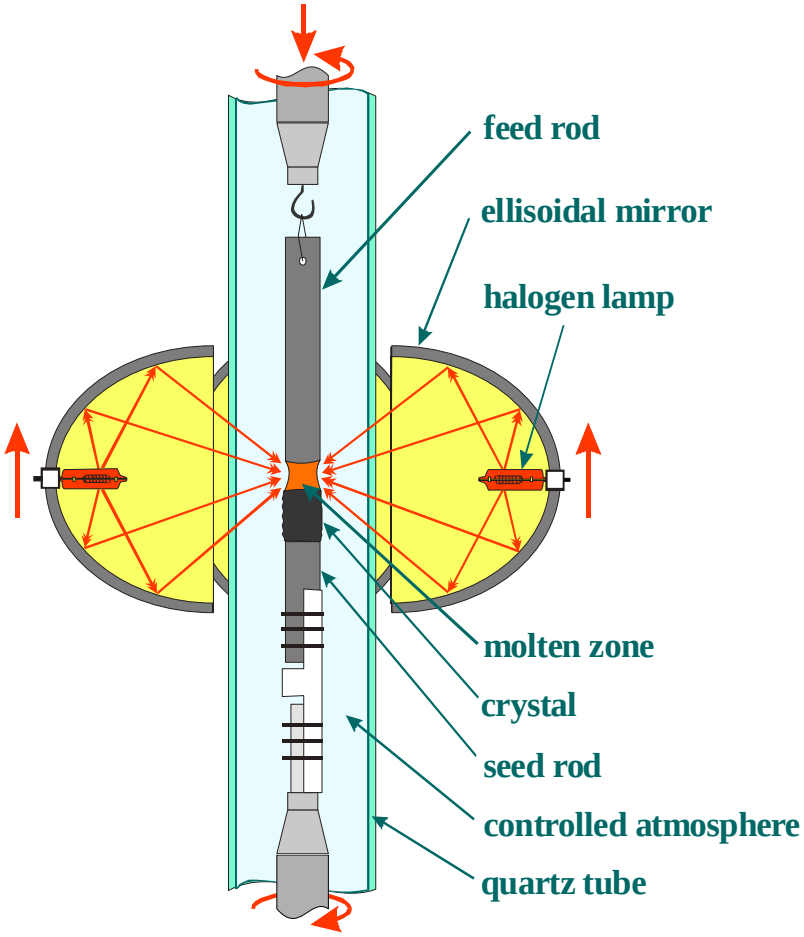

Fig. 1.2. Illustration of the four lamp ellipsoidal infra-red image furnace for TSFZ.

As shown in Fig. 1.2, sintered dense polycrystalline cylindrical rods are used as seed and feed rods. A vertical liquid zone with a controlled composition (the travelling solvent) is heated by four halogen lamps, and crystal growth is conducted by upwards transition of the molten zone, with both the feed and the seed rods counter-rotated during the growth. Since the surface tension is the principal force supporting this molten zone, a straight feed rod and good shape of the liquid zone are needed for continuous

crystal growth.

This thesis, after the literature review on the family of Na_xCoO_2 and their derived superconductors, consists of a report on a systematic study of single crystal growth of Na_xCoO_2 by TFZM and on the intrinsic properties of the resultant high quality single crystal samples. The properties of the derived superconductor also will be reported.

Chapter 2 Literature review on sodium cobaltates

2.1. Introduction

The present review deals with all the phases of sodium cobaltate. With sodium content x increasing to 1.0, there are four thermodynamically stable phases in the Na_xCoO_2 system that have been previously reported [21]. In all the phases, sheets of edge-sharing CoO_6 octahedra are interleaved by sodium ions along the *c*-axis direction, delineated as (i) α-Na_xCoO_2 ($0.9 \leq x \leq 1$) having the O3 structure (with O referring to the octahedral coordination of the Na ions and 3 the number of layers in a repeat), (ii) $\acute{\alpha}$-$Na_{0.75}CoO_2$ (Ó3 structure, i.e. monoclinic distortion of O3 phase), (iii) β-Na_xCoO_2 ($0.55 \leq x \leq 0.6$) having the P3 structure, and (iv) γ-Na_xCoO_2 ($0.55 \leq x \leq 0.74$) having a P2 phase. For these phases, chemical or electrochemical methods can be used to adjust the sodium composition within these structures. Thus, lower Na content phases have been obtained by de-intercalation of their higher x counterparts [22]. In addition, intercalation can be used to increase the sodium content of the higher Na phases to even higher phases. For example, γ phase from x = 0.7 up to x = 1.0 [22].

Among them, α- phase, $\acute{\alpha}$-phase, and β-phase have three-layer structures; only γ-phase has a two-layer structure. The richness in the structure of the phases, physics, and

chemistry had remained largely unexplored until recently. This review will not be systematic, but will rather analyse the most important study results obtained so far, in the author's opinion, and will try to underline the research directions for the author's work. I will review the basic properties of the Na_xCoO_2 family of compounds as well as the superconducting phase $Na_xCoO_2 \cdot yH_2O$. The review will start with the preparation methods for the two-layer phase (including de-intercalation methods) and the properties of these compounds, from powders to thin films, and finally to single crystals. There is then a review of the remarkable phase $Na_{0.5}CoO_2$, which is a charge-ordering insulator. Later, the review concentrates on the three-layer phases, and finally comes to the complex superconducting phases. There is an emphasis on compound fabrication and crystal structure for the various phases. The related physical and chemical properties will also be reviewed.

2.2. Two-layer Na_xCoO_2

2.2.1. Polycrystalline samples and physical properties

In March 2003, Takada et al. announced the discovery of superconductivity in a compound in this family with two-dimensional CoO_2 layers [9]. They reported that by using a chemical oxidation process (as shown in Fig. 2.1) from $Na_{0.7}CoO_2$, a

superconductor, $Na_{0.3}CoO_2 \cdot 1.3H_2O$ with a T_c of about 5 K, was obtained. This discovery has generated enormous interest in the research community. Earlier interest was focused on the understanding of the surprisingly high thermoelectric power of the metallic conductor $Na_{0.7}CoO_2$ [23, 24].

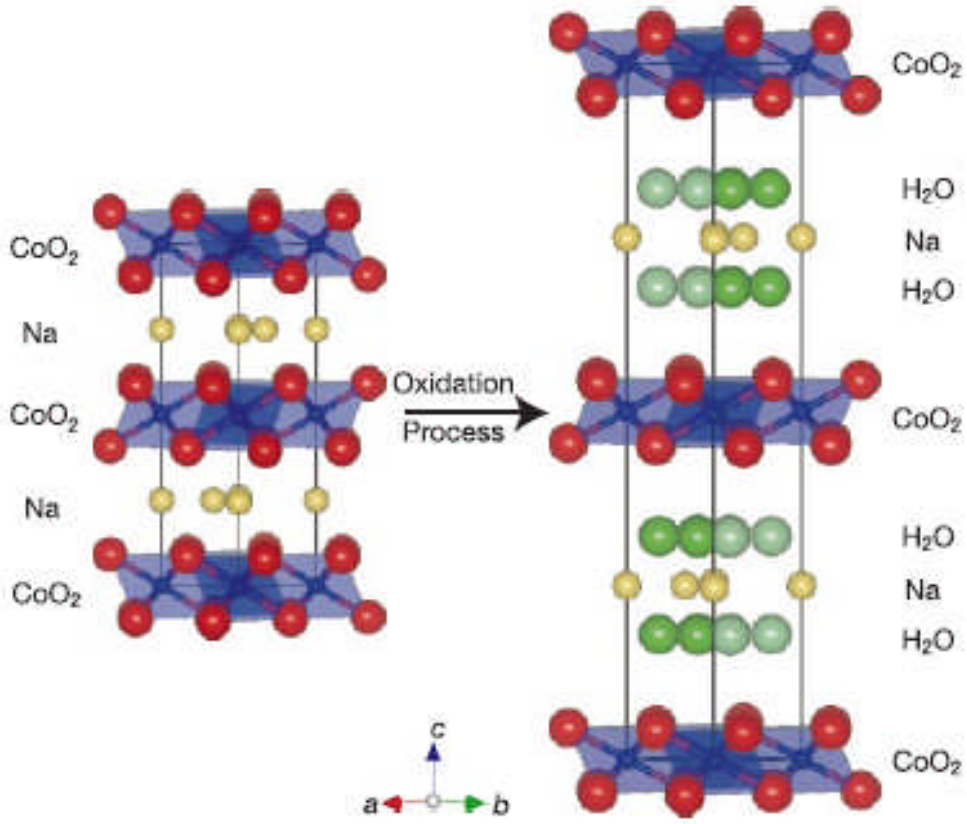

Fig. 2.1. Structural views of $Na_{0.7}CoO_2$ (left) and $Na_xCoO_2 \cdot yH_2O$ (right), where Na and H_2O sites are partially occupied. $Na_{0.7}CoO_2$ was prepared by solid-state reaction under oxygen gas flow. A fivefold excess of Br_2 with respect to the Na content was dissolved in acetonitrile (CH_3CN). A well pulverized powder of $Na_{0.7}CoO_2$ was immersed in the Br_2/CH_3CN solution for 5 days to de-intercalate Na ions; then the product was filtered, washed with CH_3CN and distilled water, and finally dried in ambient atmosphere [9].

Two-layer γ-Na_xCoO_2 has a hexagonal structure with the space group symmetry of $P6_3/mmc$ and lattice parameters $a = b = 2.840$ Å and $c = 10.811$Å [7]. The in-plane direction of the CoO_6 octahedron in CoO_2 alternates with the nearest CoO_2 layers, as shown on the left of Fig. 2.1.

There have been extensive efforts to fabricate and precisely control the Na content for polycrystalline samples [10, 25-33]. Based on the results of thermogravimetric (TG) analysis on the phase formation, T. Motohashi et al. employed a "rapid heat-up" (RHU) technique to heat the mixed raw materials to obtain Na_2CO_3 samples with precisely controlled Na contents by avoiding Na evaporation [27].

Samples of γ-Na_xCoO_2 with precisely controlled Na content were obtained. In this procedure, a powder mixture of Na_2CO_3 and Co_3O_4 in an appropriate ratio is put in an Al_2O_3 crucible and directly placed in a furnace preheated to 700-900 °C to be fired for 12 h in air. The temperature is adjusted to correspond to the Na content, and in general, powders with higher sodium content need a lower sintering temperature.

To obtain samples with Na contents lower than the as-grown Na_xCoO_2, a chemical de-intercalation method has usually been used. Utilizing one of the three oxidizing agents: I_2, Br_2 [34], and NO_2BF_4 [35], a Na-rich sample is immersed in an acetonitrile (CH_3CN) solution of the oxidant for one or several days with stirring at room temperature, and the product is then washed several times with CH_3CN, and finally

dried. Karppinen et al. [37] demonstrated the results on oxygen non-stoichiometry and the actual Co valence in $Na_xCoO_{2-\delta}$. Low sodium content samples were de-intercalated from $0.70 \leq x \leq 0.78$ powder samples. It was found that the oxygen vacancies increase as x decreases, until it finally reaches the threshold value of 0.35. Their research suggested that the oxygen non-stoichiometry parameter is the dominant influence on the cobalt valence, rather than the x parameter in two-layer Na_xCoO_2.

The electrochemical method also can be used for intercalation of sodium from the parent compounds of Na_xCoO_2 bronze [25, 26, 38], while maintaining the parent crystal structure in most cases. This method provides an easy way to approach large single crystal samples. As Na_xCoO_2 compounds are conductors, they are used as cathodes during the intercalation or de-intercalation at room temperature. Discharge potentials ($2.0 < V < 3.5$ V) have been used as a function of the composition. The electrochemical intercalation of sodium in all these materials is reversible within their range of existence. Since the electropositive metals can be easily changed in this material, the electric properties and other properties can be chemically or electrochemically tuned over a wide range, and this is one reason why Na_xCoO_2 is attractive. The holes arising from sodium non-stoichiometry during the de-intercalation process can be partly compensated by electrons resulting from the oxygen non-stoichiometry [38], and this agrees well with the results from chemical de-intercalation [37]. Both methods are widely used in the fabrication of low sodium content Na_xCoO_2 [39, 40].

Another study [41] on the *ab* face of Na_xCoO_2 (x = 0.79) presents interesting results. When the sample was examined under a dry nitrogen flux by conducting probe atomic force microscopy (CP-AFM), the surface conductivity and surface profile of Na_xCoO_2 could be reversibly modified by an electrochemical method. This has attracted further interest in these compounds, because it indicates the potential of sodium cobaltate to be used in nanoscale rewritable media.

In 2004, Sakurai et al. [30, 31] synthesized powder samples of Na_xCoO_2 (x = 0.70, 0.72, 0.74, 0.76, 0.78, 0.80, 0.82, and 0.84) by conventional solid state reaction from stoichiometric mixtures of Na_2CO_3 (99.99%) and Co_3O_4 (99.9%) in flowing oxygen. Samples were carefully characterized by X-ray diffraction analysis (XRD), inductively-coupled plasma atomic emission spectroscopy (ICP-AES), and redox titration. It was found that two-layer Na_xCoO_2 is formed only in the narrow range of $0.70 \leq x \leq 0.78$. The magnetic properties strongly depend on the Na content. A sharp peak at $T_p = 16$ K and an anomaly at $T_k = 9$ K, as well as a transition at $T_c = 22$ K and a broad maximum at $T_m = 50$ K were found for $Na_{0.78}CoO_2$. A type of weak ferromagnetic transition seems to occur at T_k. The transition at T_c caused by spin density wave formation was observed clearly for $x \geq 0.74$ with constant T_c and T_p independent of x. Furthermore, a phase separation into Na-rich and Na-poor domains occurs for $x > 0.78$.

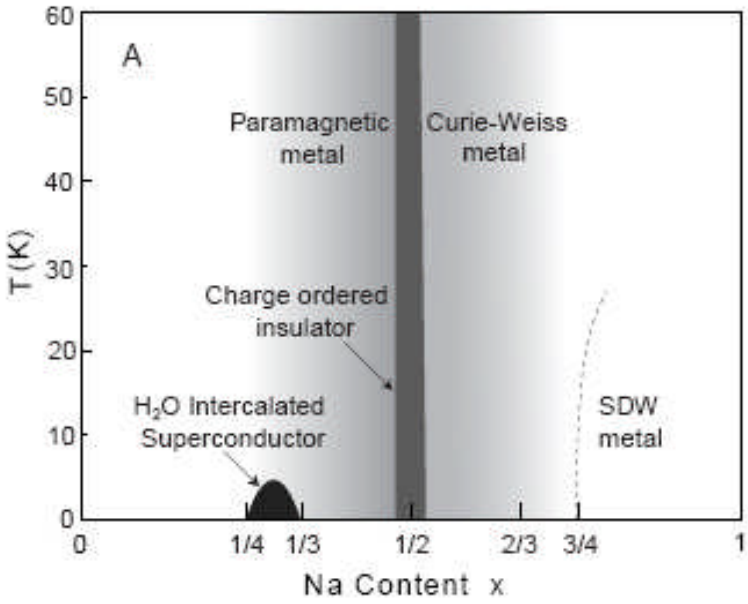

Fig. 2.2. The phase diagram of non-hydrated Na_xCoO_2 [10].

By changing the Na content x, using a series of chemical reactions from x = 0.75, it has been found that Na_xCoO_2 exhibits metallic behaviour over a wide range ($x \leq 0.75$), but an insulating state exists at x = 0.5 [10]. As x increases from 0.3, the ground state goes from a paramagnetic metal to a charge-ordered insulator (at x = 0.5) to a 'Curie-Weiss metal' ($x \approx 0.7$), and finally to a weak-moment magnetically ordered state ($x > 0.75$). The metallicity in the phase diagram of layered Na_xCoO_2 is shown in Fig. 2.2. The authors suggested that insulating behaviour is based on strong coupling between the electronic charge carriers (holes) and the Na ions. Recently Wu et al. [36] refined the magnetic phase diagram and proposed a magnetic structure for $Na_{0.55}CoO_2$, as shown in Fig. 2.3.

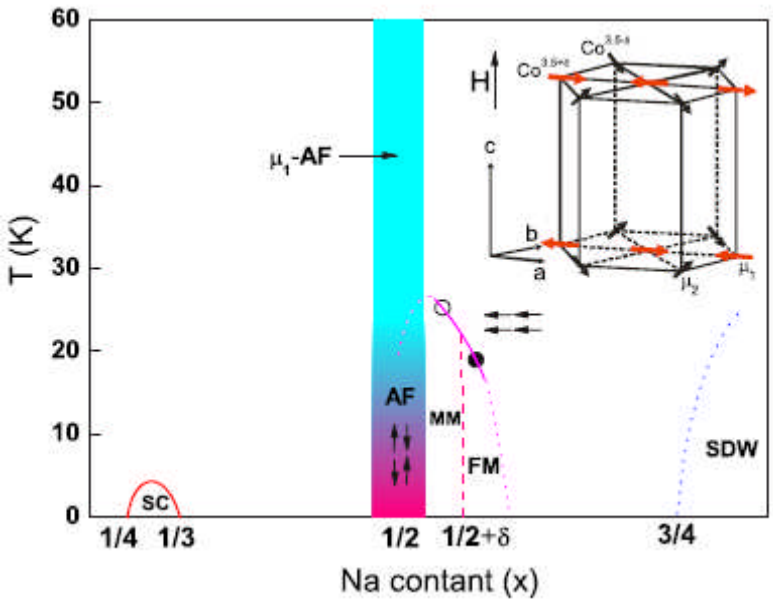

Fig. 2.3. The renewed magnetic phase diagram of Na_xCoO_2. μ_1-AF, antiferromagnetism of $Co^{3.5+\delta}$; AF, antiferromagnetism of $Co^{3.5-\delta}$; FM, ferromagnetism of $Co^{3.5-\delta}$; MM, metamagnetism of $Co^{3.5-\delta}$; SC, superconductivity; and SDW, spin density wave. The open and filled circles stand for the ferromagnetic transition points for $Na_{0.52}CoO_2$ and $Na_{0.55}CoO_2$, respectively. The inset figure shows the magnetic structure proposed for x = 0.55 with field H//c plane [36].

Cui et al. [33] studied the structure and transport properties of polycrystalline samples of Na_xCoO_2 (x = 0.52, 0.56, 0.6, 0.68, 0.72, 0.76, 0.8), where x represents the nominal Na content. ICP-AES results confirmed that the ratio of Na to Co was in good agreement with the nominal value, with minor increases for x = 0.68, 0.72, 0.76. With increasing Na content, the in-plane lattice parameter *a* increases, while lattice parameter *c* decreases. The temperature dependence of the electrical resistivity shows that all the samples remain metallic, and the resistivity reaches a minimum around x = 0.68. This

indicates that the insulating phase (x = 0.5) exists only in a very narrow sodium range. An electron diffraction study [29] revealed an extensive series of ordered Na ion-Na vacancy superlattices which existed beyond the simple hexagonal average structure. The superlattice was found in a $Na_{0.71}CoO_2$ sample (Fig.2.4).

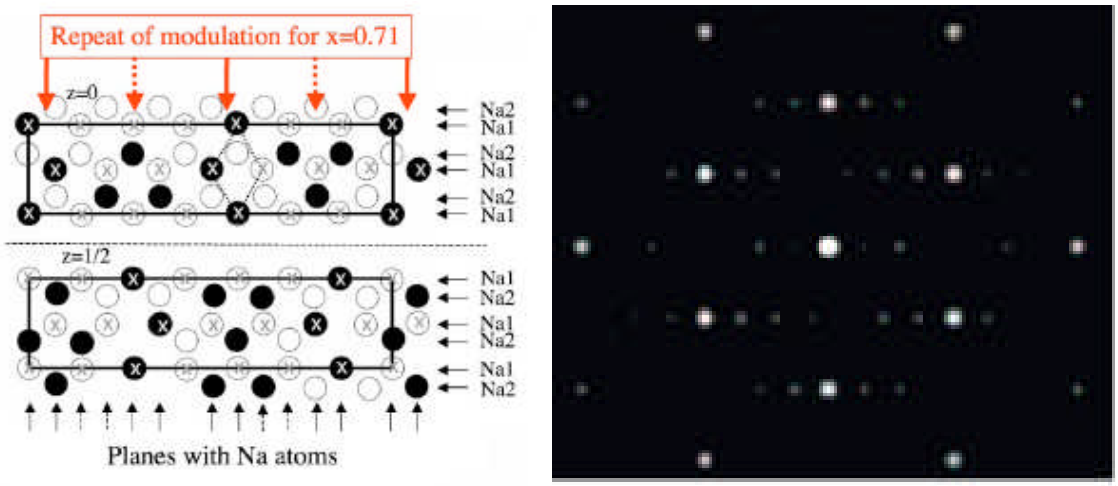

Fig. 2.4. Model for the Na planes of $Na_{0.71}CoO_2$ (left) and electron diffraction pattern of $Na_{0.71}CoO_2$ (right). The Na planes at both z = 0 and z = 1/2 are given. Occupied Na positions are given as black dots and Na vacancies by open circles. X indicates the positions of the underlying Co atoms. On the right of each model, it is indicated whether the Na atoms are at a Na1 or a Na2 site [29].

^{23}Na nuclear magnetic resonance (NMR) and superconducting quantum interference device (SQUID) magnetometer studies on nominal $0.50 \leq x \leq 0.70$ powder samples give evidence for the order of the Na ions and of the Co charges in the CoO_2 planes [32]. Although Co charge order did not occur in ref. 11, it is a mystery as to whether the Co

charge order is an intrinsic property of the CoO_2 planes which governs ground state properties and drives the Na ordering as a side effect, or conversely, has become an extremely important step to understand the physics of sodium cobaltates.

2.2.2. Effects of elemental doping

In order to investigate the thermoelectric properties and the electronic transport properties of the cobalt oxide Na_xCoO_2 system, many researchers have focused on doping effects [42-52]. Doping of alkaline-earth metals into Na sites will change the carrier concentration, and doping of transition metal into Co sites will change the electronic spin state. The effects on the thermoelectric properties of doped samples were investigated by Yakabe et al. [44], who doped Na sites with 5 % Li, La, Ba, Ca, Mn, Cu, and Ag. It was found that in alkaline-earth metal doping, the effective carriers are electron holes. The Ag doping improved the thermoelectric power but reduced the resistivity, although this could not be explained by conventional band theory.

Y. G. Zhao's group [49-51] systematically studied the doping effects on Co sites, with $\leq$ 5 % doping with Mn, Ti, and Ga. A resistivity upturn was observed at low temperatures for both Mn and Ti doped samples, while it does not appear in the Ga doped samples. Early researches [46-48] reported that an electrical upturn was also observed in Ni doped samples, while the upturn was absent in Cu doped samples. Pb doped samples

showed improved thermoelectric properties [45] because Pb in Co sites increased the charge carrier concentration by reducing the Co^{3+}/Co^{4+} ratio. Low level doping with 3 % Mn on Co sites resulted in a metal-insulation transition at about 35 K [49]. This differs from the results on $NaCo_{1-x}Cu_xO_2$ [46].

Samples with higher Mn doping (> 4 %) [52] show an electrical resistivity upturn at low temperature, which can be attributed to the scattering of conduction electrons by the spin frustration. The resistivity, magnetoresistance, and specific heat can be fitted by $\rho = \rho_0 + aT^2 + b\ln T$, $M = M_0 + a' T^2 + b' \ln T$, and $C/T = \gamma + \gamma T^2 + \alpha \ln T$, respectively. The results suggest that the Mn doping on Co sites increases magnetic fluctuations in the cobalt oxides, leading to possible quantum critical behaviour.

2.2.3. Thin film growth and physical properties

The Na_xCoO_2 series have the ground states of a two-dimensional triangular lattice. For the purposes of fundamental research and applications, many efforts have been focused on the fabrication of Na_xCoO_2 thin film with modulated sodium concentrations. Due to the high vapour pressure of Na in these materials, the incongruent melting of Na_xCoO_2, and the complex relations between the film and the substrate, the epitaxial growth of high-quality, single phase thin film is much more difficult than for ordinary materials, even with no mention of controlling x.

In 2005, Oht et al. reported the growth of epitaxial Na_xCoO_2 thin film using reactive solid-phase growth via lateral diffusion of sodium [53], the so-called "reactive solid-phase epitaxy (R-SPE) method". Although the precise control of the sodium content and related characterizations need to be improved, this work has opened the door to achieving success. x = 0.68 and 0.75 thin films have been fabricated on sapphire (0001) substrates via the lateral diffusion of sodium into Co_3O_4 (111) films by pulsed-laser deposition (PLD) [54, 55]. Sodium contents were well controlled with a capped-sandwich lateral diffusion scheme. The thin film quality is as decent as that of single crystals. A $Na_{0.83}CoO_2$ epitaxial thin film was prepared by the R-SPE method [57]. The temperature-dependent photoemission has been studied on the as-grown film; the results suggest that the large thermoelectric power at high temperatures should be treated within the correlated hopping model. Son et al. [58] grew epitaxial thin films on sapphire substrates by the PLD method. The deposition rate controlled the phase structure. A γ-phase thin film was grown at the low deposition rate of 0.02 Å/pulse using the eclipse method. When the deposition rate was increased, mixed β- and γ-phase was observed. At the high deposition rate of 0.2 Å/pulse, single phase β-$Na_{0.6}CoO_2$ thin film was deposited in the island growth mode. The γ-$Na_{0.7}CoO_2$ thin film exhibits spiral surface growth with highly crystallized texture compared to that of the β-$Na_{0.6}CoO_2$ thin film.

2.2.4. Single crystal growth and physical properties

2.2.4.1. Single crystal growth by the flux method

Large single crystals are required for measuring the thermoelectric properties and other anisotropic properties of these sorts of compounds. However, it is difficult to grow large Na_xCoO_2 crystals. In 1997, Terasaki et al. first grew $NaCo_2O_4$ single crystals by the flux method, with the largest size 1.5 x 1.5 x 0.01 mm^3. Since then, the flux method has been widely used in the single crystal growth of Na_xCoO_2 [59-67].

Fujita et al. [60, 61] studied the flux growth of two-layer γ-Na_xCoO_2 and its high-temperature thermoelectric properties. Single crystals were grown from the molten materials using NaCl as the flux. The starting materials were well mixed in the ratio of Na_2CO_3 : Co_3O_4 : NaCl = 1 : 1 : 7. The mixture was heated in an Al_2O_3 crucible at 1223 K for 12 h in air and slowly cooled down to 1123 K at the rate of -0.5 K/h. This was followed by washing away of the NaCl flux with pure water. The largest size of the flaky resultant samples was about 5 x 3 x 0.05 mm^3; the typical size was 1.5 x.1.5 x 0.03 mm^3 (as shown on the left of Fig. 2.5). These single crystals with metallic lustre are thin in the *c*-axis direction and can be cleaved along the *ab* plane. Single crystals grown by the same procedure were used in many studies [64-66]. The in-plane resistivity and thermal conductivity of single crystal $Na_{0.7}CoO_2$ were measured down to

40 mK. A Fermi-liquid state at low temperature is characterized by the largest Kadowaki-Woods ratio ever observed. Comparison with other materials suggests that the giant electron-electron scattering is due to magnetic frustration or to the proximity of a nearby magnetic quantum critical point [65]. Wang et al. [64] investigated the electronic structure and charge for $Na_{0.7}CoO_2$ single crystals by means of an optical spectroscopy probe. The in-plane optical conductivity spectra show two broad interband transition peaks at 1.6 eV and 3.1 eV, and a weak mid-infrared peak at 0.4 eV. The origin of the interband transitions and the low-frequency charge dynamics is also discussed in Ref. [64].

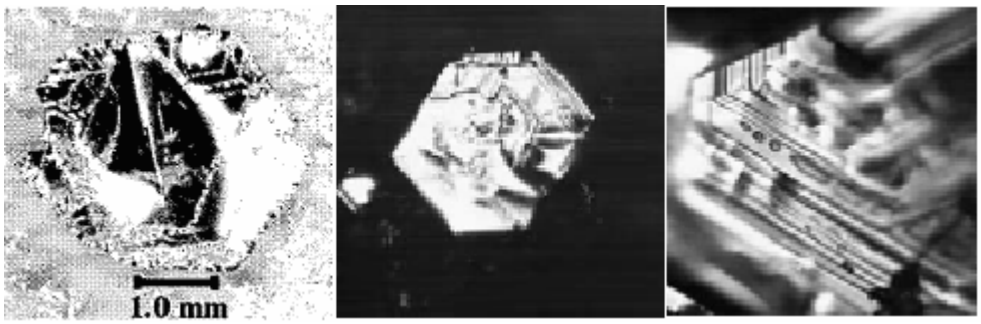

Fig. 2.5. An optical micrograph of a sample prepared by Fujita et al. (left) [61], and typical $Na_{0.7}CoO_2$ single crystals packeted parallel to the ab plane (middle and right) [68].

Single γ-$Na_{0.7}CoO_2$ crystals can be grown from a higher flux ratio (Na : Co : NaCl = 1 : 1 : 10) mixture by the same procedure [68]. The resultant hexagonal thin platelets with a typical size of 3 x 3 x 0.1 mm^3 seem have better morphology than the crystals grown

from the lower flux ration (as shown on the right of Fig 2.5). When B_2O_3 was used as the flux with Na_2CO_3 : B_2O_3 = 8 : 1 [63], γ-$Na_{0.6}CoO_2$ single crystals were grown with a typical size of 3 x 3 x 0.1 mm^3. (The Na content is inaccurate, however, as otherwise the compound would be β-phase.)

2.2.4.2. Single crystal growth by optical floating zone method

Solution growth by using NaCl (or B_2O_3) flux was performed, but that unfortunately led only to thin crystals, where the NaCl flux wash in water will lead to non-stoichiometric and possibly contaminated samples. This kind of crystal can't be used for superconducting phase studies, for the compound can be partially decomposed during the intercalation process, resulting in highly defective crystals containing Na-poor phases.

Large and high quality single crystals of γ-phase Na_xCoO_2 were grown by the floating-zone technique in an image furnace [10, 52-60], and their chemical, thermal, and structural behaviour, and their physical properties were carefully studied. The details of crystal growth will be discussed in Chapter 3.

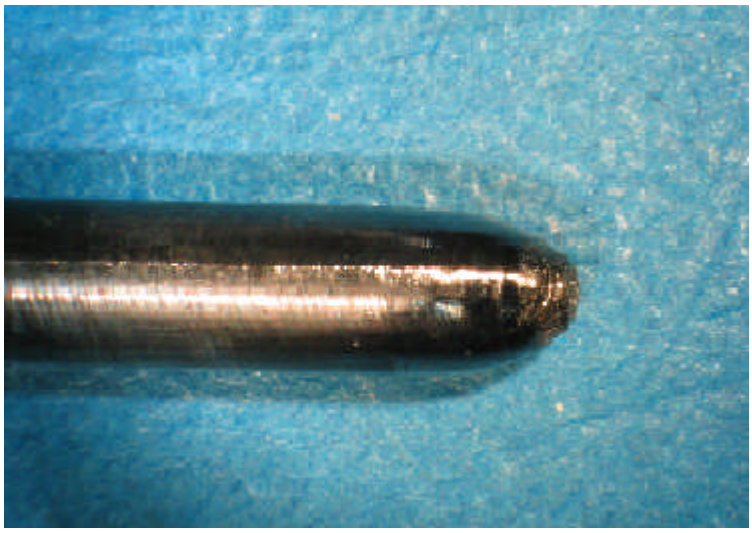

Fig. 2.6. Typical $Na_{0.82}CoO_2$ single crystal grown by the floating-zone technique in an image furnace (Φ 6 × 80 mm^3).

Bayrakci et al. systematically studied the physical properties of high-quality single crystals of $Na_{0.82}CoO_2$ [69-73]. Susceptibility, specific heat, and muon spin rotation measurements revealed bulk antiferromagnetism with Néel temperature T_N = 19.8 ± 0.1 K and an ordered moment perpendicular to the CoO_2 layers. The susceptibility exhibits a broad peak around 30 K, characteristic of two-dimensional antiferromagnetic fluctuations. The magnetic order encompasses nearly 100 % of the crystal volume. The in-plane resistivity is metallic at high temperatures and exhibits a minimum at T_N. Anisotropic dc magnetic susceptibility and μSR measurements on the x = 0.82 composition both showed that the Co spins were oriented along the *c* axis [69]. Neutron scattering measurements demonstrated that $Na_{0.82}CoO_2$ exhibits *A*-type antiferromagnetic order, and the corresponding spin-wave dispersions were characterised. The antiferromagnetism coexists with metallic conductivity. The in-plane

and out-of-plane exchange constants resulting from a fit to a nearest-neighbour Heisenberg model are similar in magnitude [73]. Spectral ellipsometry measurements on a $Na_{0.82}CoO_2$ crystal demonstrated two prominent transitions as a function of temperature [72]. The first one at 280 K involves marked changes of the electronic and lattice responses that are indicative of charge ordering in the CoO_2 layers. The second transition at T_N = 19.8 K reveals sizable spin-charge coupling.

When the field was parallel to the *c*-axis, a metamagnetic transition from an antiferromagnetic state to a quasiferromagnetic state was found at 8 T at low temperatures for a Na = 0.85 single crystal sample, but when the field was perpendicular to the *c*-axis, no transition was found below 14 T [74]. High-resolution thermal expansion measurements on $Na_{0.80}CoO_2$ single crystal revealed the continuous behaviour of the paramagnetic-antiferromagnetic phase transition at T_M = 21.7 K, with critical exponent α = 0.18. The thermal expansion was highly anisotropic [76]. Schulze et al. [77] found a direct link between low temperature magnetism and high temperature sodium order in Na = 0.8 and 0.85 single crystals. The impact of ordered Na^+ Coulomb potential on the CoO_2 physics is evidenced opening new ways to experimentally revisit the Na_xCoO_2 phase diagram.

2.2.5. Theoretical explanations

There have been many efforts to explain the novel physical properties found in γ-phase Na_xCoO_2 [78-83]. However, such basic issues as the low energy electronic structure and the Fermi surface topology in the cobaltates have not been well understood [80]. Density functional calculations were used to study the doping dependence of the electronic structure and magnetic properties in Na_xCoO_2 for x = 0.3, 0.5, and 0.7, and a weak itinerant ferromagnetic state is predicted for all doping levels in the range x = 0.3 to x = 0.7, with competing but weaker itinerant antiferromagnetic solutions [78]. The puzzle of the discrepancy between the angle resolved photoemission spectroscopy (ARPES) results and the local density approximation (LDA) Fermi surfaces was resolved by showing that the small e'_g Fermi surfaces in Na_xCoO_2 are destroyed by Na disorder [79]. In order to explain how strong correlations drive orbital polarization and the band narrowing observed in ARPES, Zhou et al. [80] adopted a multiorbital Hubbard model and obtained a quasiparticle dispersion and a Fermi surface topology that were in good agreement with experiments. The 3D Hubbard model calculation results indicated that the spin fluctuations that give rise to superconductivity in $Na_xCoO_2 \cdot yH_2O$ and the 3D magnetism in non-hydrated Na_xCoO_2 share the same origin [82]. The unexpected experimental results showed that signatures of strong correlations are present in the Na-rich regions of γ-Na_xCoO_2 and absent in the Na-poor regions (x = 0.3), which can be explained by density functional theory and dynamical mean-field

theory calculations. The Na potential was shown to be a key element in understanding correlations in this phase [83].

2.3. Charge ordered insulator $Na_{0.5}CoO_2$

2.3.1. Crystal structure of $Na_{0.5}CoO_2$

$Na_{0.5}CoO_2$ is not a thermodynamically stable phase, but it is obtained from the parent compounds γ-Na_xCoO_2 [6, 16, 87-95] or α-Na_xCoO_2 [96] by a de-intercalation process, as described in Section 2.2.1, and the resulting structures are determined by the structures of the parent sodium cobaltates. In all the phases, sheets of edge-sharing CoO_6 octahedra are interleaved by sodium ions. The stacking sequence of the oxygen layers gives the number of sheets within a unit cell.

Neutron diffraction data [87] has shown that the average crystal structure of $Na_{0.5}CoO_2$ at room temperature belongs to Space group *Pmmn*, with parameters: a = 5.6305 Å, b = 11.1299 Å, and c = 4.8758 Å. The structure undergoes several phase transitions below 100 K, and becomes a magnetically ordered insulator at low temperatures. The crystal structure involves an ordering of the Na ions into zigzag chains, which is confirmed by semi-quantitative analysis of the electron diffraction data, as shown in Fig. 2.7.

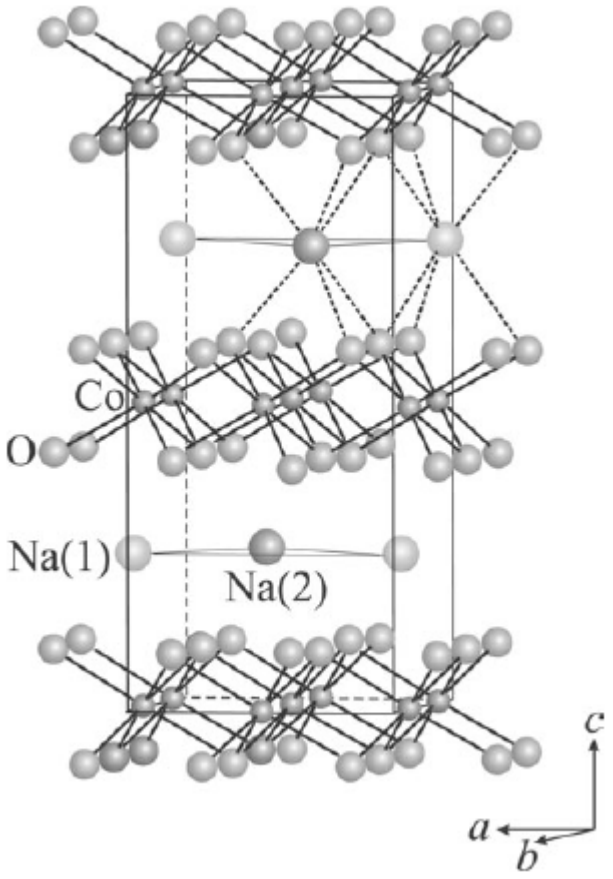

Fig. 2.7. The crystal structure of $Na_{0.5}CoO_2$ obtained from γ-Na_xCoO_2, showing layers of edge-shared CoO_6 octahedra and the triangular prismatic coordination of Na within the intermediary layers [87].

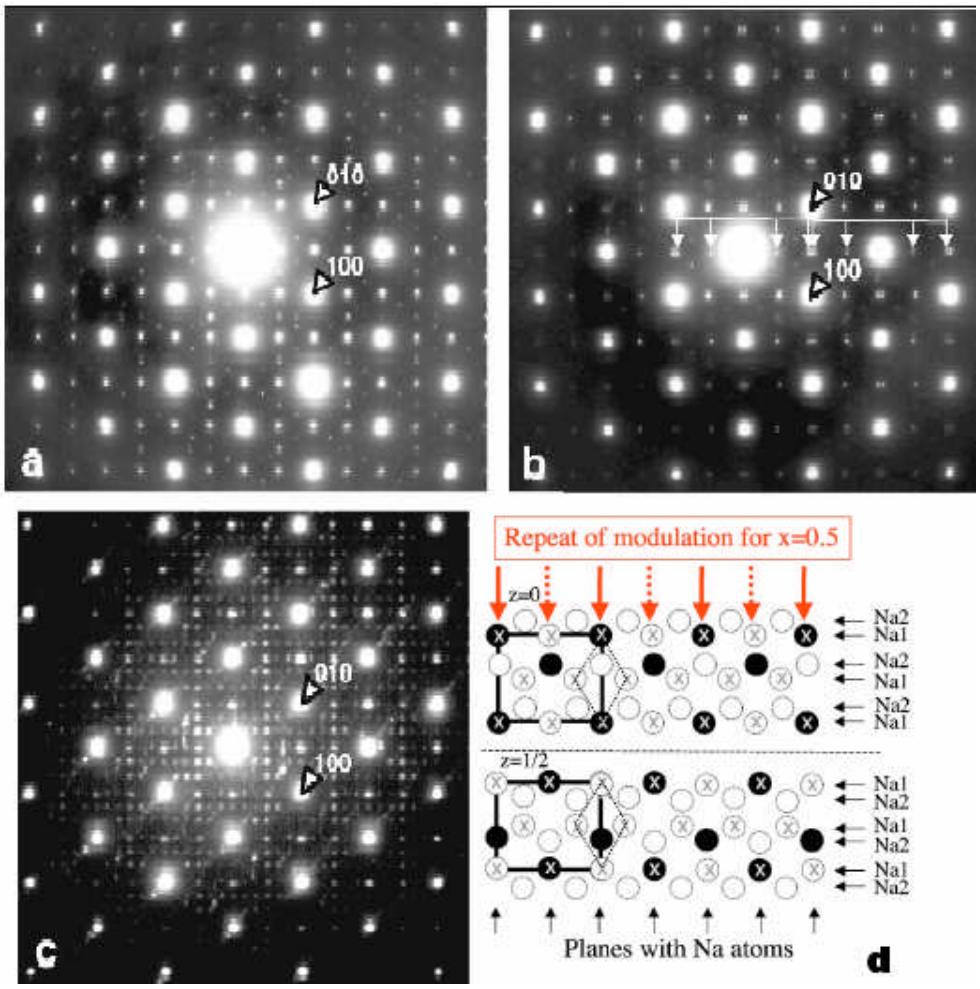

Fig. 2.8. [001] diffraction patterns of $Na_{0.5}CoO_2$: (a) pattern of commensurate superstructure was taken almost immediately expose to the electron beam, (b) pattern of incommensurate superstructure was taken after exposure to the electron beam; (c) diffraction pattern taken at about 100 K with extra reflections; such diffraction patterns were only observed in a few areas. White arrows in (b) indicate the first and second order superstructure reflections of the central spot and the 110 spot. (d) Model for the Na planes of $Na_{0.5}CoO_2$. Both the Na planes on z = 0 and z = 1/2 are given. Occupied Na positions are shown as black dots and Na vacancies by open circles. X indicates the positions of the underlying Co atoms. On the right of each model it is indicated whether the Na atoms are at a Na1 or a Na2 site [29].

An electron diffraction study [29] revealed an extensive series of ordered Na ion/Na vacancy superlattices, which went beyond the simple hexagonal average structure. The clearest superlattice was found in $Na_{0.5}CoO_2$ sample (Fig. 2.8), and it showed the presence of lines of Na ions and vacancies rather than simply maximized Na-Na separations.

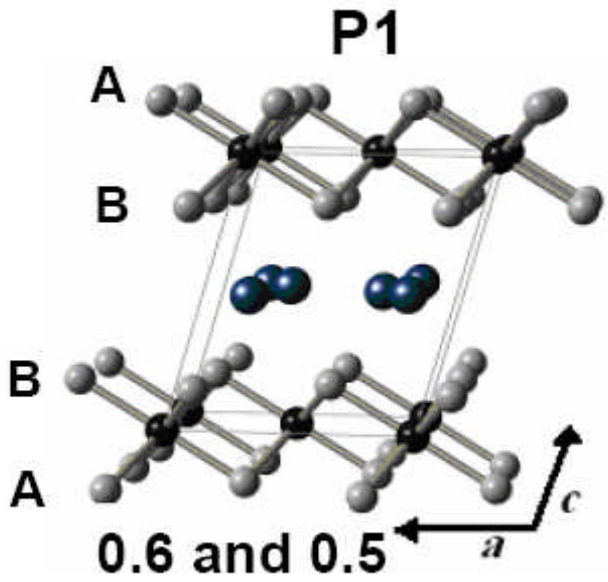

Fig. 2.9. The crystal structures of $NaCoO_2$ phases (x = 0.6, 0.5) derived from three-layer $NaCoO_2$. The smaller and larger black spheres represent Co and sodium ions, respectively, while the grey spheres are the oxygen ions.

$Na_{0.5}CoO_2$ derived from three-layer Na_xCoO_2 [96] only has one octahedral layer (space group *C2/m*), where the sodium ions are in trigonal prismatic coordination (see Fig.

2.9). The unit cell parameters are a = 4.8809(1) Å, b = 2.81535(9) Å, and c = 5.7738(2) Å. β = 105.546(2)°.

2.3.2. Magnetic structure of $Na_{0.5}CoO_2$

The relationship between the ordering pattern of Co sites and that of Na ions is very important for determining the electronic structures and the magnetic moments of Co atoms. From the data taken from various methods (magnetic susceptibility, specific heat, NMR, nuclear quadrupole resonance (NQR), and neutron scattering), Yokoi et al. [93] found two now well-known transitions for $Na_{0.5}CoO_2$ (as shown in Fig. 2.10). Pseudo-gap-like behaviour was observed in this phase. The Co sites with the larger quadrupole frequency, ν_Q, have larger magnetic moments. These moments align antiferromagnetically at 87 K with their direction within the plane, while the Co sites with smaller ν_Q have smaller moments. They align in the direction parallel to the c axis. The proposed magnetic structures for $Na_{0.5}CoO_2$ are shown in Fig. 2.11.

From polarized and unpolarized neutron scattering measurements, the simplest magnetic structure in single crystals of $Na_{0.5}CoO_2$ was proposed, as shown in Fig. 2.12 [16]. The solid circles represent ‘‘non-ordered’’ Co ions, and the open circles represent magnetically ordered Co ions, where the arrows indicate the directions of the magnetic moments. The shaded parallelogram outlines the magnetic unit cell.

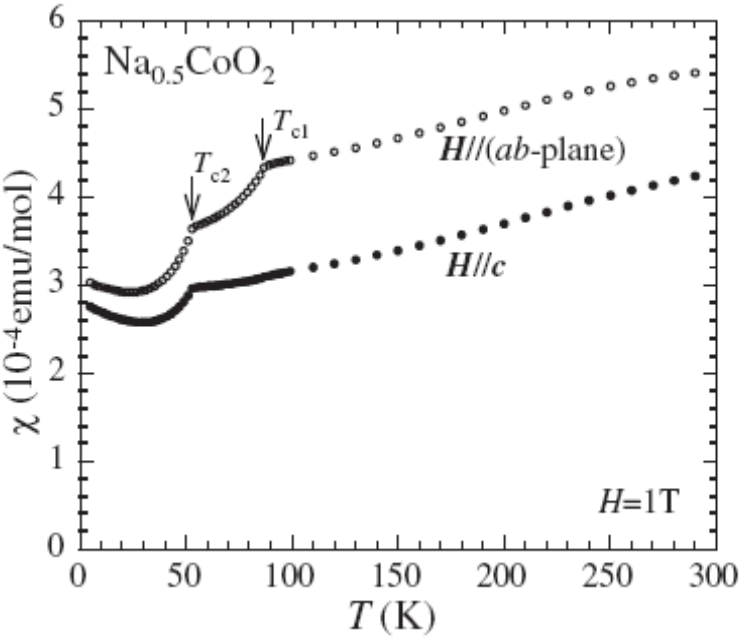

Fig. 2.10. Magnetic susceptibilities measured for a single crystal of $Na_{0.5}CoO_2$ with a field of 1 T parallel and perpendicular to c. At 87 K, the anomaly is very small for H//c, while the anomalies are significant at 53 K for directions of H that are both perpendicular and parallel to the c-axis [93].

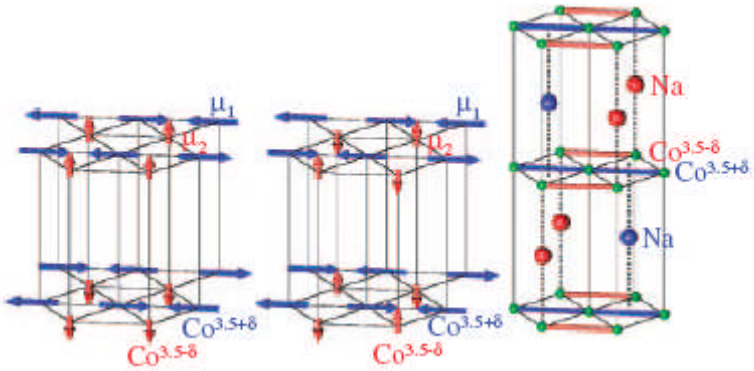

Fig. 2.11. Magnetic structures proposed [93] for $Na_{0.5}CoO_2$ are shown with ordered pattern of Na atoms. The close relationship between the ordering patterns of the Na atoms and the Co moments can be seen.

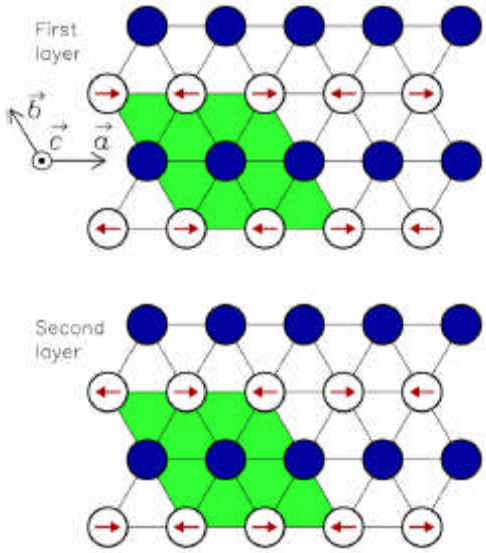

Fig. 2.12. Model of the spin arrangement in $Na_{0.5}CoO_2$. The two CoO_2 layers in the magnetic unit cell are depicted, and, for clarity, only Co ions are shown [16].

The electronic structure [84] and optical spectra [85] of $Na_{0.5}CoO_2$ have been calculated within the local density approximation (LDA). The results agree well with some experimental data. Charge disproportionation (CD) and spin differentiation in $Na_{0.5}CoO_2$ were studied by the correlated band local density approximation + Hubbard U (LDA + U) approach [86, 98], and valuable models have been proposed. The optical conductivity in $Na_{0.5}CoO_2$ was calculated from the tight binding approximation [99]. The calculated gross features agree well with the experimental findings. Choy et al. [100] demonstrated that at a filling factor of n = 1.5, a hexatic insulating state obtains in the extended Hubbard model on a triangular lattice. Their model is capable of explaining the Hall coefficient both qualitatively and quantitatively. Neutron powder diffraction was utilized to probe the crystal structure of layered $Na_{0.46}CoO_2$ over the

temperature range of 2 – 600 K [101]. They argued that changes in the Na (1)-O bond lengths observed at the magnetic transition at 88 K reflect changes in the electronic state of the CoO_2 layer [88]. Transport measurement on the x = 0.5 powder sample with pressure up to 30 GPa demonstrated a paradoxical result [95]: with the pressure increasing, the transition temperature at 53 K passes from an insulating to a metallic state. J. Y. Son [102] successfully grew $Na_{0.5}CoO_2$ thin films on (001) sapphire substrate by the PLD method. Epitaxial thin film with high crystallinity was obtained from Na de-intercalation of epitaxial $Na_{0.7}CoO_2$ in a solution of iodine-dissolved acetonitrile. The $Na_{0.5}CoO_2$ thin film showed layer-by-layer growth closely following an ideal step flow growth mode. The charge-ordered insulator property of $Na_{0.5}CoO_2$ thin film was confirmed by experiments.

2.3.3. Other physical properties of $Na_{0.5}CoO_2$

Raman scattering experiments have been performed on $Na_{0.5}CoO_2$ single crystal as a function of temperature ($10 \leq T \leq 300$ K), a structural instability and a metal–insulator transition have been observed [94]. Three additional phonon modes (at 414, 437, and 496 cm^{-1}) were observed compared to samples with x = 0.82. Combined variable temperature transmission electron microscopy and Raman scattering were used to investigate the structural transformations [103]. Structural transitions in the temperature range from 80 to 1000 K were directly identified, and the observed superstructures

agree with the Na-ordering model. The Raman scattering measurements revealed phase separation and a systematic evolution of the active modes along with phase transitions. This work demonstrates that the combination of electron diffraction and Raman spectroscopy measurements is an efficient method for studying the cation ordering and phase transitions in related systems. The charge ordering in $Na_{0.5}CoO_2$ single crystal has also been studied by infrared reflectivity [104].

Using high-resolution photoemission spectroscopy [105, 106], the electronic structures of insulating cobaltates were systematically studied. It was found that the a_{1g} band, which forms a large hexagonal Fermi surface centred at the Γ(A) point, shows a dispersion kink at a binding energy of approximately 100 meV [105]. Xia et al. [106] found an insulator-like low-energy state with a weakly k-modulated gap due to particle–hole instability on the Fermi surface for $Na_{0.5}CoO_2$.

^{59}Co NMR studies have been performed in metallic $Na_{0.5}CoO_2$ in the temperature range of 350 – 100 K [107]. The NMR results, together with the susceptibility, indicate the presence of Co^{3+} ions with $S = 0$, as well as the magnetic Co^{4+} ions. Ning et al. [108] presented ^{59}Co NMR evidence for charge ordering below 51 K and evidence that the insulating ground state of the itinerant antiferromagnet $Na_{0.5}CoO_2$ (T = 86 K) is induced by charge ordering.

2.4. Unusual physical properties phase γ'-$Na_{0.75}CoO_2$

2.4.1. Crystal structure

$Na_{0.75}CoO_2$ is a rather unusual metal. It is interesting because of its magnetic and thermoelectric properties. Neutron scattering has revealed spin correlations which are ferromagnetic in the *ab* plane and antiferromagnetic in the stack direction. Below about 22 K the compound is ordered in this way, with a small moment of about 0.2 μ_B per Co atom. Photoemission spectroscopy (PES) has shown that there is a single large Fermi surface (FS) in this latter concentration region [109, 110]. The Fermi surface measured by photoemission is a cylinder around the stack axis. It has a complex crystal structure. Quite early [21] research demonstrated a monoclinic distortion of the O3 phase, and powder neutron diffraction data [88] indicated that there was a narrow two-phase region with 31.1 % H1 type $Na_{0.71}CoO_2$ (a = 2.8314 Å, c = 10.8756 Å) and 68.9 % H2 type $Na_{0.77}CoO_2$ (a = 2.84126 Å, c = 10.8144 Å), but the $Na_{0.75}CoO_2$ derived from three-layer Na_xCoO_2 [96] has a one-layer CoO_2 monoclinic cell with space group C2/m (a = 4.9043 Å, b = 2.8723 Å, c = 5.7789 Å, β = 111.764^o). In this review, I take an average structure for this phase with a monoclinic cell, as shown in Fig. 2.13.

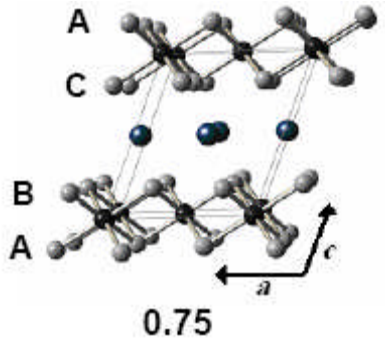

Fig. 2.13. The crystal structures of $Na_{0.75}CoO_2$ derived from three-layer $NaCoO_2$. The small and large black spheres represent Co and sodium ions, respectively, while the grey spheres are the oxygen ions [96].

2.4.2. Sodium pattern and magnetic structure of $Na_{0.75}CoO_2$

Long range sodium ordering has been reported, however, the ordering pattern of $Na_{0.75}CoO_2$ appears to be controversial [29, 111-113]. Up to now, no electronic pattern has been resolved. This is mainly because of the difficulty in accurately determining the Na content and the sensitivity of sodium ordering to small variations in x or to the synthesis method. Fig 2.14 shows the neutron diffraction results and the proposed pattern of sodium ions in this most studied phase. Neutron diffraction shows Na^+ order for x = 0.75 at T = 150 K. Superlattice reflections form rings around hexagonal Bragg reflections, and some higher-order harmonics are observed [111]. The Na ion ordering pattern proposed for x = 0.75 [113] indicates that sodium ions at Na(1) positions may hop (arrows) onto unoccupied neighbouring Na(2) positions (solid triangles), but

sodium ions at Na(2) positions (triangle centres) cannot. This is because edge-sharing triangles cannot be occupied simultaneously. NMR data also suggest a similar selective mobility in $Na_{0.75}CoO_2$ [113].

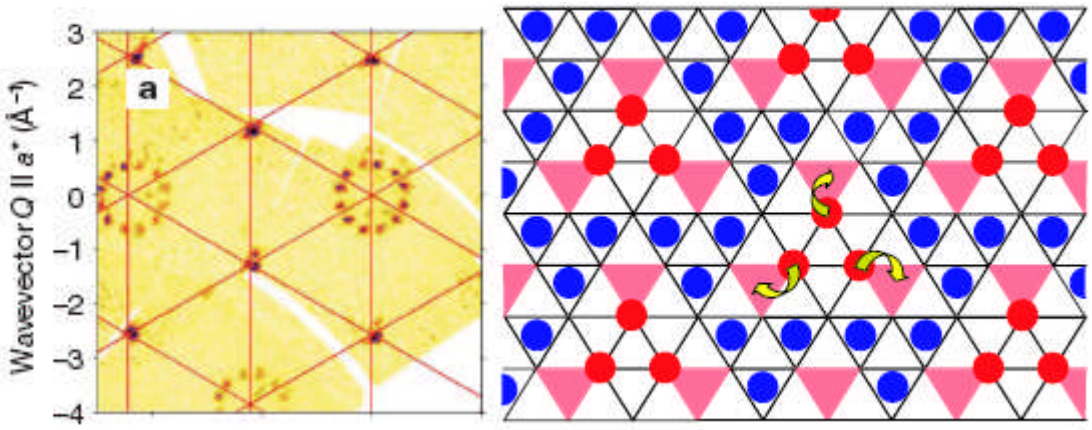

Fig. 2.14. Neutron diffraction results showing ordering of Na^+ (left [111]) and the Na ion ordering pattern proposed for x = 0.75 (right)[113].

Helme et al., using polarized and unpolarised neutron scattering measurements, confirmed the ferromagnetic correlations within the CoO_2 layers and revealed antiferromagnetic correlations perpendicular to the layers. Their results are consistent with an *A*-type antiferromagnetic ordering. They estimate the interlayer and intralayer exchange constants to be 12.2 ± 0.5 meV and -6 ± 2 meV, respectively. The magnetic fluctuations in $Na_{0.75}CoO_2$ were found to be highly three dimensional [114]. Fig. 2.15 shows that the simplest spin arrangement consistent with the observations is the *A*-type antiferromagnet.

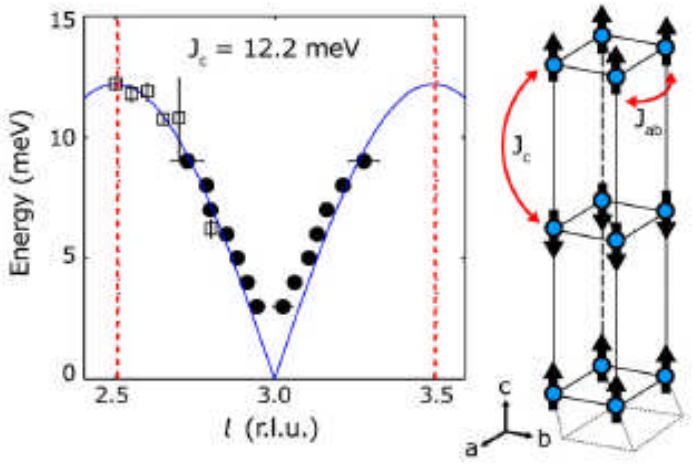

Fig. 2.15. Left: The magnon dispersion of $Na_{0.75}CoO_2$ parallel to the (00l) direction, measured on IN8 at a temperature of 1.5 K. Right: The magnetic structure on which the spin-wave model is based, showing the two exchange constants J_{ab} and J_c, and the spin directions [114].

Later, they presented experimental results [115] that provide information on the spin anisotropy and the magnetic structure of Na_xCoO_2. They reported low-energy neutron inelastic scattering measurements of the magnetic excitations in the magnetically ordered phase of $Na_{0.75}CoO_2$. The energy spectra suggested the existence of two gaps and can be well fitted by a spin-wave model. The in-plane anisotropy is the puzzling feature of their work. The gap energies decrease with increasing temperatures, and both gaps are found to have closed when the temperature exceeds the magnetic ordering temperature, $T_m \approx 22$ K.

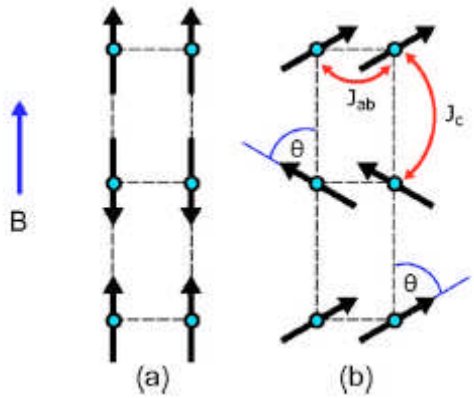

Fig. 2.16. (a) The ordered A-type antiferromagnetic structure in the a-c plane, with an external magnetic field B applied parallel to the magnetic moments. (b) Above a critical field B_{sf} the system undergoes a spin-flop transition to a phase with spins at an angle θ to the c axis [115].

First-principles calculations were used to analysis the exchange mechanisms of $Na_{0.75}CoO_2$ [116], and the results agree with the neutron results [117], favouring the antiferromagnetic stacking of ferromagnetic planes. It was found that interplane coupling to second neighbours plays an important role in the out-of-plane magnetism. It was suggested that the exchange between the six next-nearest neighbours in adjacent planes needs to be taken into account when doing calculations.

2.4.3. Crystal growth and physical property measurements

As detailed in 2.2, $Na_{0.75}CoO_2$ samples were prepared by the RHU technique [27, 118-121], the flux method [122, 123], or the floating zone technique [124-129]. The

optical floating zone (FZ) technique is the best way to prepare large crystals of Na_xCoO_2 for experiments where size is important, such as inelastic neutron scattering and anisotropic property measurements. Prabhadran et al. [124] systematically investigated the growth of Na_xCoO_2 single crystals by this technique. It was found that the oxygen annealing will change the magnetic properties of the material, especially at low temperature. Na loss during the growth was reduced by using a high-pressure growth atmosphere. They concluded that there is an optimum O_2/Ar ratio near 4 : 1 for good crystal quality and minimum Co_3O_4 impurity content. High quality large single crystals also can be obtained by using the FZ technique under a low oxygen atmosphere [125-129].

Early research [27] found a simultaneous enhancement of the thermopower with reduced resistivity in $Na_{0.75}CoO_2$, with S reaching a high value of 120 μV/K at 300 K. There are five Raman active phonons with positions around 195 cm^{-1} (E_{1g}), 482 cm^{-1}, 522 cm^{-1}, 616 cm^{-1} ($3E_{2g}$), and 663 cm^{-1} (A_{1g}) that appear in x = 0.75 sodium cobaltate. The Raman spectra change along with the intercalation of H_2O and changes in the superconducting properties [123].

A study on polycrystalline samples [119] found a magnetic transition of the second order at 22 K. All the measurement results indicated that this unusual electronic state may be attributed to the strongly correlated electrons in $Na_{0.75}CoO_2$. The μ^+SR spectroscopy indicated that this magnetic transition was an intrinsic change in the

magnetism of the sample [120]. Magnetic susceptibility, resistivity, magnetoresistance, and heat capacity measurements on single crystals of $Na_{0.75}CoO_2$ indicated a bulk phase transition at 22 K. These data are consistent with the formation of an antiferromagnetic spin-density-wave (SDW) at 22 K, with the easy axis for magnetization along the *c* axis. The SDW transition in this compound is found to be sensitive to the preparation conditions, and no SDW transition was observed in polycrystalline powder [125, 126].

The crystal samples exhibit a sharp first-order phase transition at 340 K. M.-H. Wangbo and D. Dai [128] proposed the use of a modified Curie-Weiss law to analyse the magnetic susceptibilities of $Na_{0.75}$ CoO_2, and their study showed that the low-spin Co^{4+} (S = 1/2) ions were responsible for the anisotropic magnetic properties of $Na_{0.75}CoO_2$ and suggested that the six nearest-neighbor Co^{3+} ions of each Co^{4+} ion had adopted the intermediate-spin electron configuration. This proposal resolved the conflict between the magnetic structure derived from neutron scattering studies below 22 K and that deduced from magnetic susceptibility measurements between 50 and 300 K. Ga or Mn doping studies found that Ga doping increases the electronic resistivity of $Na_{0.75}CoO_2$, while 5 % Mn doping causes a metal-insulator transition at low temperature [51].

2.5. Three-layer Na_xCoO_2

2.5.1. Crystal structure

Compared with the widely studied aforementioned phases of Na_xCoO_2, there has only been little research focus on three layer sodium cobaltates. The research has been hampered by difficulties in single crystal growth, as well as by phase separation effects for high Na content samples [6]. Some physical properties are even decided by the sample preparation process. For instance, no superconductivity has been found in sodium cobalt oxyhydrates obtained from a parent polycrystalline sample of β-$Na_{0.6}CoO_2$ [130], but sodium cobalt oxyhydrates obtained from both single crystal and powder samples of β-$Na_{0.6}CoO_2$ have shown superconductivity with a T_c of about 4-5 K [131, 132].

In three-layer structured Na_xCoO_2, crystallographic studies have been reported for x = 1 (single crystals [133], polycrystalline powder [136]), x = 0.92 (polycrystalline powder) [96], and x = 0.60 [130], 0.61 [134], and 0.67 [135] (polycrystalline powder). At x = 1 and 0.92, the reported three-layer structure is trigonal (*R-3m* with a = 2.889 Å and c = 15.60 Å), and at x = 0.6, the reported structure is also trigonal (*R-3m* with a = 2.8256(4) Å and c = 16.466(2) Å), while at x = 0.61, the crystal structure is two-layer hexagonal (*$P6_3/mmc$*, with a = 2.83287(2) Å, c = 10.8969(1) Å). However, at x = 0.67, the crystal structure is single-layer monoclinic (*C2/m*, with a = 4.9023(4) Å, b = 2.8280(2) Å, c = 5.7198(6) Å, and β = 105.964°). The three-layer structure is shown in Fig.2.17, where

the unit cell is defined by three CoO_2 identically orientated planes in an ACBACB [96] or ABCABC [130] hexagonal stacking arrangement.

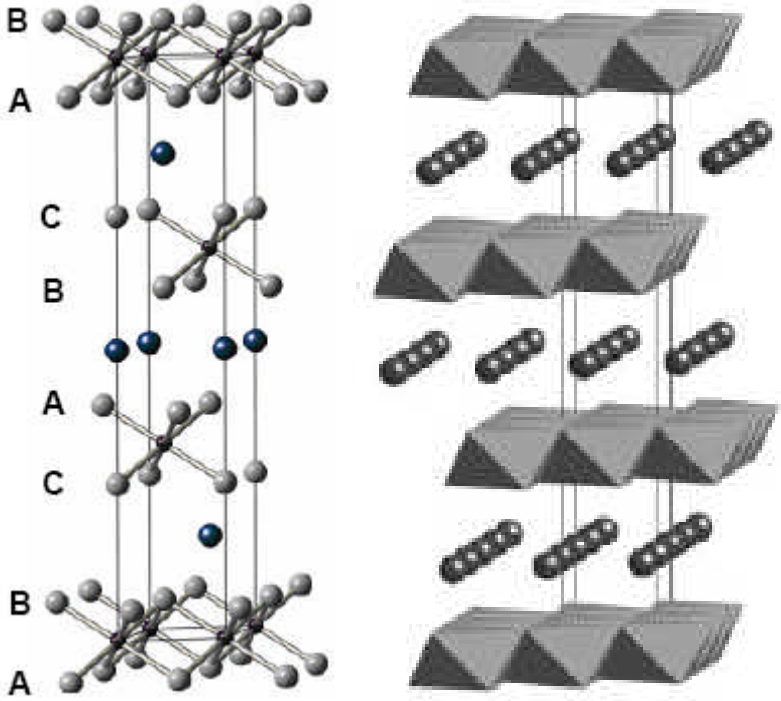

Fig. 2.17. Left [96]: The crystal structure of $Na_{0.92}CoO_2$. Smaller and larger black spheres represent Co and sodium ions, respectively, while the grey spheres are the oxygen ions. Right [130]: The crystal structure of $Na_{0.6}CoO_2$.

2.5.2. Sodium ion ordering and magnetic state

The strong correlation between the Na vacancies and the doped holes clearly determines the electronic and magnetic properties of the sodium cobaltates [111]. Sodium ions

between the CoO_2 layers play an important role for the understanding of the magnetic properties and electronic structure in three-layer Na_xCoO_2. Both the β- and α-phases have sodium ion ordering in different patterns. Zandbergen et al. [29] studied the Na ordering by electron diffraction, and two types of [001] diffraction patterns were observed for $Na_{0.64}CoO_2$. Both show incommensurate superstructure reflections, but they differ in (a) not showing and (b) showing the presence of reflections at 1/2,0,0 and similar positions. Some of these reflections are circled in (b). The incommensurate vectors $\mathbf{q}_1$ and $\mathbf{q}_2$, which are of equal length and make an angle of 3.6° with the [11-20] and $[\bar{1}2\bar{1}0]$ directions are indicated with white arrows in (a).

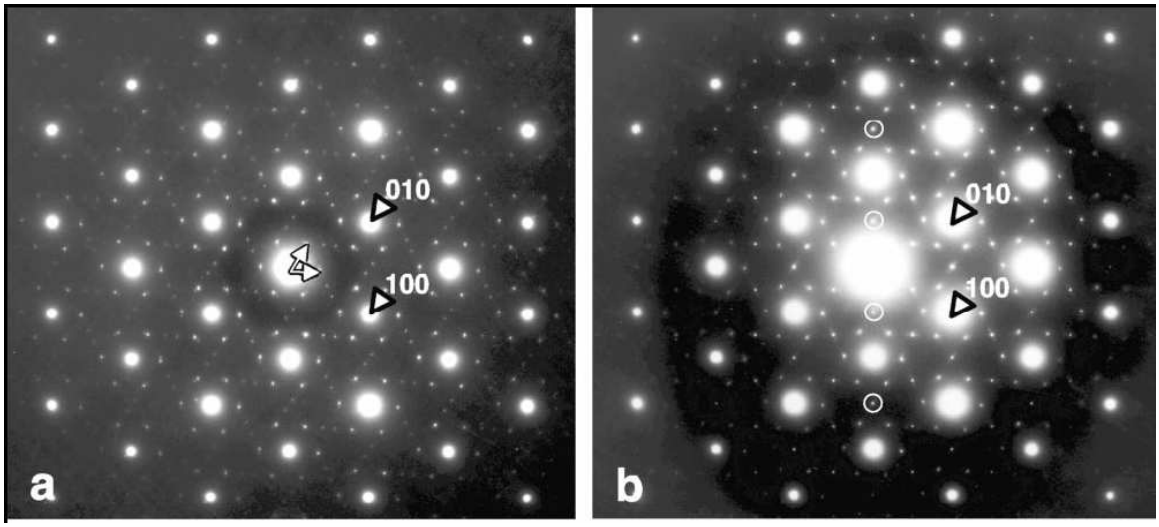

Fig. 2.18. (a) and (b) show the two [001] diffraction patterns observed for $Na_{0.64}CoO_2$ [29]. The arrows indicate the incommensurate vectors $\mathbf{q}_1$ and $\mathbf{q}_2$ in (a), and the circles indicate the extra reflections in (b).

The nature of the underlying magnetic state is still debated. Bernhard et al. [137] studied Na_xCoO_2 ($0.78 \leq x \leq 0.97$) by muon spin rotation. They proposed that the intrinsically inhomogeneous magnetic state can be described in terms of hole-doping (Na vacancy) induced magnetic clusters. However, this state cannot be discussed in terms of chemical inhomogeneity or of impurity phases.

2.5.3. Sample preparation and physical properties

The sample preparation method strongly impacts on the structure and physical properties. β-$Na_{0.6}CoO_2$ synthesized by a solid state reaction of Na_2CO_3 and Co_3O_4 at 610 ℃ for 3 days is a three-layer structured powder, and the derived cobalt oxyhydrate has no superconductivity [130]. When using the RHU method with same starting materials, the powder has a two-layer structure, and the derived oxyhydrate shows superconductivity at 4.5 K [131]. When β-$Na_{0.6}CoO_2$ is prepared by conventional solid state reaction using Co and anhydrous NaOH as starting materials, followed by 5 days of heating at 550 °C, the powder has a monoclinic structure, and the derived oxyhydrate has superconductivity at 3.7 K [132].

Small β-$Na_{0.57}CoO_2$ single crystals (1.5 x 1.5 x 0.01 mm^3) can be grown from a NaCl flux, where the NaCl is mixed in a molar ratio Na : Co : NaCl = 1 : 1 : 7. The mixture is then fired at 950 °C for 12 h and then slowly cooled down to 850 °C [138]. α-Na_xCO_2

single crystals also can be grown from a NaCl flux with a molar ratio Na : Co : NaCl = 1 : 1 : 4 or 1 : 1 : 5 [139, 133]. Bigger single crystals of Na_xCoO_2 were grown by a flux technique [141, 63] using Na_2CO_3 and Co_3O_4 powders as the starting materials. A mixture of NaCl, Na_2CO_3, and B_2O_3 was used as the flux. The typical dimensions of the obtained $Na_{0.9}CoO_2$ crystal were 3 x 3 x 0.1 mm^3, while those of $Na_{0.6}CoO_2$ were 6 x 6 x 0.1 mm^3. Investigation [140] on an as-grown $Na_{0.9}CoO_2$ crystal indicated a transition from a paramagnetic to an incommensurate spin-density wave state (IC-SDW) at 19 K and suggested that the oscillating moments of the IC-SDW are directed along the *c* axis. The $Na_{0.6}CoO_2$ crystal is paramagnetic down to 1.8 K, and the magnitude of the electronic specific-heat parameter indicates that Na_xCoO_2 is unlikely to be a typical strongly correlated electron system.

The growth of large β-Na_xCO_2 single crystals still remains a big challenge for the researcher, even using the FZ method, and only poor quality ingots, including mixtures of Na-poor phase, β-Na_xCO_2, and Co_3O_4 can be obtained [142]. High quality large single crystals of α-Na_xCO_2 can be grown by the FZ method [143]. For the α-Na_xCoO_2 single crystal with $x \approx 1$, crystallographic, magnetic, and NMR measurements indicated that the stoichiometric Na_1CoO_2 was a non-magnetic insulator, as expected for homogeneous planes of Co^{3+} ions with $S = 0$. Because of a slight average Na deficiency, phase separation led to a segregation of Na vacancies into the well-defined, magnetic, $Na_{0.8}CoO_2$ phase [12]. With $x \leq 0.97$, no detectable phase segregation was found [137, 143]. The cobalt spin susceptibility corresponding to Na_1CoO_2 phase was measured

using ^{23}Na NMR. It was found to be almost zero, in agreement with the low-spin 3+ charge state of all the cobalt atoms. This single state of Co ions in CoO_2 planes was confirmed by ^{59}Co NMR, giving evidence of a single non-magnetic Co^{3+} state in Na_1CoO_2 [11]. The phonon properties of the insulating phase of Na_1CoO_2 were systematically studied by theoretical calculations [144] For the Ni doped $Na_{0.9}CoO_2$, it was found that thermoelectric efficiency is enhanced upon nickel substitution in the sodium cobaltate [145].

Single phase thin films of Na_xCoO_2 have been grown by Krochenberger et al. [146], using pulsed laser deposition. The $Na_{0.58}CoO_2$ film grown on $SrTiO_3$ (100) substrate maintained its metallic behaviour down to 4.2 K. Later, Na_xCoO_2 (x = 0.51, 0.54, and 0.59) thin films with *c*-axis texture down to the substrates were grown. The substrates were $SrTiO_3$ (100) with a 5° vicinal cut towards [010]. An unusual large resistivity anisotropy ratio ρ_c/ρ_a of 680 has been found in x = 0.54 films, thus making it possible to develop a strategy for the fabrication of Na_xCoO_2 based thermoelectric thin film devices.

2.6. $Na_xCoO_2 \cdot yH_2O$ superconductor

2.6.1. Crystal structure

Motivated by the discovery of superconductivity in two-dimensional CoO_2 layers [9], many efforts have been made to investigate the structural details of the water intercalated superconductor $Na_xCoO_2 \cdot yH_2O$, for an understanding of the crystal structure is fundamental to interpreting the physical and chemical properties.

The crystal structure of superconducting $Na_xCoO_2 \cdot yH_2O$ differs from the parent material's crystal structure, and the structural details differ from the model for structure refinement. Even different data (XRD data or neutron data) for refinement may result in differences in the structural details. In general, superconducting $Na_xCoO_2 \cdot yH_2O$ derived from γ-Na_xCoO_2 and β-Na_xCoO_2 has a hexagonal $P6_3/mmc$ space group structure (No. 194), while that from α-Na_xCoO_2 has a trigonal R-3m space group structure (No. 166). All superconducting phases have two layers of H_2O/D_2O between the CoO_2 layers. The crystallographic symmetry does not change during the Na de-intercalation and H_2O intercalation processes. The small differences in the unit cell parameters shown in Table 2.1 may come from errors in the Na and H_2O content determination.

Table 2.1. Structure details and unit cell parameters of $Na_xCoO_2 \cdot yH_2O$ at room temperature.

Parent phase	β [134]	γ [9]	γ [148]	γ [149]	α [150]
Space group	P63/mmc	P63/mmc	P63/mmc	P63/mmc	R-3m
Data source	Neutron	XRD	neutron	XRD	XRD
Co site	*2a*	*2a*	*2a*	*2a*	*3b*
O site	*4f*	*4f*	*4f*	*4f*	*6c*
M1 site	*6h(Na)*	*2d(Na)*	*2b(Na)*	*4e(Na/H_20)*	*6c(Na/H_20)*
M2 site	*2b(Na)*	*2b(Na)*	*2c(Na)*	*2d(Na)*	
W1 site	*24l(D_2O)*	*12k(H_2O)*	*12k(D_2O)*	*12k(H_2O)*	*18h(H_2O)*
W2 site	*24l(D_2O)*	*12k(H_2O)*	*12k(D_2O)*	*12k(H_2O)*	*18h(H_2O)*
a(Å)	*2.81693(5)*	*2.8230(2)*	*2.8232(1)*	*2.81693(5)*	*2.8231(9)*
b(Å)	*19.6449(6)*	*19.6207(14)*	*19.530(1)*	*19.6449(6)*	*29.506(7)*

Takada et al. systematically studied the oxidation state of cobalt in the $Na_xCoO_2 \cdot yH_2O$ superconductors [15, 149-151], and it was found that the oxidation number of cobalt is about 3.46, which is significantly lower than the value (3.64) deduced from the Na to Co stoichiometry ratio, x. This may be explained by the presence of an oxygen deficiency or excess protons. They also found that the Na content decreased during the water intercalation process, Raman spectroscopy indicated that the ingoing species

substituting for the Na1 ion is the H_3O^+ ion, therefore, the reaction corresponding to the water intercalation should be as follows:

$$Na_{0.406}CoO_2 + (0.140 + n)\ H_2O \rightarrow$$

$$Na_{0.337}(H_3O)_{0.070}CoO_2 \cdot nH_2O + 10.070\ Na^+ + 10.070\ OH^-$$

Na_xCoO_2 also experienced reductive insertion of H_3O^+ ions according to the following reaction:

$$Na_{0.337}(H_3O)_{0.070}CoO_2 \cdot nH_2O + 0.246H_2O \rightarrow$$

$$Na_{0.337}(H_3O)_{0.234}CoO_2 \cdot nH_2O + 0.041\ O_2$$

Although it is not clear whether the reactions occurred sequentially or simultaneously, they modified the refinement structure model by the occupation of the M sites not only by Na^+ ions, but also by oxonium (H_3O^+) ions.

The two typical superconductor structures are given in Fig. 2.19. The figure in the middle shows the D_2O ice structure [129]. For comparison, the small figure between these two structures shows the ice molecule superimposed on the water block in the structure of the superconducting phase, demonstrating that the dimensions of the water block are close to those found in free ice. The crystal structure of the α-Na_xCoO_2

derived superconductor (R-3m) is shown in the right figure. The stacking sequence of O atoms are represented by A, B, and C, which denote their positions in cells.

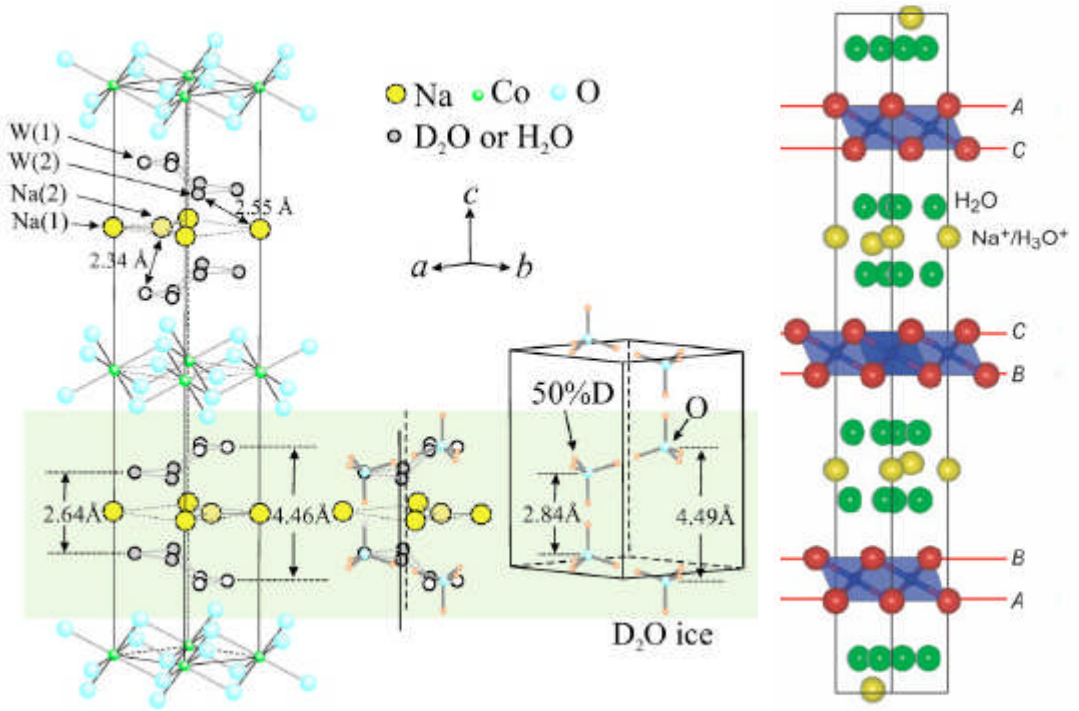

Fig. 2.19. Structural models [148] for the $Na_xCoO_2 \cdot 1.4(D_2/H_2O)$ superconductor: Left: $P6_3/mmc$ structure of the γ-Na_xCoO_2 derived superconductor. The figure in the middle shows the D_2O ice structure [153]. The figure on the right shows the crystal structure of the α-Na_xCoO_2 derived superconductor (R-3m) [150].

In contrast to the well known fact that the parent materials only show a significant expansion along the *c*-axis with increasing temperature, the unit cell parameters for the $P6_3/mmc$ superconductor show expansion in both the *a*- and *c*-axis parameters with increasing T [148, 149].

2.6.2. Superconducting phase diagram

The dependence of the superconducting T_c on the degree of electronic band filling is one of the most fundamental issues. It was found that there is an optimal T_c, which occurs in a narrow range of Na concentrations (and therefore electron concentrations) [152], for two-layer derived superconductors. As shown in Fig. 2.20, the single phase sample with sodium content of $x \approx 0.30$ displays the highest T_c at 4.3 K, while the overdoped or underdoped samples show lower T_c.

Milne et al. [14] revised the diagram, both in terms of Na content x and the Co valence state, as shown in Fig.2.21. They found that their results were consistent with a report [151] that intercalation of H_3O^+ ions into Na_xCoO_2 occurred, together with water, indicating that Na substoichiometry alone does not control the electronic doping of these materials. In their superconducting phase diagram, the optimal T_c is within a Co valence range of 3.24–3.35. The critical role of dimensionality in achieving superconductivity differs only in the interlayer spacing. However, the maximum T_c occurs near the average cobalt oxidation state of +3.5, when considering only Na control of the electronic doping [155, 163].

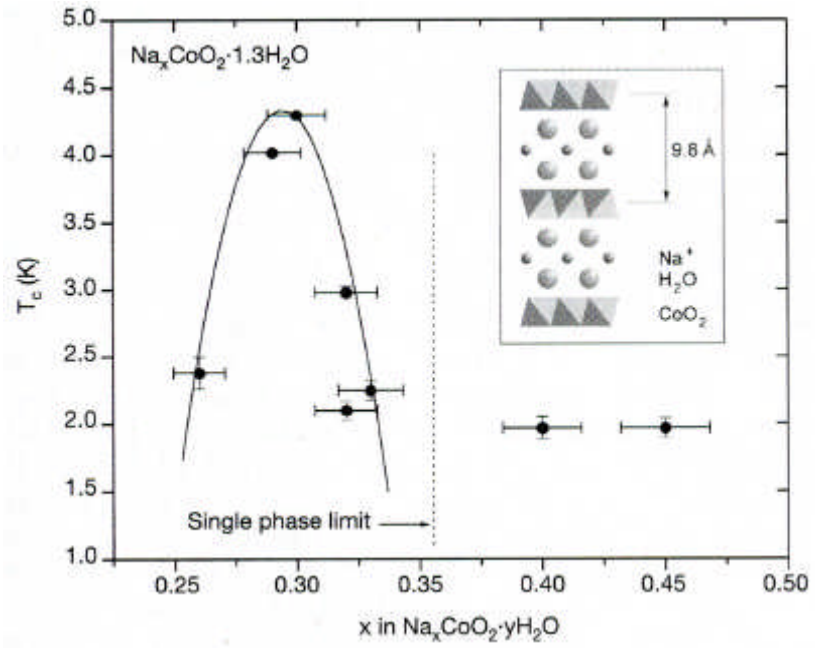

Fig. 2.20. The superconducting phase diagram for $Na_xCoO_2 \cdot 1.3H_2O$. Inset shows the schematic structure [152].

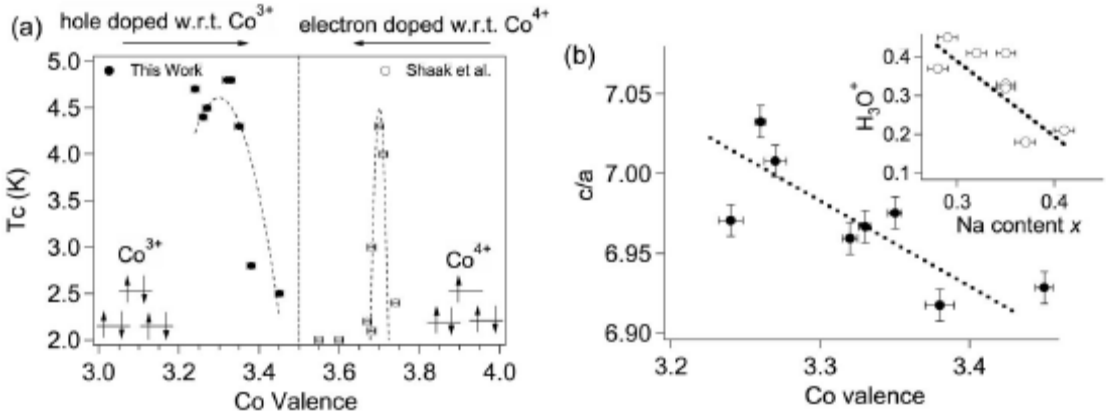

Fig. 2.21. (a) T_c vs. Co valence for superconducting cobaltate. The left curve is from titration data, while the right hand curve describes oxidation states based solely on Na content, from Schaak et al. [152]. (b) The variation of the c / a ratio as a function of the cobalt oxidation state. The inset show the variation of the H_3O^+ content of particular

samples as determined from measurements of the Na content and the Co oxidation state. Dashed lines are only guides to the eye [14].

Superconductors derived from α-phase are less stable in laboratory air at ambient temperature compared with those from γ-phase [154]. Both α- and β-$Na_xCoO_2 \cdot 1.3H_2O$ have lower superconducting T_c values at 4.2 and 4.3 K, respectively. D_2O intercalation in either α- or β-$Na_xCoO_2 \cdot 1.3H_2O$ also yields slightly lower T_c at about 0.2 K [131,132].

2.7.3. Sample preparation and physical properties

When the Na de-intercalated samples (x = 0.22–0.45) are immersed in deionized water or kept in 100% relative humidity atmosphere at room temperature, the superconducting phase begin to appear. Single phase powder samples normally need 3–7 days to achieve this [14, 151-155]. Large single crystals are very hard to obtain, because during the water intercalation process, the *c*-axis parameter doubles. This large increase in thickness along the *c*-axis is visible to the naked eye, and the morphology exhibits layered cracks perpendicular to the *c*-axis [142].

$Na_xCoO_2 \cdot 1.3H_2O$ superconductor is in a metastable state [156]. It exhibits a systematic variation of T_c as a function of time. Immediately after synthesis, this compound is not a

superconductor, even though it contains appropriate amounts of Na^+ and H_2O. The samples become superconducting with low T_c after about 90 h. T_c continually increases until it reaches a maximum value after about 260 h. Then T_c drops drastically, and the sample becomes non-superconducting approximately 100 h later [155]. It needs more than one day to show superconductivity in a 75% relative humidity atmosphere, and reaches the maximum T_c after about 7 days. T_c and the superconducting volume fraction are almost invariant between 7 days and 1 month's duration [157]. The research revealed that the two O-H covalent bonds in $Na_{0.3}CoO_2 \cdot 1.3H_2O$ superconductor differ in strength by about 18 % [158]. Superconducting epitaxial thin films of $Na_{0.3}CoO_2 \cdot 1.3D_2O$ grown by pulsed laser deposition technique have been reported. This provides an additional path for experimental research and future applications [159].

Nuclear quadrupole resonance (NQR) studies found that a low T_c sample has a larger residual density of states (DOS) in the superconducting state and a smaller increase of $1/T_1T$ ($1/T_1$ is the spin-lattice relaxation rate)just above T_c than a high T_c sample. This is seemingly associated with the two dimensionality of the CoO_2 plane, which is considered to be one of the most important factors for the occurrence of superconductivity [160].

T_c decreases with increasing pressure at an average rate of -0.49 ± 0.09 K/GPa up to 2.36 GPa. The decreasing T_c behavior in different pressure regions indicates that the electronic and magnetic states of Co are primarily responsible for the superconductivity

[161]. Measurements of the pressure dependence of T_c (up to 1.6 GPa) also support the assumption of two-dimensional superconductivity in these materials [162].

Magnetic research on $Na_{0.3}CoO_2 \cdot y1.3D_2O$ revealed that the superconducting phase has a larger susceptibility than $Na_{0.3}CoO_2$ and a higher degree of anisotropy for in- and out-of-plane [127]. The in-plane anisotropy of magnetic fluctuations in $Na_xCoO_2 \cdot y1.3D_2O$ were determined by Michioka et al., and they suggested that there was a change in the electronic state in the CoO_2 plane around 150 K [164].

A ^{59}Co Knigt shift measurement indicated that the electron pairing in the superconducting state is in the spin singlet form [165]. The electron momentum distribution in bulk $Na_xCoO_2 \cdot y1.3H_2O$ superconductor, measured by x-ray Compton scattering, gives evidence that the small elliptically shaped pockets predicted to be the electronically dominant Fermi surface sheet do exist [166].

Raman spectroscopy studies [123, 167, 168] have shown a broad electronic continuum, with a pronounced peak at around 100 cm^{-1} and a cut-off at approximately 600 cm^{-1}. Since the discovery of this superconductor, considerable theoretical work has been done on this material [169-177]. The superconductivity of $Na_xCoO_2 \cdot y1.3H_2O$ is often assumed to be unconventional, in that the Cooper pairs are not in a spin singlet state with *s*-wave symmetry. There are number of proposals [174-177] for the pairing symmetry, but still no solid evidence for any particular pairing state up to now. I. I.

Mazin and M. D. Johannes [177] based their conclusions on 3 criteria used to test each of the 25 symmetry-allowed pairing states. These are (1) two-dimensionality [137, 161, 162]; (2) absence of a finite superconducting gap [179]; and (3) absence of superconductivity-induced spontaneous magnetic moments below the critical temperature T_c [177]. Surprisingly, the possible pairings have *f*-wave symmetry, which contradicts many experimental results. The experimental reports are often contradictory, however. For instance, ^{59}Co nuclear quadrupole resonance measurements suggest non-*s*-wave superconductivity [178], but Mn doping effects studied by X-ray absorption spectroscopy indicates the coexistence of *s*-wave superconductivity in this material [179]. ^{59}Co NMR and NQR studies [180, 181] strongly suggest that the superconducting state of $Na_xCoO_2 \cdot y1.3H_2O$ is a *d*-wave state.

Chapter 3 Two-layer sodium cobaltates: crystal growth, structure, melting behavior, and electrical properties

3.1. Introduction

It is of particular interest that the Na_xCoO_2 compounds can be transformed into a superconductor with water molecules intercalated between the CoO_2 layers [9, 24, 152], as the observation of superconductivity in a transition metal oxide is a rare and exceptional phenomenon. Great efforts have been made to study the mechanism of superconductivity and the magnetic susceptibility, and to investigate basic properties, such as specific heat and electronic anisotropy [71, 162, 182-184], but even these are far from being understood. To obtain superconductivity in the compound, a controlled doping level or a particular ratio of Co^{3+}/Co^{4+} has to be achieved, and the intercalated water should also be considered as an important parameter. Although neutron and X-ray powder diffraction (XRD) were used to determine the crystal structure and the arrangement of water molecules in the sodium layer [131, 134, 148], it is rather difficult to fix the local coordination of the water molecules. Furthermore, the intercalated water in the crystal is extremely unstable; hence, the accurate characterization of the compound becomes another problem to be solved [70, 138, 156, 185]. Several models have been proposed [134, 148] to interpret the structure of the compound. There are several plausible scenarios of unconventional, non-phonon superconductivity in $Na_{0.3}CoO_2 \cdot yH_2O$, and it is expected that the water coordination also affects the electronic properties of the CoO_2 planes. Moreover, the hydrated compound is

extremely unstable under ambient conditions [156, 182] or at elevated temperatures, and it exhibits several phases with different y values on dehydration. Therefore, the availability of single crystals is important, since they allow an accurate characterization of the compound with respect to its physical, chemical, electrical, and thermal properties.

When growing Na_xCoO_2 single crystals, considerable difficulties appear on account of the high Na_2O vapor pressure, which increases exponentially from 10^{-5} to 10^{-3} Torr with heating to temperatures between 500 and 800°C, followed by a noticeable evaporation. Therefore ceramic powders were synthesized using additional Na_2CoO_3 to compensate for the Na loss during heating [138, 156], or a "rapid heat-up" technique was used [27] to avoid the formation of a non-stoichiometric compound. Solution growth using NaCl flux [60] was performed, but unfortunately, that led only to thin crystals (< 0.03 mm) or to non-stoichiometric and possibly contaminated samples. To obtain the superconducting phase, the crystal must be hydrated by chemical oxidation [9]. The compound can be partially decomposed during the oxidation process, leading to highly defective crystals containing Na-poor phases.

In this chapter, I present the floating zone (FZ) method for growing Na_xCoO_2 with varying Na content. Investigations of the resultant chemical and thermal properties, crystal structures, thermoelectricity, and superconductivity are discussed.

3.2. Experiment

Single crystals were grown in an optical floating zone furnace (Crystal System Incorporation, Japan) with 4 × 300 W halogen lamps installed as infrared radiation sources. Starting feed and seed materials were prepared from Na_2Co_3 and Co_3O_4 of 99.9 % purity, with the nominal composition of Na_xCoO_2, where x = 0.50, 0.60, 0.70, 0.75, 0.80, 0.85, and 0.90, respectively. Well-mixed powders were loaded into alumina crucibles, heated to 750°C, and kept at that temperature for one day. The heated powders were reground and calcined at 850°C for another day. They were then shaped into cylindrical bars about 6 mm in diameter and 100 mm long by pressing at an isostatic pressure of ~ 70 Mpa and then sintering at 850°C for 1 day in flowing oxygen to form the feed rods.

Each sintered feed rod was pre-melted with a mirror scanning velocity of 27 mm/h, while traveling the upper and lower shafts to densify the feed rod. After pre-melting, the ~ 20 mm long rod was cut and used as the first seed, and thereafter the grown crystal was used as the seed. The feed rod and the growing crystal were rotated at 15-30 rpm in opposite directions. In an attempt to reduce the volatilization of Na and obtain large and stoichiometric crystals, I applied traveling rates of 1-2 mm/h under pure oxygen flow of 200 ml/min throughout the growing procedure. The initial growth compositions together with the analyzed crystal data are given in Table 3.1.

To obtain superconductivity, the Na was partly extracted by placing crystals in a 6.6 mol Br_2/CH_3CN solution for 100 h and then washing them out with H_2O or D_2O solution [9]. Alternatively, the electrochemical technique was also applied, using an aqueous solution of NaOH as an electrolyte to partially extract the Na [89]. This technique needs a longer time for de-intercalation, and the resulting superconducting transitions are generally sharper.

Table 3.1. Possible co-existent phases in the Na_xCoO_2 single crystals and their crystallographic data.

Sample no.	Feed rod composition	Comments (phases, impurities)	Crystal formula	Lattice parameters *a* (Å)	Lattice parameters *b* (Å)
A	$Na_{0.50}CoO_2$	Na-poor phase, Co_3O_4	$Na_{0.55}CoO_2$	-	-
B	$Na_{0.60}CoO_2$	Na-poor-, β phase, Co_3O_4	$Na_{0.60}CoO_2$	2.819(3)	11.111(8)
C	$Na_{0.65}CoO_2$	ά-, β-phase, Co_3O_4	$Na_{0.65}CoO_2$	2.828(5)	10.921(2)
D	$Na_{0.70}CoO_2$	ά-, β-phase, Co_3O_4	$Na_{0.75}CoO_2$	2.842(5)	10.814(7)
E	$Na_{0.75}CoO_2$	ά-, γ-phase, Co_3O_4	$Na_{0.72}CoO_2$	2.843(6)	10.808(5)
F	$Na_{0.80}CoO_2$	α-,ά-phase, Co_3O_4	$Na_{0.87}CoO_2$	2.841(4)	10.839(5)
G	$Na_{0.82}CoO_2$	γ-phase, Co_3O_4	$Na_{0.73}CoO_2$	2.843(0)	10.817(0)
H	$Na_{0.90}CoO_2$	α-,ά-phase, Co_3O_4	$Na_{0.82}CoO_2$	2.841(9)	10.820(7)

ά-phase: $x = 0.75$; β-phase: $0.60 \geq x \geq 0.55$; γ-phase: $0.74 \geq x \geq 0.55$; $(0.75 < x < 0.90)$: α + ά phases ; $(0.60 < x < 0.75)$: ά-phase + $Na_{0.6}CoO_2$ [186].

Thermogravimetric and differential thermal analysis (TG-DTA) was performed to study the melting behavior, as well as the time and temperature dependence of the water loss

in the compound. Single crystal XRD measurements were carried out with an x-ray diffractometer (Philips PW 1710) using Cu *K*a radiation, a scanning rate of 0.02° per second, and $\theta - 2\theta$ scans from 5° to 90°. The lattice parameters obtained from XRD data were refined using the commercial program PowderCell. The chemical composition was determined by energy dispersive x-ray spectroscopy (EDX), including microanalysis. The as-grown crystals were cleaved parallel to the *a*-axis, and the composition of Na and Co was determined across the cleaved section.

3.3. Results and discussion

3.3.1. Melting behavior of two-layer Na_xCoO_2

The melting behavior of a $Na_{0.7}CoO_2$ crystal was investigated by DTA-TG measurements and with a high temperature optical microscope. A small single crystal was placed in a Pt crucible and then heated in the DTA-TG apparatus (NETZSCH STA-449C) at 7.5 °C/min up to 1200–1250°C in flowing oxygen. Two peaks with onset T_1 = 1035°C and T_2 = 1092°C on the DTA curve correlate very well with the weight loss observed by TG, as shown in Figs. 3.1(a) and 3.2(b), respectively. No weight changes were observed below 980°C.

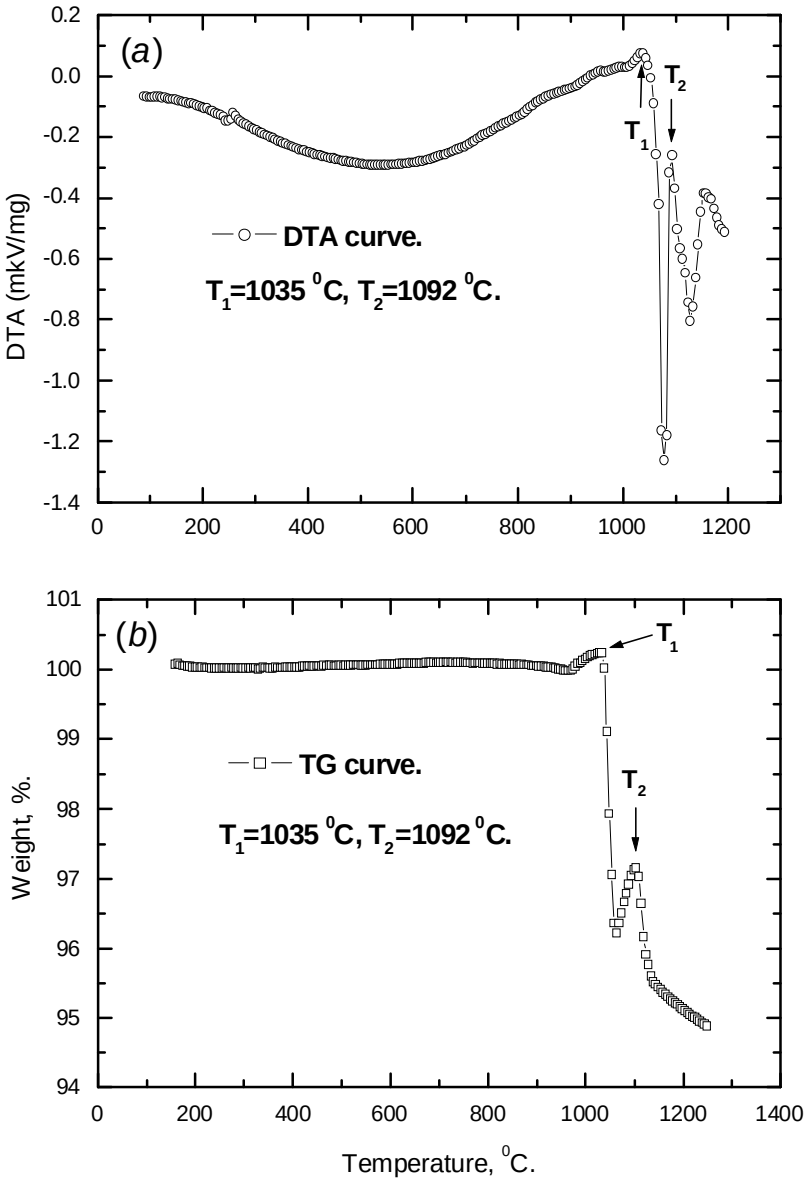

Fig. 3.1. DTA-TG analysis by melting single crystalline $Na_{0.7}CoO_2$, with heating at 7.5 °C/min up to 1200–1250°C in flowing oxygen. T_1 = 1035°C, T_2 = 1092°C. (a) The melting behavior of the compound, and (b) the temperature dependence of the weight loss.

A high temperature optical microscope study of the crystal reveals that the liquid phase appears at T_1 = 1035°C, but the solid phase (crystal) still remains up to T_2 = 1092 °C, so that there is a coexistence of solid and liquid phases. The investigations indicate that

thermal decomposition of $Na_{0.7}CoO_2$ is accompanied by a weight loss down to 96.2 wt% and the compound decomposes into a sodium-rich liquid and a cobalt-rich solid phase [186, 187], assuming that the chemical reaction of the melt proceeds as follows:

$$Na_xCoO_2 -> CoO + \text{liquid (Na-rich)} + xO_2 - (T>1100°C) - > [Na_xCoO_{1.65}] *$$

* = homogeneous melt.

The dissolution of CoO occurs in the Na-rich melt by taking up oxygen from the environment. Thus, it results in an increase of weight, because the oxidation state of cobalt is significantly higher in the melt, i.e., $Co^{+2.7}$, according to the chemical reaction equation shown above. A sharp weight loss down to 95.5 wt% occurs at T_2 = 1092°C, and the melt starts to become homogeneous and stable. A nearly constant weight of 95.5–94.9 wt% is obtained in the temperature range of 1120–1200°C, where the melt becomes homogeneous. A monotonic weight loss in the melt may occur under constant heating. Evidently, the melting behavior described so far indicates that the compound melts incongruently.

3.3.2. Crystal growth, morphology, and composition

When sintering Na_xCoO_2 at high temperatures, the decomposition of Na_2O can cause weight loss and lead to an inhomogeneous compound. During growth, a white powder consisting of Na_2O is observed to volatilize and be deposited on the inner wall of the

quartz tube. From weighing, a total weight loss of ~6 wt% is estimated. This value is in agreement with the data shown in Fig. 3.1(b), neglecting the tiny loss of oxygen caused by the change in the cobalt valence state. The main loss of Na_2O is found during the pre-melting procedure and is estimated to be ~5 wt%. This is probably caused by incompletely reacted Na_2O when the mixtures are calcined and sintered prior to pre-melting. An additional ~1 wt% loss is estimated after the crystal growth.

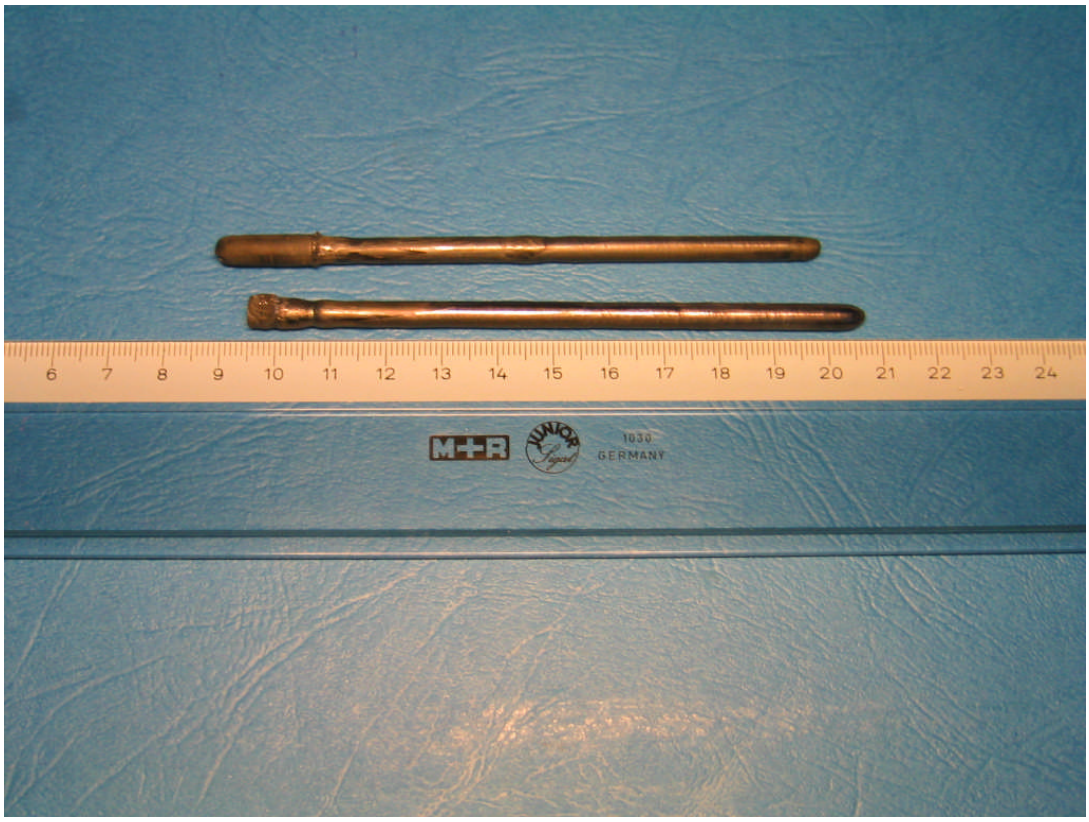

Fig. 3.2. Typical $Na_{0.82}CoO_2$ (upper) and $Na_{0.75}CoO_2$ (lower) single crystal ingots obtained by the optical floating zone technique.

Large single crystals of Na_xCoO_2 were obtained with variable Na content, using a growth rate of 2 mm/h in flowing oxygen atmosphere. During growth, it has been

observed that the molten zone was stable and that it was easy to form the ά-phase of Na_xCoO_2 with sodium content x = 0.75, while it was hard to grow the *β*-phase with x = 0.55 and 0.60, and *γ*-phase with x = 0.65 and 0.70. EDX (energy dispersive X-ray analysis) results indicated that as-grown Na_xCoO_2 with the lower sodium content of x = 0.65 consists of multi-phases such as Na_2O, Co_3O_4, and Na-poor phases. Co-existent phases and inhomogeneous composition are always observed in the compounds with initial x = 0.70, 0.80, and 0.82, as listed in Table 3.1.

Fig. 3.2 shows typical as-grown crystal ingots of $Na_{0.82}CoO_2$ and $Na_{0.75}CoO_2$. The XRD *00l* diffraction patterns indicate nearly pure phases of both *γ*- and *á*-Na_xCoO_2 crystals, as shown in Fig. 3.3.

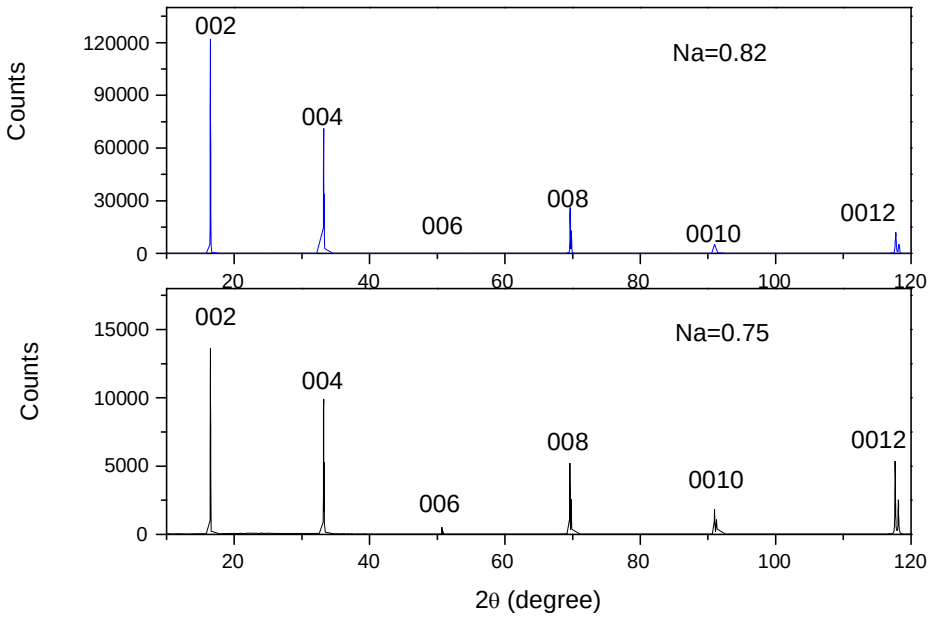

Fig. 3.3. 001 XRD patterns showing pure γ-phase $Na_{0.82}CoO_2$ (upper panel) and γ-phase $Na_{0.75}CoO_2$ (lower panel). The split peaks are $CuKa_1$ and $CuKa_2$ for the higher and lower intensity, respectively.

Both crystals were identified to have a hexagonal structure with two sheets (prismatic, P2) of edge-shared CoO_6 octahedra in a unit cell for the *γ*- and *ά*-phase, respectively. The lattice parameters and cell volumes were determined by least squares refinement of the XRD data and correspond to the space group $P6_3/mmc$ (P2), respectively. The crystallographic data are given in Table 3.1.

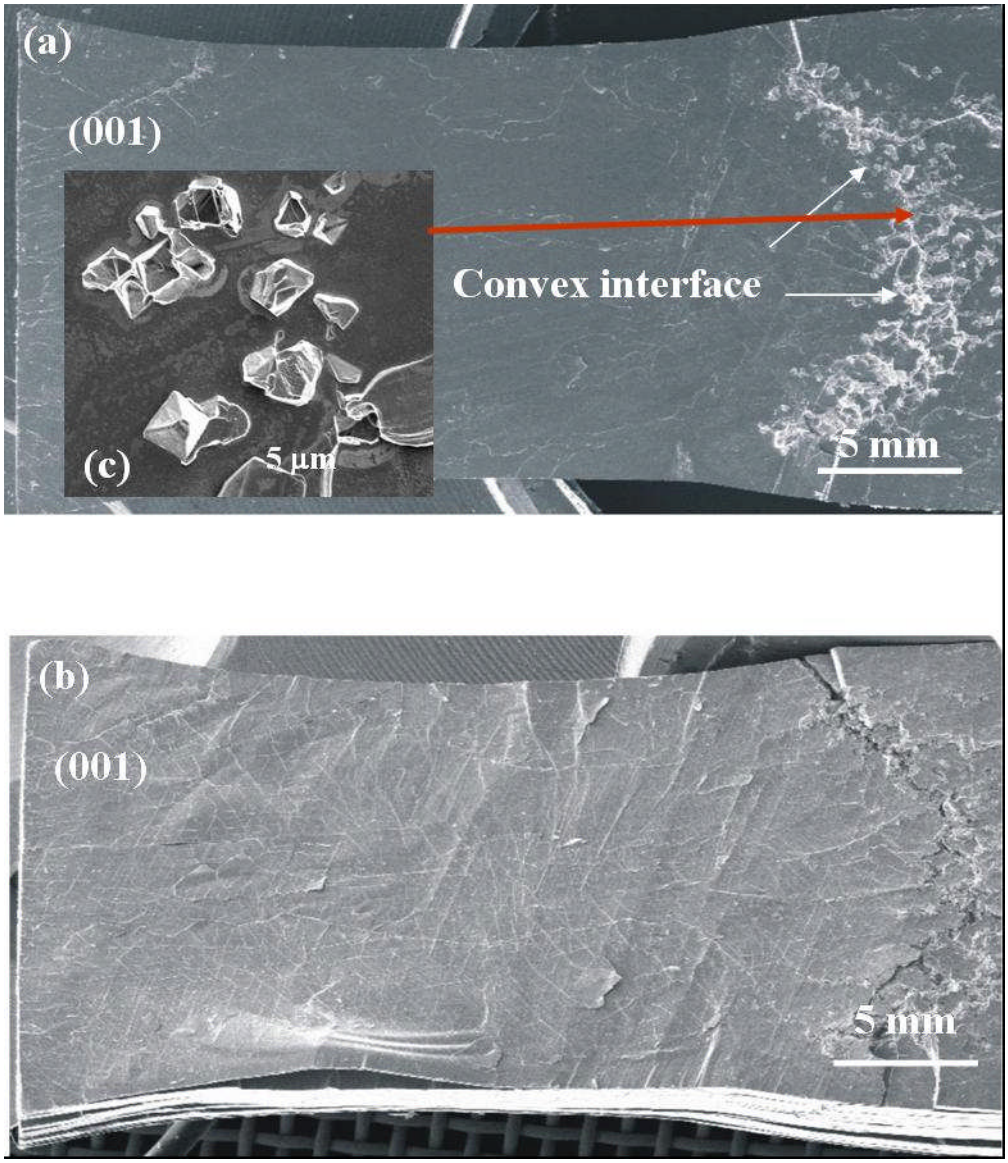

Fig. 3.4. Two halves of an as-grown crystal ingot with a cleaved 001 surface: (a) As-cleaved half ingot of $Na_{0.7}CoO_2$, showing CoO_2 inclusions gathered at the growth boundary (b) The other half of the ingot transformed to $Na_{0.3}CoO_2 \cdot yH_2O$, showing the removal of the CoO_2 inclusions after de-intercalation followed by hydration. (c) The enlarged CoO_2 inclusions.

Fig. 3.4(a) displays one-half of an ingot showing crystal platelets with the *00l* face of several cm^2 areas cleaved from the ingot with a sharp scalpel. Fig. 3.4(b) shows the other half after water intercalation. Crystal grains were found to grow preferentially along the *a* crystallographic axis, parallel to the rod axis.

A convex growth interface is observed to be the boundary between the regions of smaller and larger diameter of the crystal ingot, as shown in Fig. 3.4. The smaller diameter part was formed when the molten zone was at lower temperatures, and the larger diameter one was formed at higher temperatures. Therefore, the unequal diameter for an ingot indicates that temperature fluctuations occurred at the molten zone during growth. According to the temperature-composition relationship, a fluctuation in the heating temperature may result in a composition change of the molten zone, leading to an inhomogeneous compound. Fig. 3.4(a) shows that many tiny crystal grains of CoO_2 gather at the boundary of the growth front. These grains can be removed by the de-intercalation treatment, as shown in Fig. 3.4(b) and the inset of Fig. 3.4(a), respectively. It is important to maintain a stable molten zone by applying a constant heating temperature to grow a high quality single crystal.

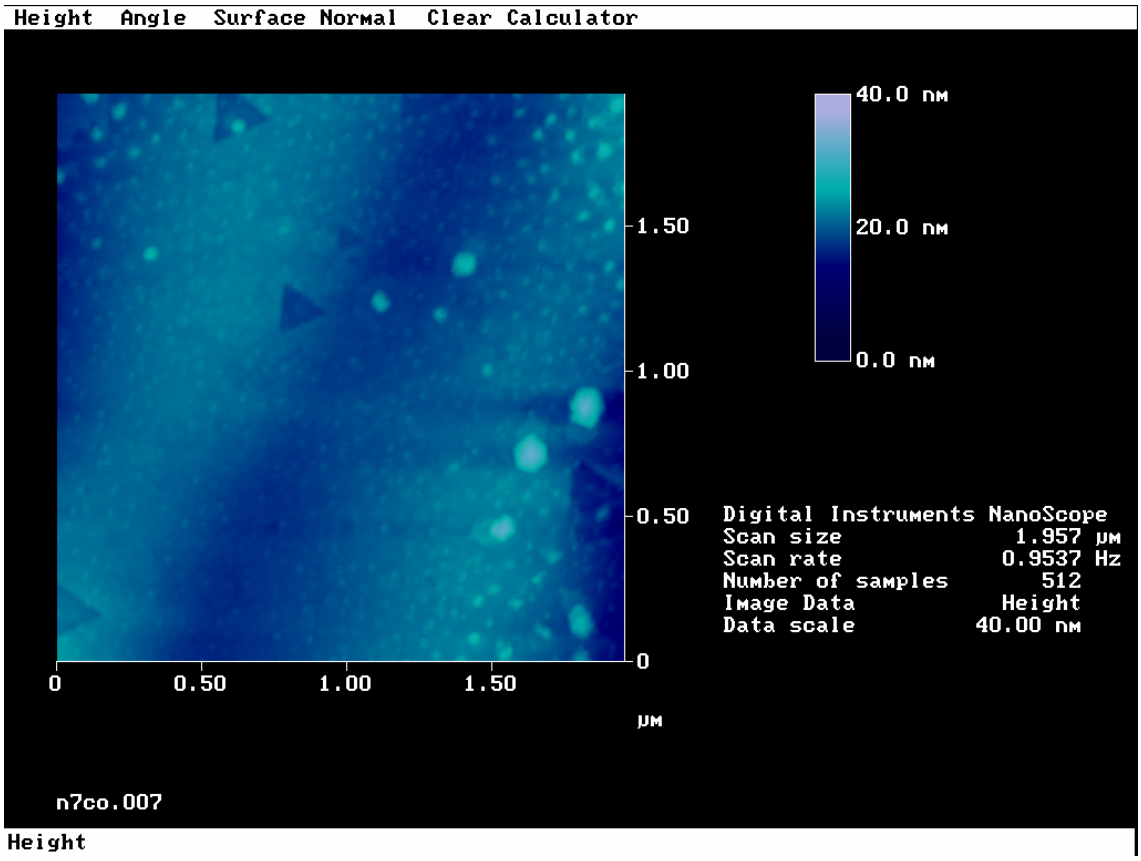

Fig. 3.5. Typical terraced pits on the (110) face of as-grown $Na_{0.7}CoO_2$ single crystal.

In order to understand the detailed structures of these materials, atomic force microscopy (AFM) and transmission electron microscopy (TEM) were used. Figure 3.5 shows an AFM image taken from the freshly cleaved (110) face of $Na_{0.7}CoO_2$ single crystal. It can be seen that there are some triangular pits at specific sites, which may be attributed to the defects in the as-grown crystal.

High-resolution TEM (HRTEM) images taken from the ingot in Figure 3.4(a) are shown in Figure 3.6. The identical *d*-spacing of 1.09 nm is consistent with the *d*-value of (001), indicating single-crystal characteristics, with a cleavage surface along [001].

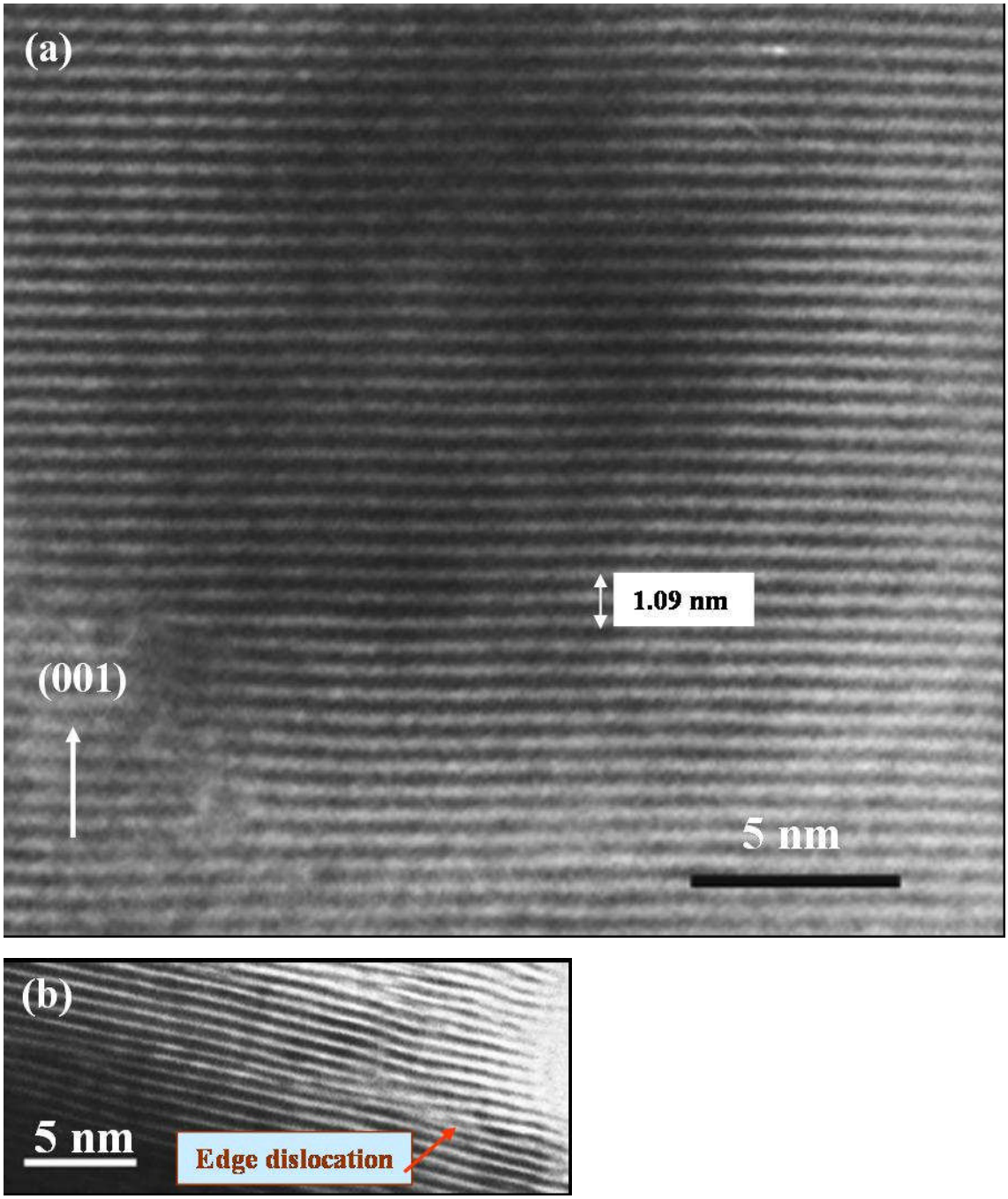

Fig. 3.6. (a) HRTEM image showing the layered structure of a $Na_{0.7}CoO_2$ single crystal; (b) HRTEM image of an edge dislocation in the same crystal.

The composition distribution along the ingot of $Na_{0.75}CoO_2$ was determined using EDX. The crystal was scanned through a 3 mm segment along the growth direction in order to

determine the Na/Co compositions. The average value of the Na composition was calculated from four measured points in the central and edge regions of the crystal. It was found that the Na content varied with the temperature fluctuations during the growth. At the beginning of the growth the temperature fluctuations were high and caused a high variation of the composition, $\Delta x \approx 0.11$, determined within 2 cm from the seeding part of the ingot. Further away from the seeding part, the variation of Na content is smaller, $\Delta x \approx 0.06$, when the molten zone is maintained in a stable state by a constant temperature. A volatilized white Na_2O powder accumulates on the inner wall of the quartz tube after the growth is completed. The loss of Na may result in a reduction of its concentration in the as-grown crystal. White Na_2O powders also form on the surfaces of crystals if the samples are stored under ambient conditions. Therefore, the freshly grown crystals must be stored in an evacuated container or a desiccator to avoid decomposition.

3.3.3. Sodium extraction and water hydration

By chemically extracting additional sodium from the structure of $Na_{0.75}CoO_2$ and following this by hydration, I obtained the superconducting phase of the compound with the composition $Na_xCoO_2 \cdot yH_2O$ ($0.26 \leq x \leq 0.42$, $y = 1.3$). Crystals of Na_xCoO_2 with $x = 0.3$ resulted from a treatment in 6.6 mol Br_2/CH_3CN, and the details of the oxidation process are described in Ref. [70]. Na extraction from the crystals was also carried out

by the electrochemical method. The composition $Na_{0.3}CoO_2$ could be achieved in an aqueous solution of NaOH using a constant current of 0.5 mA and a voltage of 1.0 V for over 10 days. Compared to the published 1–5 days extraction time for $Na_{0.7}CoO_2$ powders [9, 152], a longer time is needed for single crystal samples to complete the extraction, also depending on the dimensions of the sample. This can be attributed to the fact that the Na extraction process takes place along the *100* direction, and the chemical bonding period of Na–O–Na in the NaO layer for single crystal is an order of magnitude greater and more perfect than that of nanoscale powders, which are randomly distributed.

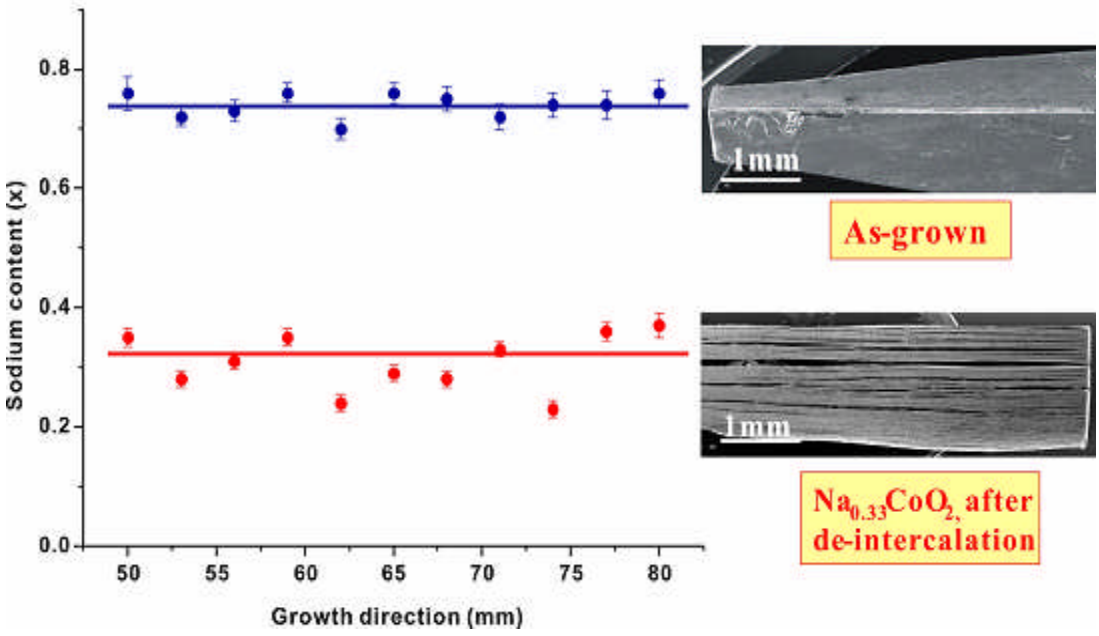

Fig. 3.7. Sodium distributions along the growth direction for the as-grown $Na_{0.75}CoO_2$ single crystal before and after Na-extraction.

Before and after the extraction treatment, the sodium composition distribution across the crystals was determined by EDX. Fig. 3.7 shows a plot of the sodium distribution in the central area along the crystal growth direction. This analysis indicates that the change in the sodium content of the resulting crystals after de-intercalation was $\Delta x \approx 0.3$. The sodium intercalant layer expanded with decreasing Na content, because the Na removal results in Co oxidation (where Co^{3+} ions are oxidized to the smaller Co^{4+} ions), and thus the CoO_2 layers are expected to shrink [156]. This suggests that a decreased bonding interaction between the layers with decreasing Na content may result in a readily cleaved plane.

The Na-extracted samples are then hydrated by immersing them in de-ionized water at room temperature to obtain the superconducting phase. After hydration a large increase in thickness is visible to the naked eye, and the morphology exhibits layered cracks perpendicular to the *c*-axis. The typical crystal morphologies are shown in Fig. 3.8. (a, c) and (b, d) show morphologies formed by Na-extraction and H_2O-intercalation, respectively.

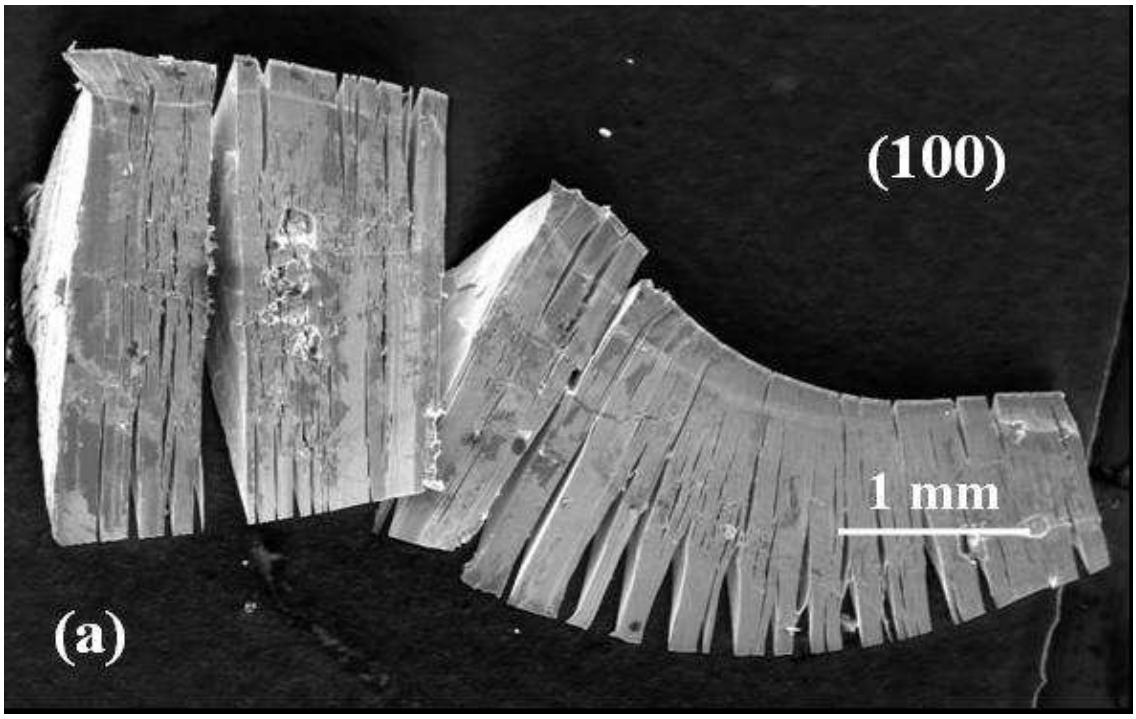
(100)
1 mm
(a)

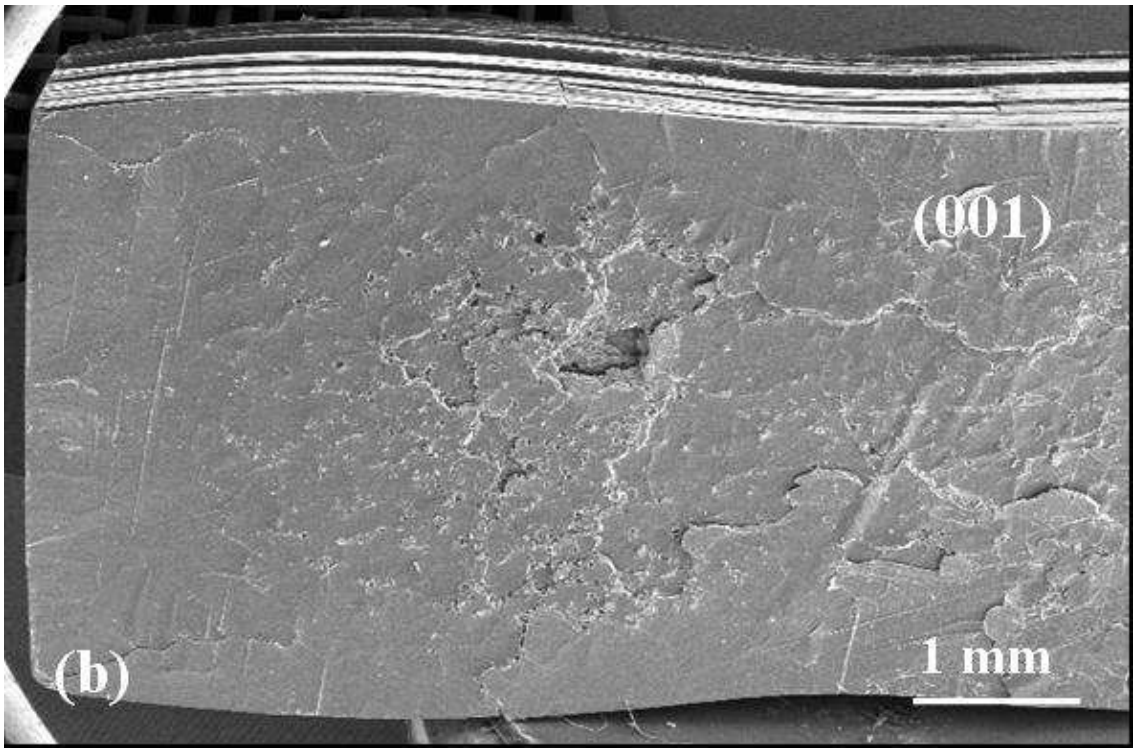
(001)
1 mm
(b)

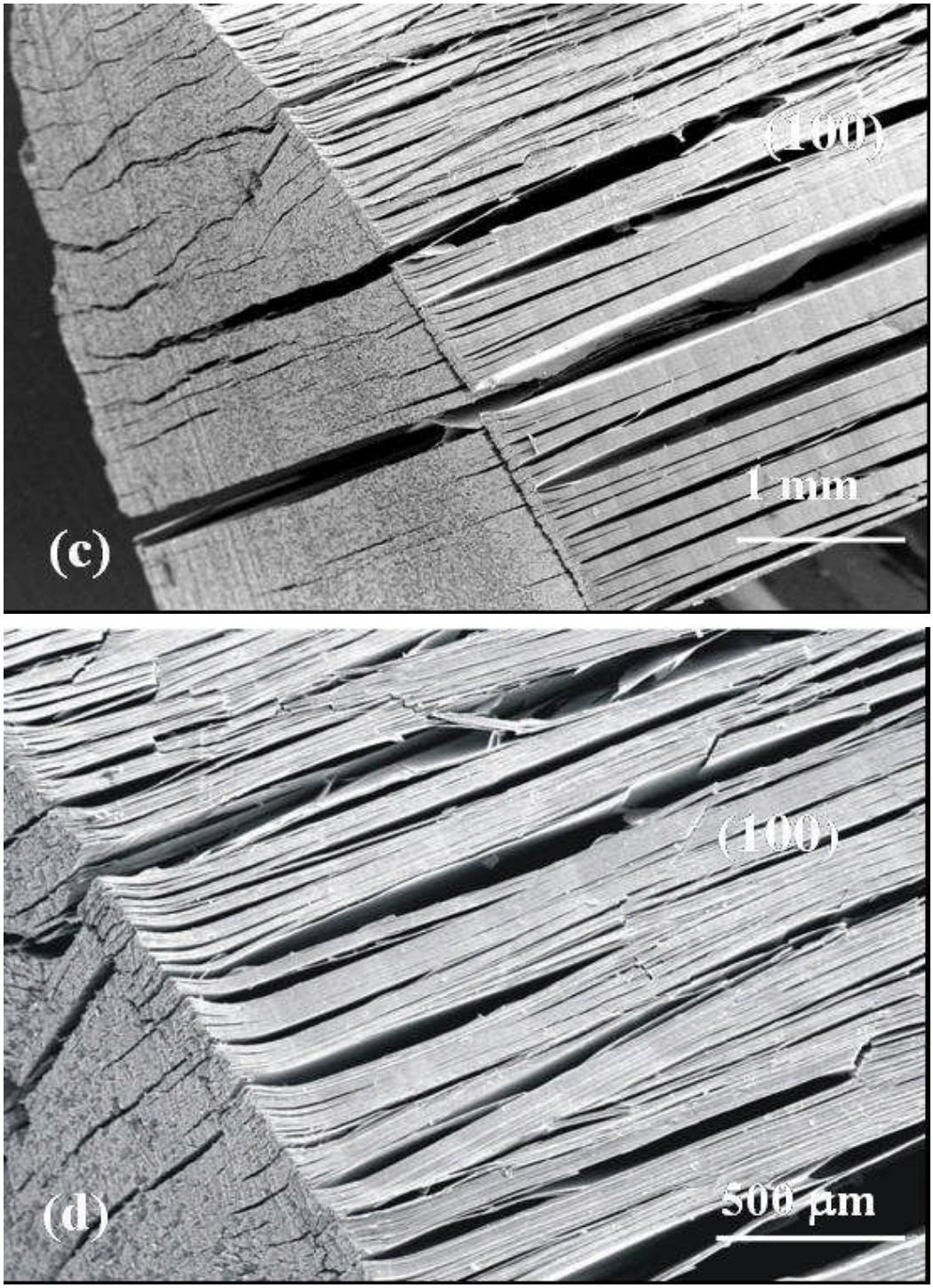

Fig. 3.8. Typical crystal morphologies showing the layered structure of Na_xCoO_2 single crystals. Intercalant layers appeared after de-intercalation using (a) Br_2/CH_3CN solution (2 days) and (b) H_2O to wash out Na ions. (c) "Booklet"-like crystals obtained by the electrochemistry method using NaOH solution (7 days); (d) the same electrochemistry method crystals after a further washing with D_2O.

3.3.4. Hydration dynamics

The high sensitivity of the X-ray diffraction procedure allows us to observe the phase formation as well as its dissolution during the hydration and dehydration of $Na_{0.3}CoO_2$. Fig. 3.9 shows the 002 reflections obtained from a crystal with hydration time from 0 min up to 10 days. It is not surprising to observe the coexistence of the two phases with y = 0 and 0.6 (Fig. 3.9, 0 min) prior to hydration, since the non-hydrated sample of $Na_{0.3}CoO_2$ was stored in air and readily absorbs water to form a partial hydrate under ambient conditions (Fig. 3.10(c)). After heating the sample at 150^{o}C for 15 minutes, the y = 0.6 phase could be removed. As hydration proceeded, the y = 0.6 phase reformed and vanished after 10 days, when the fully hydrated phase of y = 1.3 was formed. Assuming that the initial diffusion paths of the water molecules ran along the Na-plane to fill the partially occupied sites, this process would not stop until water saturation occurred in these planes. According to the 002 reflection patterns, the expansion of the *c*-axis per intercalant layer is about 1.3 Å, averaged between the non-hydrated $Na_{0.3}CoO_2$ (11.2 Å) and the partially hydrated $Na_{0.3}CoO_2 \cdot 0.6H_2O$ (13.8 Å). This value is smaller than the diameter of an oxygen ion (~2.8 Å), suggesting that in this partial hydrate, the Na ions and the H_2O molecules are accommodated in the same plane.

As shown by the hydration process in Fig. 3.9, the y = 1.3 phase is formed predominantly and becomes the sole phase within 10 days, with nearly complete elimination of both the y = 0 and y = 0.6 phases. These results suggest that the sample is

fully hydrated with four water molecules, forming clusters of $Na(H_2O)_4$ in the structure. Thus, the optimal superconducting phase of $Na_{0.3}CoO_2 \cdot yH_2O$ (y = 1.3, n = 4) is achieved with $T_c \approx 4.9$ K [70]. No evidence of the formation of the phases with y = 0.3 (n = 1), 0.9 (n = 3), or 1.8 (n = 6) is observed during the 10-day hydration process. This clearly demonstrates that the initial intercalation process takes place with two water molecules, followed by a group of four to form two additional layers between the Na and the CoO_2. Increasing the hydration time further, beyond 15 days, may lead to an additional phase of y = 1.8 [40].

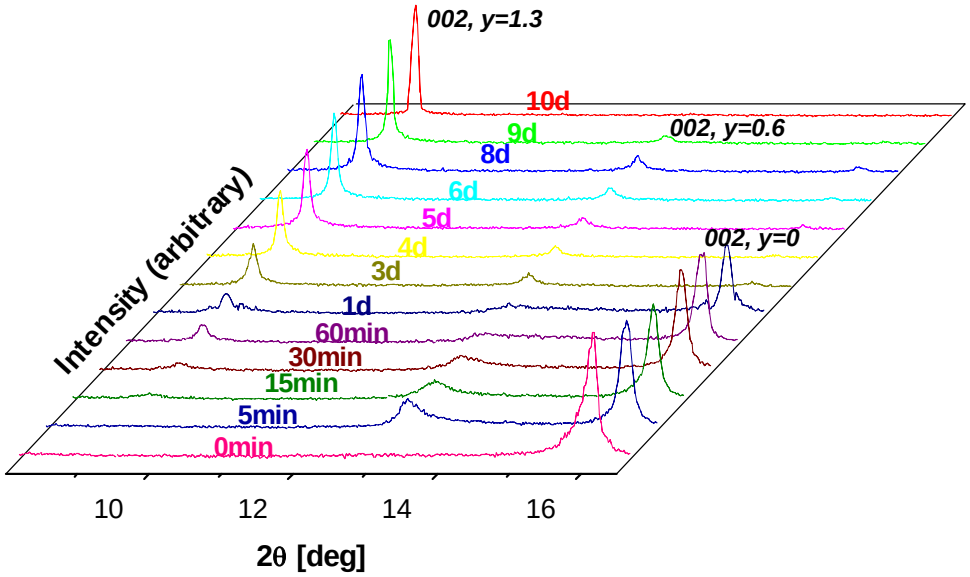

Fig. 3.9. The 002 reflections show the hydration dynamics of the water molecule intercalation in $Na_{0.3}CoO_2$. The process indicates that two water molecules (y = 0.6, n = 2) are inserted into a formula unit initially and that this is followed by a group of four to form a fully hydrated phase (y = 1.3, n = 4) [40].

With increasing intercalation time, the y = 1.3 phase starts to form after a hydration time of 15 min. The diffraction data in Fig. 3.11 show that the 002 intensity of this phase tends to be stronger, indicating that more water molecules are accommodated in the lattice, resulting in an increase in the phase volume, while the opposite is true for the

non-hydrated y = 0 phase. The fully hydrated sample will lose water after being moved to ambient conditions, and mixture phases are formed with y = 0, 0.3 (n = 1), 0.6 (n = 2), or 1.3 (n = 4) (see Fig. 3.10(a) and (b)).

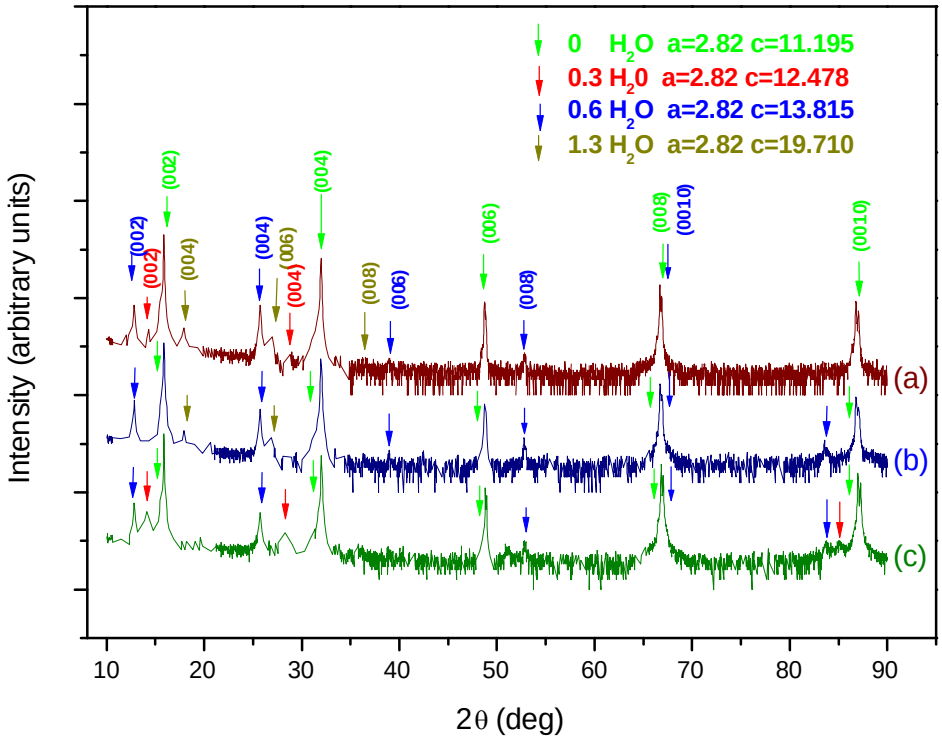

Fig. 3.10. XRD patterns and lattice constants for $Na_{0.3}CoO_2 \cdot yH_2O$ under changing ambient conditions: (a) From humid to dry air for 2 days after full hydration. (b) From humid to dry air for 5 days after full hydration. (c) From dry to humid air for 5 days before hydration.

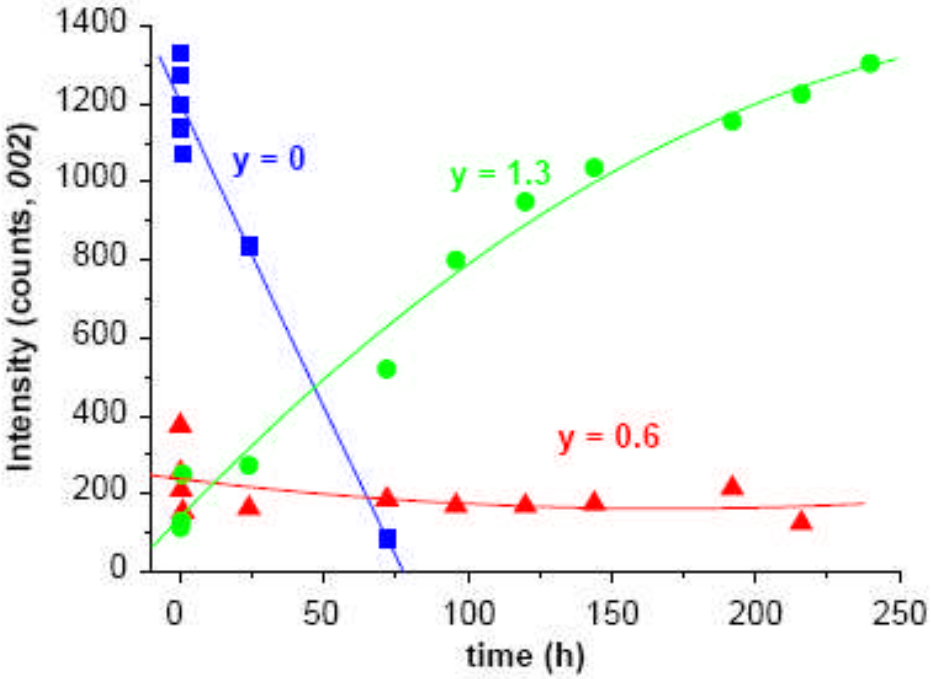

Fig. 3.11. Time dependence of the 002 counts for y = 0, 0.6 and 1.3, respectively, indicating that the volume of the fully hydrated y = 1.3 phase increases while the y = 0 phase rapidly decreases. The y = 0.6 phase is rather stable.

3.3.5. De-intercalation process

The specimens of $Na_{0.3}CoO_2$ were first treated by an over-hydration time of 15 days, and the dehydration process was then carried out by heating the sample. The process was monitored by thermogravimetry. The results in Fig. 3.12 are given as a thermogravimetric curve obtained from an over-hydrated sample heated at 0.3 ^{o}C /min in a flowing oxygen environment. There are five plateaus observed as a change of weight during heating of the sample.

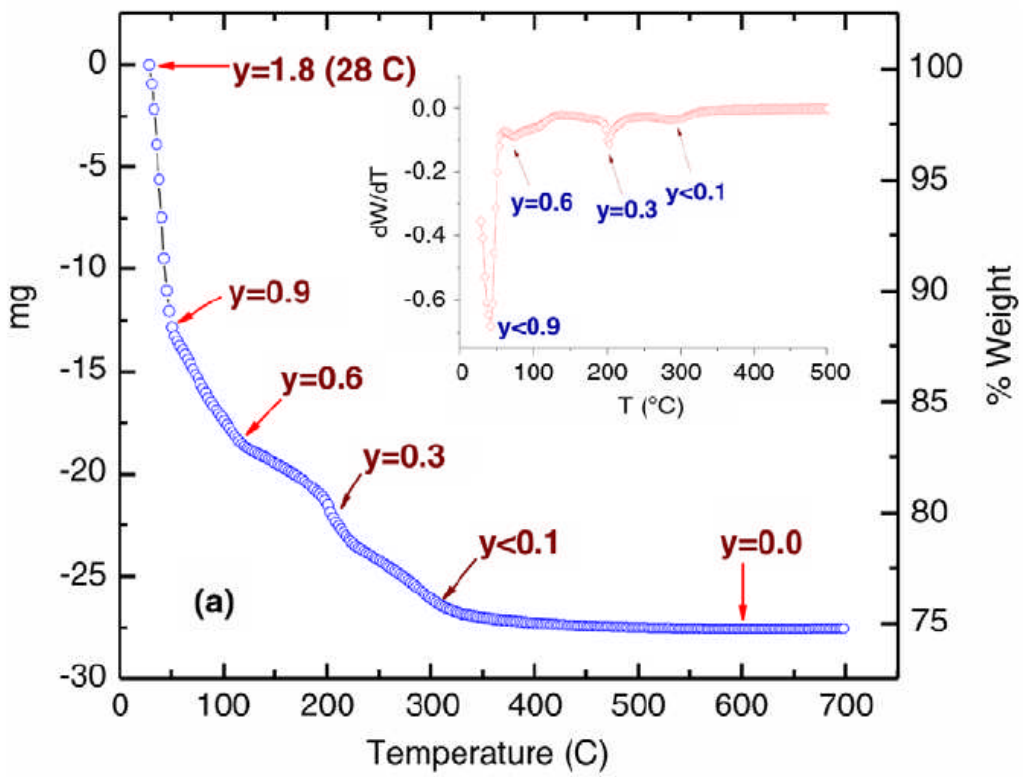

Fig. 3.12. Thermogravimetric analysis of an over-hydrated (15 days) $Na_{0.3}CoO_2 \cdot 1.8H_2O$ (112.9650 mg) sample, showing the temperature dependence of the weight loss for the compound heated at 0.3 ^oC/min in flowing oxygen. Inset: the derivative curve.

Analysis of the XRD data suggests that each plateau corresponds to a particular dehydrated phase with a different number of crystal water units (as shown in Fig. 3.13, [40]), i.e., y values. The y values are calculated from the weight loss. Note that there are turning points between every two plateaus at elevated heating temperatures, which are similar to a phase transition. These can be seen clearly in the derivative of the weight loss curve in the inset of Fig. 3.12. The first sharp loss of weight is estimated to be about 13 mg, observed between 28 and 50^{o}C. This value resulted from the initial water

content of y ≈ 1.8, indicating that the sample was over-hydrated with the composition $Na_{0.3}CoO_2 \cdot 1.8H_2O$.

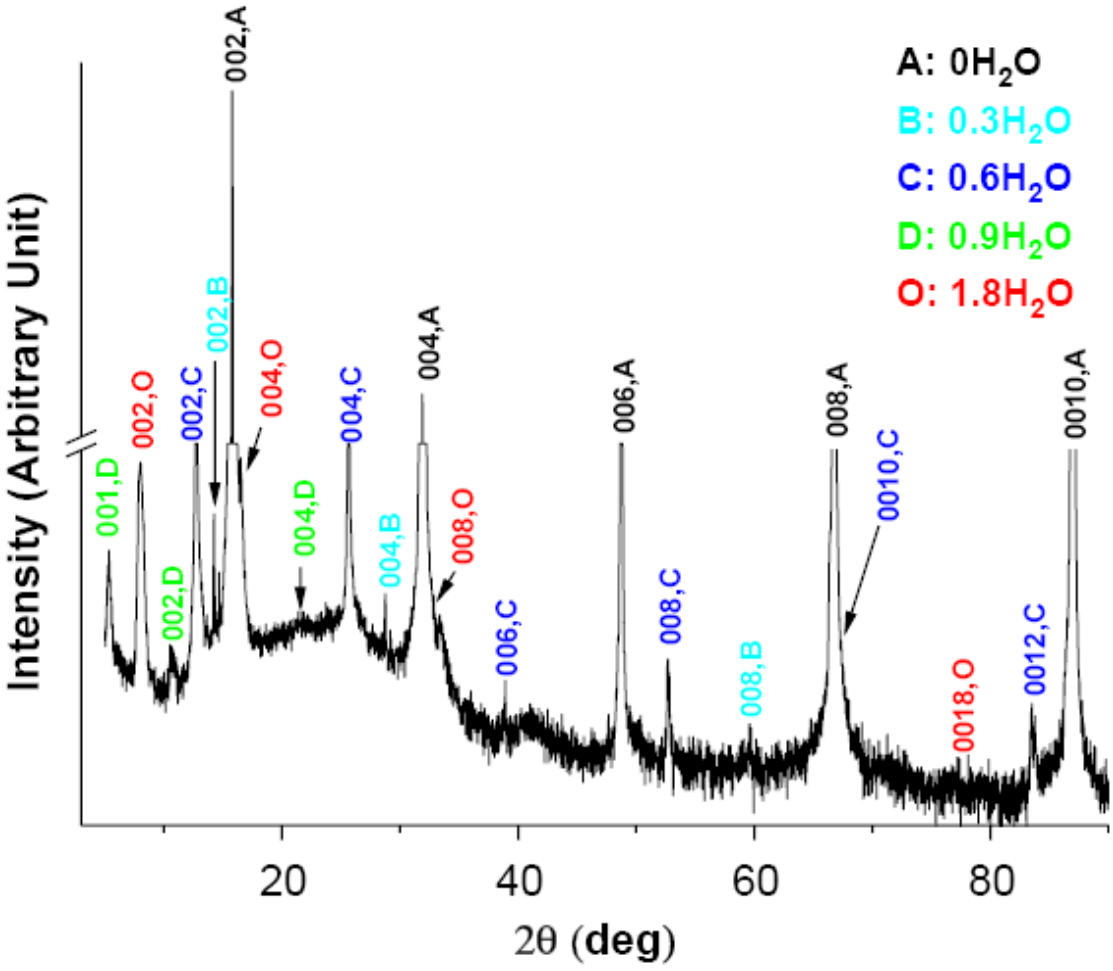

Fig. 3.13. The 0 0 l X-ray diffraction pattern for $Na_{0.3}CoO_2 \cdot yH_2O$ showing the mixture of hydrates with y = 0, 0.3, 0.6, 0.9, and 1.8, respectively [40].

For an over-hydrated sample, it is assumed that six water molecules are inserted below, in, and above each Na ion site to form a cluster of $Na(H_2O)_6$. The XRD data indicate that this results in the y = 1.8 phase with lattice constant c = 22.38 Å. The process described above reduces the water content from y = 1.8 (n = 6) to y = 0.9 (n = 3), corresponding to a loss of about three water molecules from each sodium site. It is

noticeable that the y = 1.3 phase is not observable from a turning point in Fig. 3.12. The indication of this rapid loss of water confirms that both the over-hydrated phase (y = 1.8, n = 6) and the optimum hydrated phase (y = 1.3, n = 4) are extremely unstable at around room temperature. The result was reproduced with another sample of partially hydrated $Na_{0.3}CoO_2 \cdot 0.9H_2O$ (107.7800 mg), as shown in Fig. 3.14.

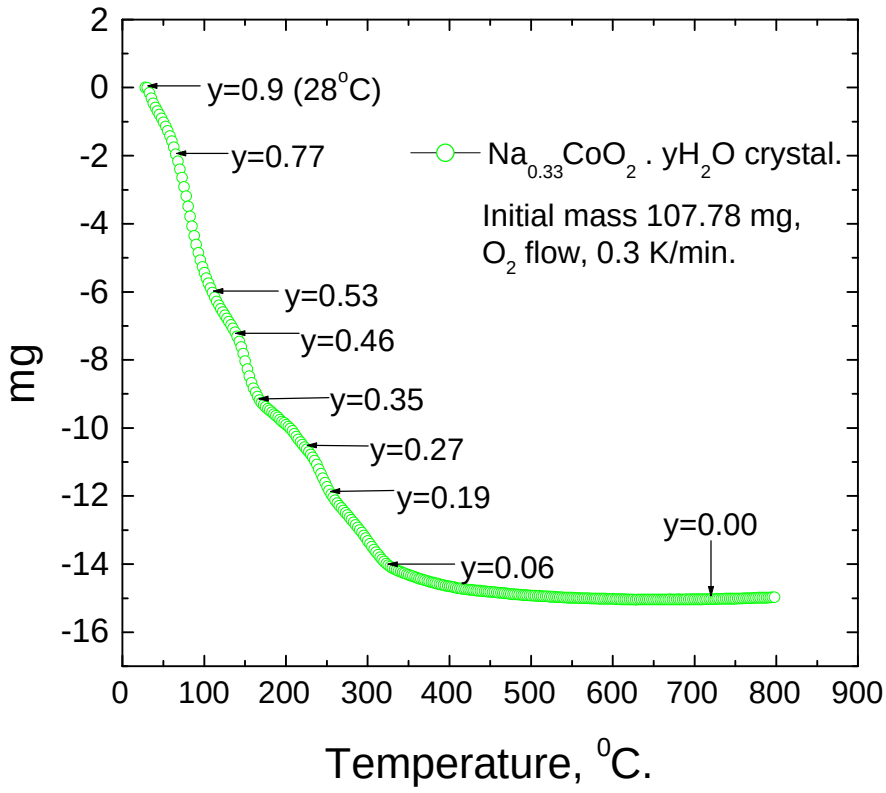

Fig. 3.14. Thermogravimetric results from another sample of partially hydrated $Na_{0.3}CoO_2 \cdot 0.9H_2O$ *(107.7800 mg).*

3.3.6. Electrical properties

The time dependence of the in-plane and out-of-plane resistivity shows anisotropic behavior for single crystals. I demonstrated the time dependence of the resistivity for single crystals during the hydration process. Fig. 3.15 shows that the resistivity plateau increases stepwise for increasing doping times t_0, $t_{0.5}$, t_1, t_2, t_3, t_4 t_5, and t_6, and then sharply and gradually decreases at t_8 and t_{24}, respectively. During hydration, some water molecules enter to intercalate between the CoO_2 and Na layers, so that the CoO_2 layers are separated by a tri-layer of $H_2O/Na/H_2O$ in the compound. The dominant effect is to expand the *c*-axis lattice parameters, from about 11.2 Å without water (non-superconducting phase of $Na_{0.3}CoO_2$) to 12.5 Å (semi-hydrated phase of $Na_{0.3}CoO_2 \cdot 0.6H_2O$), and then to 19.5 Å when the system becomes superconducting (fully hydrated phase of $Na_{0.3}CoO_2 \cdot 1.3H_2O$).

The experiments indicate that a stepwise increase in the form of resistivity plateaus occurs at a constant chemical doping level as the CoO_2 layers are increasingly separated by the intercalation of water. This phenomenon is more significant in ρ_c than ρ_{ab}, showing its anisotropic behavior. Interestingly, the resistivity decreases rapidly when the water doping level reaches that at t_8 and then slowly decreases again at t_{24}, monotonically decreasing with further doping. The increase of the 002-reflection intensity suggests that it is the increasing volume of the superconducting phase from the

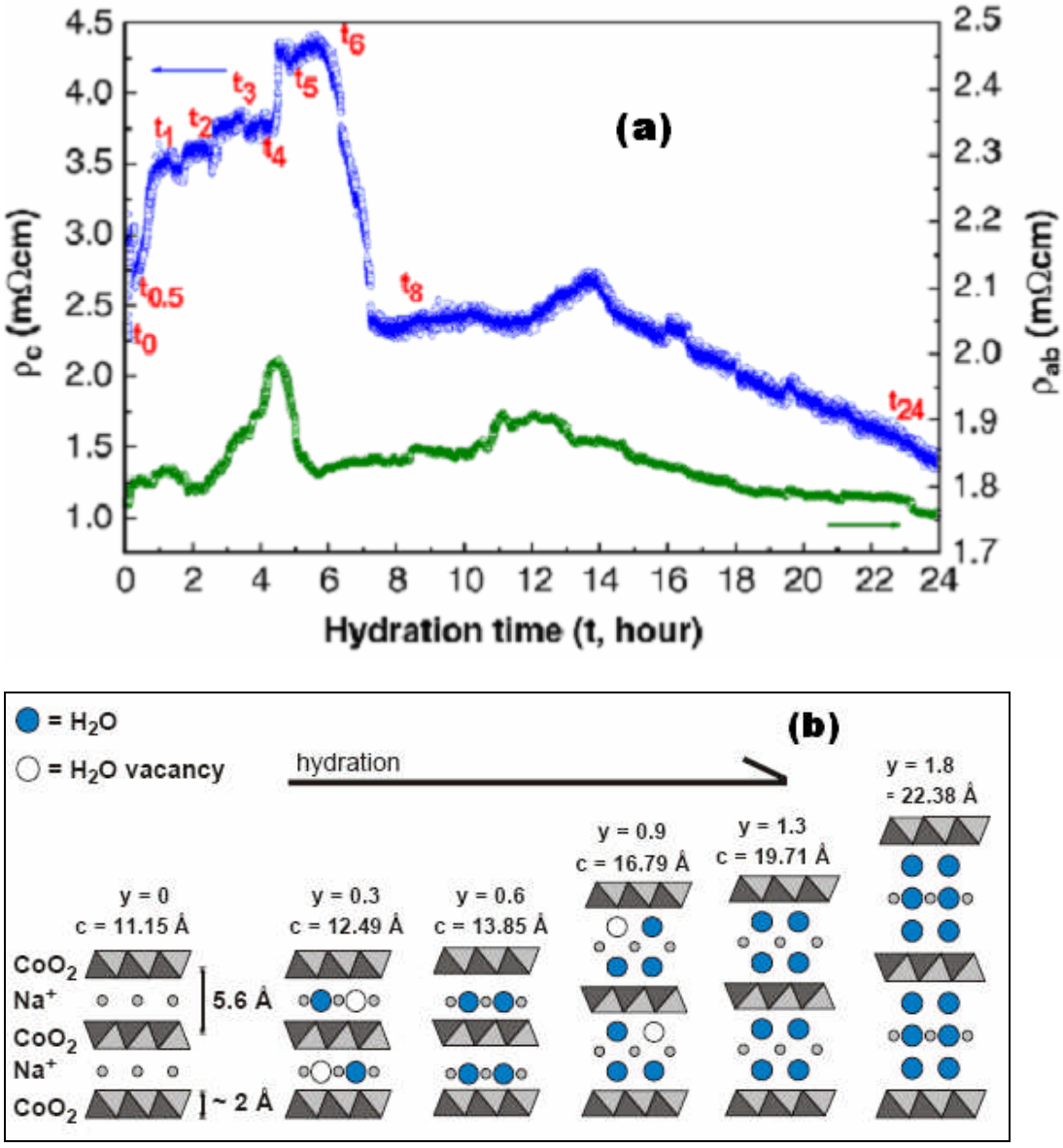

Fig. 3.15. (a) Time dependence of the in-plane and the out-plane resistivity for $Na_{0.3}CoO_2 \cdot yH_2O$ single crystal during a constant hydration process. (b) Schematic representation of the structures of the possible ordered phases with y = 0, 0.3, 0.6, 0.9, and 1.3, respectively.

constant doping process that brings down the room temperature resistivity. The results reveal that there is an interesting correlation between the CoO_2 layers and the

superconducting temperature, i.e., the Co-O distance decreases with increasing T_c [134]. The layer thickness of CoO_2 changes from 1.93 Å for the non-superconducting phase to 1.84 Å for the superconducting phase [148].

Fig. 3.16 demonstrates the time dependence of the resistivity for non-hydrated single crystals under ambient conditions. It shows that the resistivity of the sample increased from t_1 to t_2 and then sharply and gradually decreased to a stable level for in- and out-of-plane, respectively. The in-plane sample had absorbed water to form a partially hydrated phase under ambient conditions before the measurement. During the first stage, absorbed water molecules intercalate between the CoO_2 and Na layers, expand the c-axis lattice parameters, and finally form some fully hydrated phase of $Na_{0.3}CoO_2 \cdot 1.3H_2O$ (Fig. 3.10(c)). The fully hydrated phase is not stable under ambient conditions; it rapidly loses intercalated water to form the most stable phase of $Na_{0.3}CoO_2 \cdot 0.6H_2O$ within several hours. The ρ_c curve has several plateaus and tiny peaks, but ρ_{ab} only has one big transition at t_2, showing its anisotropic behavior under ambient conditions.

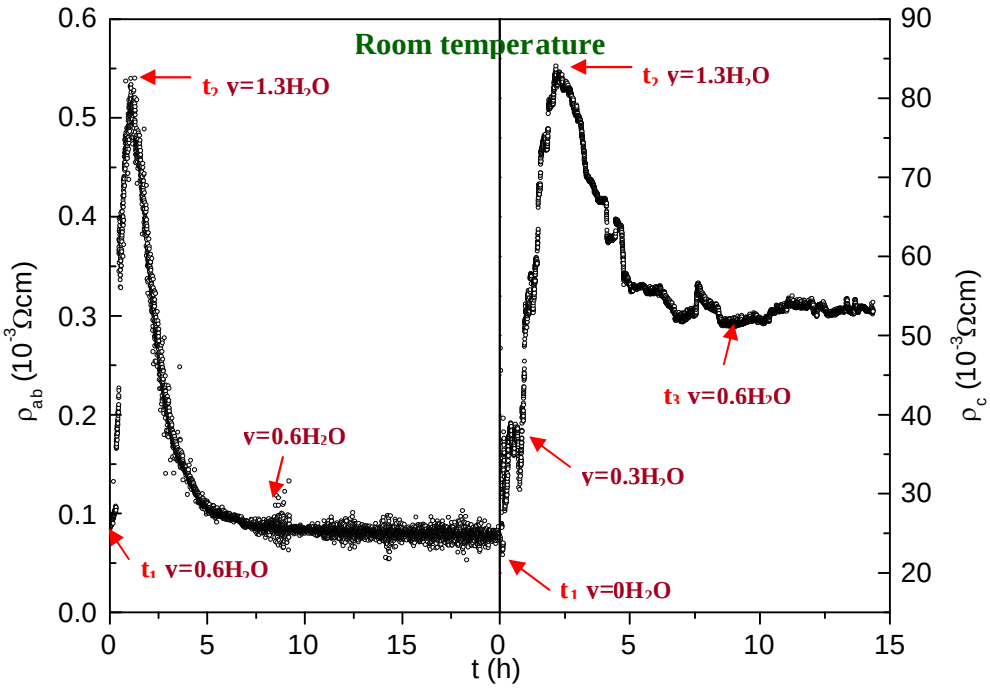

Fig. 3.16. Time dependence of the in-plane (left) and out-of-plane (right) resistivity, ρ_{ab} and ρ_c, of $Na_{0.3}CoO_2$ single crystals.

It is clear that the layer thickness of CoO_2 shrinks after reaching full hydration or doping to y = 1.3 and a change in the oxidation state of Co occurs. This is because the oxidation state directly corresponds to the carrier density in the CoO_2 layers and there is some electron transfer from the cobalt ions [9]. Nevertheless, the change in the room temperature resistivity during the doping process is not only influenced by the expanded spacing in the system, but also by a redistribution of the charge in the CoO_2 layers. It has been observed that the resistivity plateaus are changed in a stepwise manner due to the rapid kinetics of doping water, but isolation of the intermediate plateaus for their

detailed structure and physical study would, although interesting from a fundamental point of view, be quite difficult.

3.4. Conclusion

This investigation on growing a series of two-layer Na_xCoO_2 single crystals was performed by the optical floating zone technique using a variety of Na contents. A high quality compound was formed at x = 0.75, i.e. ά-phase, while other phases with lower sodium content of x < 0.70 (β-phase with x = 0.55 and 0.60, and γ-phase with x = 0.65 and 0.70, respectively) are observed always to contain Na_2O, Co_3O_4, and Na-poor phases, while the pure phase was formed in the tail of the ingot. The availability of the Na_xCoO_2 crystals gives us the opportunity for a more accurate characterization with respect to various aspects: structure, thermoelectric and electric behavior, and superconductivity.

Using TG-DTA it has been found that Na_xCoO_2 is an incongruently melting compound. Both non-hydrated and fully hydrated crystals are exceptionally sensitive under ambient conditions. The study of XRD and TG indicates that the semi-hydrated phase $Na_xCoO_2 \cdot 0.6H_2O$ is more stable than the other compositions under ambient conditions. The hydrated compound is highly unstable with respect to its chemical, structural, and electrical properties. The data show that the water intercalation/de-intercalation

processes in $Na_{0.3}CoO_2 \cdot yH2O$ single crystals are essentially different. The intercalation process from immersing the crystals in water takes place in such a way that two water molecules per Na ion are inserted initially into the Na-planes, followed by a group of four (two more) to form a hydrated cluster of $Na(H_2O)_4$ in a formula unit. In the water de-intercalation process monitored by TG measurements, the water molecules are removed from the hydrated cluster of $Na(H_2O)_4$ one by one at elevated temperatures, starting from 50^oC. The intercalation/de-intercalation dynamics via different hydrates may lead to complex non-equilibrium states in the bulk, especially on the surface of the single crystals. There are indications of multiphase formation and their coexistence in $Na_{0.3}CoO_2 \cdot yH2O$. Their effect on the electronic and superconducting properties remains unclear. However, depending on the reaction conditions, transition-like phenomena mark phase boundaries between quasi-equilibrium states with y = 0 (n = 0), 0.3 (n = 1), 0.6 (n = 2), 0.9 (n = 3), 1.3 (n = 4), and 1.8 (n = 6). This signals that, presuming a careful control of hydration conditions, it is possible to study the cobaltates under quasi-equilibrium conditions. I therefore propose to carefully reinvestigate the recently claimed evidence for unconventional superconductivity in single crystals.

Chaper 4 Studies on a superconductor derived from two-layer sodium cobaltates

4.1. Introduction

The recently discovered superconductivity in cobalt oxide $Na_xCoO_2 \cdot 1.3H_2O$ has attracted considerable attention [9]. The new material consists of two-dimensional CoO_2 layers that bear a similarity to high-T_c copper oxide superconductors. A simple but widespread view of the electronic state is that increasing the sodium content x adds x electrons to the spin 1/2 network in the CoO_2 layer [172, 176], which is similar to the case of doping the spin 1/2 network in the CuO_2 layer of the high-T_c cuprates. However, there is a large difference between these two classes of transition-metal oxides. Namely, Co forms a triangular lattice in the cobaltate, instead of a square lattice as in the cuprates. Because of this crystal structure, exotic superconducting states are expected in the cobaltate. So far, chiral *d*-, *p*-, *f*-, and *i*-wave states [169, 172, 174, 176, 189-192], as well as an odd-frequency *s*-wave state [193], have been proposed theoretically. The *d*- and *i*-wave states are spin singlet states, while the rest are spin triplet states.

The physical properties are determined by the amount of sodium and water in $Na_xCoO_2 \cdot yH_2O$ via their influence on the Co valence state and the resulting local distortions of the CoO_6 octahedra that are present in the structure. The compound Na_xCoO_2 shows manifestations of frustration in its physical properties because Co occupies a triangular

lattice and the exchange interactions are antiferromagnetic [69,71]. The close relationship between the structural and the electronic properties establishes itself also on the Fermi surface, which is expected to show features of strong nesting [169, 193]. Furthermore, there exists evidence that the superconductivity might have an unconventional order parameter [169]. When water is introduced into the compound, it exhibits chemical and structural instabilities. The Na^+ ions are at least partially mobile at elevated temperatures and may become ordered at low temperatures depending on the composition and sample treatment. The same is proposed for the Co^{4+}/Co^{3+} charge state on the triangular lattice [87].

All of these features make the study of the physical and chemical properties of the compounds difficult. However, nearly all the studies reported so far have been conducted on either sintered specimens or poorly characterized polycrystalline samples. These materials are often found to be inhomogeneous, especially with respect to the distribution of Na^+ ions in the lattice and in the intergranular spaces, due to Na_2O decomposition in the compound, and with respect to the intercalation of water. In polycrystalline samples water may in part accumulate in the intergranular spaces. The possible presence of second phases leaves a degree of uncertainty when interpreting the structural, electrical, and superconducting properties as functions of composition, i.e., establishing a superconducting phase diagram. This problem may be circumvented by the use of high quality single crystals, the chemical composition and crystal structure of which can be properly determined.

In an early study on a sample with large Na content, x = 0.31 and T_c = 3.7 K, it was found that the spin-lattice relaxation rate $1/T_1$ showed no coherence peak just below T_c, and there is a T^n decrease [178], which suggests a non-*s*-wave superconducting state. However, the crossover from n = 3 to 1 at low temperatures, which was confirmed subsequently by other groups, was insufficient to determine the exact form of the gap function [194, 195]. The later measurements on a low-x sample with high T_c (x = 0.26; T_c = 4.6 K) found that $1/T_1$ obeys a T^3 dependence all the way down to $T = T_c/6$, indicating unambiguously that line nodes exist in the gap function [196]. The T^3 dependence of $1/T_1$ has also been observed recently down to 0.12 T_c in a sample with a very high T_c of 4.8 K [197]. It is also worth noting that the antiferromagnetic fluctuations increase with decreasing Na content and become strongest at $x \approx 0.26$, where T_c is at its highest [196]. In order to gain information on the spin-pairing symmetry, the Knight shift has been measured in a single crystal. It has been found that the shift decreases below T_c along both the *a*-axis and the *c*-axis directions [165]. This indicates that the Cooper pairs are in the singlet form.

In a conventional superconductor, electrons at the Fermi surface form Cooper pairs under an attractive interaction mediated by lattice vibrations. The manner in which electrons form these pairs can be strongly influenced by the shape of the Fermi surface. Questions regarding the origin of the pairing interaction and the nature of the superconductivity in the cobaltates has stimulated significant theoretical speculation,

most of which has focused heavily on the properties of some small elliptically shaped pockets predicted to be the electronically dominant Fermi surface sheets [69, 177, 193, 198]. However, the outcome of direct attempts to look for them has instead cast serious doubt over their existence [199-203].

Here, I use high quality single crystals to study the superconductivity in $Na_xCoO_2 \cdot 1.3H_2O$, and report a revised superconducting phase diagram and the magnetic-field (H) strength dependence of the Knight shift in the superconducting state. It also present evidence that small elliptically shaped pockets do indeed exist, based on bulk measurements of the electron momentum distribution in hydrated sodium cobalt oxides using the technique of X-ray Compton scattering.

4.2. Experiment

The single crystal of $Na_xCoO_2 \cdot 1.3H_2O$ ($x \approx 0.22–0.47$) used in this study was grown by the TSFZ method followed by Na extraction and H_2O intercalation, as described in Chapter 3. XRD measurements were carried out with the x-ray diffractometer (Philips PW 1710). The chemical composition was determined by EDX, including microanalysis and inductively coupled plasma – Auger electron spectroscopy (ICP-AES) techniques. The superconducting properties were characterized by AC susceptibility, using a superconducting quantum interference device (SQUID) magnetometer (Quantum Design, MPMS 7.0). Nuclear magnetic resonance (NMR) experiments were performed

using a homebuilt phase-coherent spectrometer. The NMR spectra were collected by changing the external magnetic field (*H)* at a fixed radio frequency (rf) and recording the echo intensity step by step. A Compton profile represents a double integral (one-dimensional projection) of the full three-dimensional electron momentum density. Five Compton profiles equally spaced between Γ-*M* and Γ-*K* were measured on the high-resolution Compton spectrometer of beamline BL08W at the SPring-8 synchrotron (Japan synchrotron radiation research institute). The measurements were made at 11 K.

4.3. Results and discussion.

4.3.1. Superconductivity

The superconducting properties of the fully hydrated single crystals were characterized by AC susceptibility using a superconducting quantum interference device magnetometer. Zero field cooling (ZFC) measurements with 10 Oe applied field are presented in Fig. 4.1 [70]. Superconducting transition temperatures T_c = 2.8–4.9 K with x ≈ 0.28–0.42 were observed, respectively. Some of my samples showed strong diamagnetic AC signals and a superconducting volume fraction as high as 20 %. The transition width for each sample is different, which is very likely caused by an inhomogeneous sodium concentration and partial hydration, which affect the superconducting state of $Na_xCoO_2 \cdot 1.3H_2O$. Fig. 4.2 shows a plot of T_c as a function of the sodium concentration of Na_xCoO_2. For samples with $0.47 \geq x \geq 0.22$ there is no

superconducting transition detectable. These data agree to some extent with a recent study that shows a constant T_c for Na contents up to 0.37. However, they conflict with the superconducting ‘‘dome’’ of $T_c(x)$ demonstrated for powder samples [152]. This latter dependence motivated the proposal that there are intrinsic critical concentrations $x_{cr1} \approx 1/4$ and $x_{cr2} \approx 1/3$ related to charge ordering instabilities of the Co^{3+}/Co^{4+}.

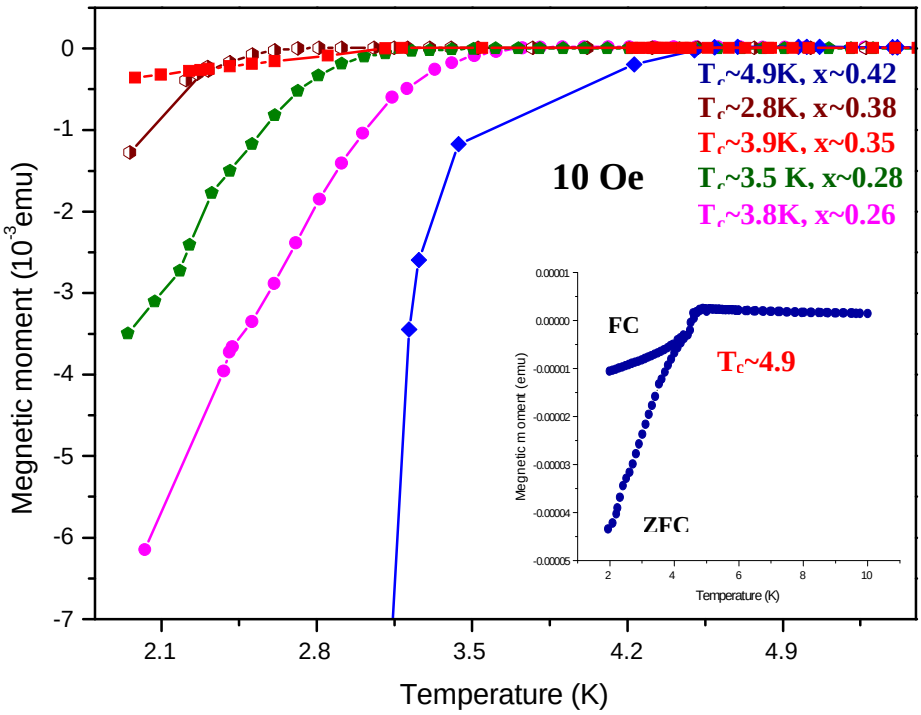

Fig. 4.1. Zero field Cooling (ZFC) magnetic characterization of the $Na_xCoO_2 \cdot 1.3H_2O$ single crystals showing the onset $T_c(x)$. Inset: ZFC and FC measurements showing that the optimum $T_c \approx 4.9$ K with $x = 0.42$ [70].

In the present single crystal study the upper limit is shifted to much higher concentrations, $x_{cr2} \approx 0.45$. This implies that a possible charge ordering at $x_{cr2} \approx 1/3$ is not relevant to the suppression of T_c.

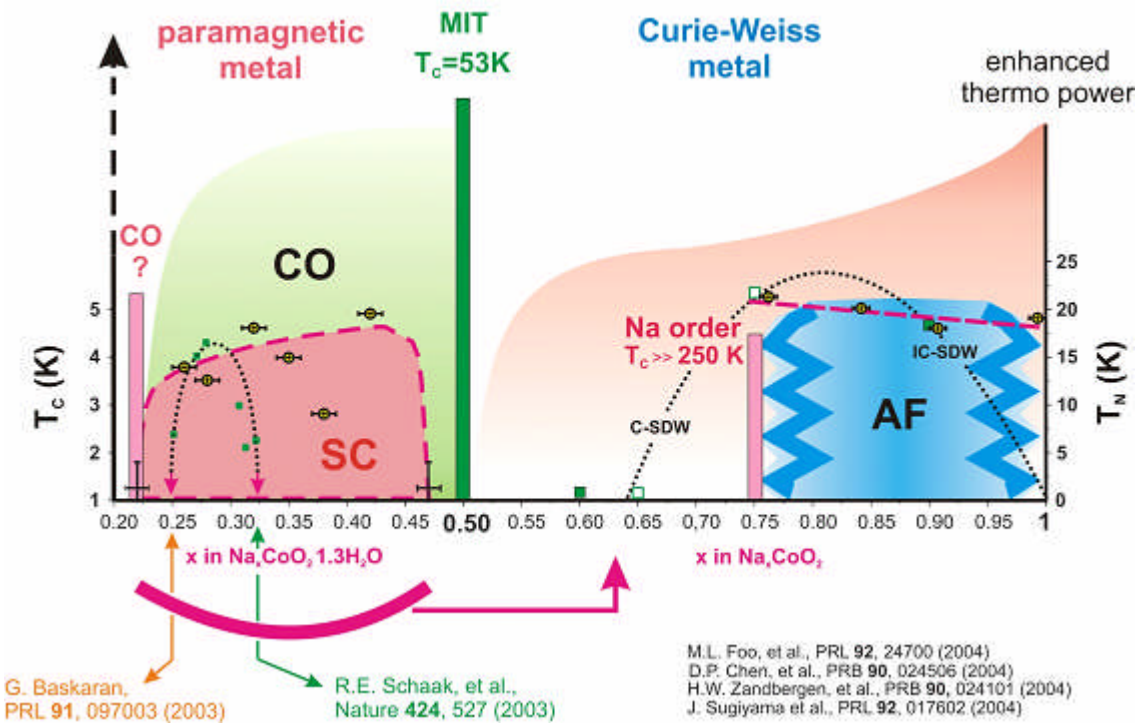

Fig. 4.2. Revised superconducting ($Na_xCoO_2 \cdot 1.3H_2O$) and non-superconducting (Na_xCoO_2) phase diagrams schematically combined. My susceptibility data (open circles) is compared to earlier data (small solid squares) and theoretical estimations (thin dashed curve). The arrows in red SC area mark a proposed charge ordering instability at x = 1/4 and x = 1/3 that is not evident in my data [152]. Green bars mark the report of charged ordered phases at x = 0.5, 0.60, and 0.65. For x = 0.5, a metal–insulator transition (MIT) is observed. The composition x = 0.5 separates the behavior of the magnetic susceptibility into a paramagnetic metallic and a Curie–Weiss-like regime. The antiferromagnetic (AF) phase shows an approximately composition-independent critical temperature T_N and fades out for a composition of x ≤ 0.75.

However, the superconducting phase now extends close to the phase line where non-hydrated $Na_{0.5}CoO_2$ shows a metal–insulator transition [87]. This is evidence for the importance of electronic correlations at higher x in the hydrated system. It is interesting to note that the Néel transition at $T_N \approx 20$ K is also only observed for higher Na concentrations with $x > 0.75$ in non-hydrated crystals and that this ordering temperature does not change appreciably with x. Bulk antiferromagnetic order has been proven using muon spin rotation (MSR) and other thermodynamic experimental techniques [69]. The exact nature of the ordering, however, still needs to be investigated further.

Evidence for superlattice formation and electronic instabilities, either due to Na or Co^{3+}/Co^{4+} charge ordering, has recently been accumulating for non-hydrated Na_xCoO_2 with $x = 0.5$, but also to some extent for other stoichiometries [29,204]. Hydration contributes to the charge redistribution due to its effect on the CoO_2 layer thickness and the formation of $Na(H_2O)_4$ clusters that shield disorder of the partially occupied Na sites. The above-mentioned instabilities should influence the superconducting state, as they modulate the electronic density of states and change the nesting properties of the Fermi surface. Further studies are needed to investigate a possible interrelation of Na content, hydration, and structural details on well-characterized samples with the highest T_c.

4.3.2. Evidence for d-wave pairing in the cobalt oxide superconductor $Na_xCoO_2 \cdot 1.3H_2O$

It has been found that the Knight shifts, both along the *a*-axis (K_a) and along the *c*-axis (K_c), decrease below $T_c(H)$ [165]. The reduction of K_a and K_c at T = 1.6 K amounts to 0.2 % and 0.13 %, respectively (for the K_c data, see Ref. [165]). The reduction in K_a is much smaller than that deduced from a powder pattern spectrum for which *s*-wave symmetry was proposed [205]. Fig. 4.3 shows the temperature dependence of the Knight shift K_a, with the field applied along the *a*-axis at low temperatures. T_c with H = 3.2 T parallel to the *a*-axis is 3.5 K, which is in good agreement with the report by Chou et al. [89].

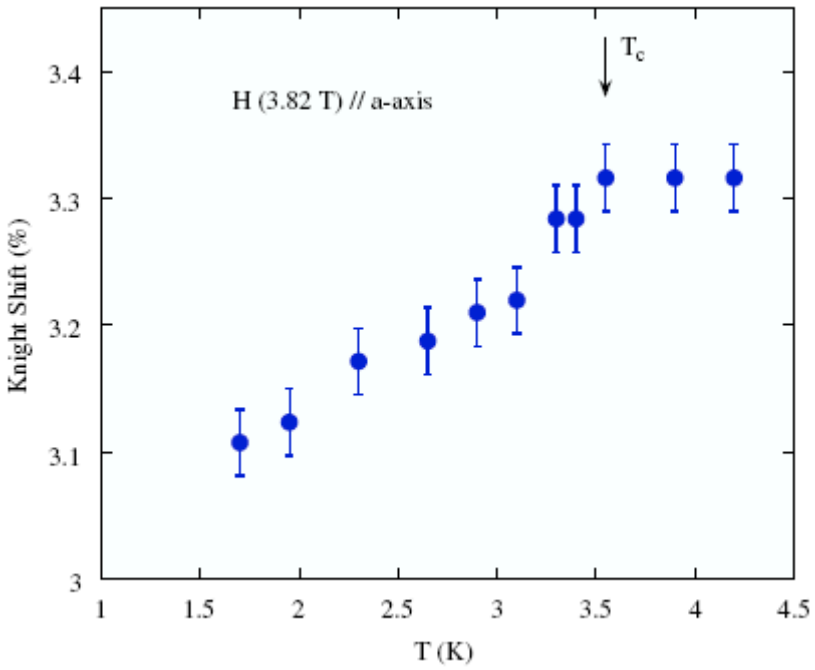

Fig. 4.3. Temperature dependence of the Knight shift for $Na_xCoO_2 \cdot 1.3H_2O$ with the magnetic field (3.82 T) applied along the a-axis (data from Ref. [165]). The arrow indicates T_c under the field.

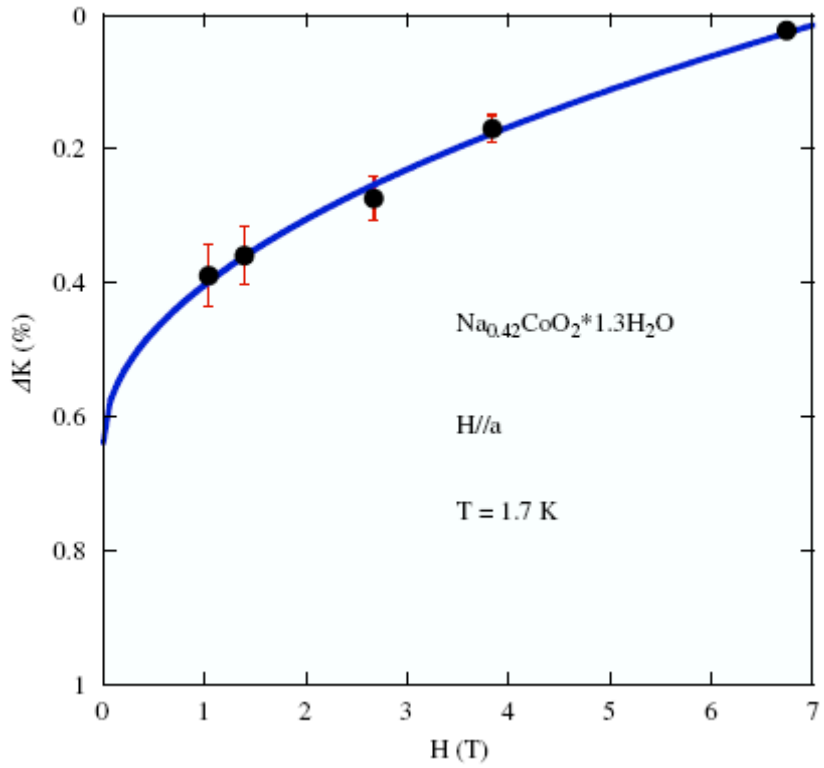

Fig. 4.4. The magnetic-field dependence of the ^{59}Co Knight shift (K) along the a-axis direction at T = 1.7 K, where $\Delta K = K_a(T = 4.2\ K) - K_a(T = 1.7\ K)$*. The curve is a fit to* $-\Delta K \propto \sqrt{H / H_{c2}}$.

As discussed in detail in Ref. [165], the reduction of K_a and K_c below $T_c(H)$ is due predominantly to the reduction of the spin susceptibility, which indicates that the spin pairing in the superconducting state is in the singlet state.

Fig. 4.4 shows the magnetic-field dependence of K_a at T = 1.7 K, where $\Delta K = K_a(T = 4.2\ K) - K_a(T = 1.7\ K)$. As seen in the figure (solid curve), the data can be fitted with

$$-\Delta K \propto \sqrt{H / H_{2c}} \quad (1)$$

with the upper critical field H_{c2} = 7 T. At H = 8.6 T, $\Delta K = 0$, confirming that the decrease of the Knight shift ceased above H_{c2}. This result adds new evidence that there are line nodes in the gap function. In the vortex state of nodeless superconductors, all quasiparticles are localized in the vortex cores [206]. In such a state, the Knight shift, which is determined from the spectrum coming from nuclei outside the vortex cores, will have no H dependence. However, if there are nodes in the gap function, the quasiparticles will be leaked out of the vortex core along the nodal directions, and their density of states will be proportional to $\sqrt{H}$ [207]. Such a feature has been observed in a typical *d*-wave superconductor, $TlSr_2CaCu_2O_7$ [208]. The results shown here indicate clearly that there is a quasiparticle density of states outside the vortex cores in $Na_xCoO_2 \cdot 1.3H_2O$.

Although a $d + id$ symmetry, which has a full gap, has been proposed theoretically for an exact triangular lattice [172, 176, 209], anisotropy of the triangles or modulation of the Fermi surface could cause the symmetry to be *d*-wave with line nodes.

4.3.3. Elliptical hole pockets in the Fermi surfaces of hydrated sodium cobalt oxides

A superconducting sample was produced by the chemical intercalation of deuterium oxide (with D_2O used rather than H_2O to allow future neutron experiments on the same sample) by submersion in liquid D_2O for three months at 5 °C [89]. Subsequent to the

Compton experiment, a measurement of the sample's magnetization showed that it was superconducting at a temperature of 3.5 K.

The spectrometer consists of a Cauchois-type crystal analyzer and a position-sensitive detector, with a full width at half maximum (FWHM) resolution at the Compton peak of 0.115 a.u. (1 a.u. of momentum = 1.99×10^{-24} kg m s^{-1}) [210, 211]. For the Compton profile, ~ 600 000 counts in the peak data channel were accumulated, and the Compton profile was corrected for possible multiple-scattering contributions. A two-dimensional momentum density, representing a projection down the *c*-axis of the full three-dimensional density, was reconstructed from five profiles using tomographic techniques [212] and then folded back into the first Brillouin zone (BZ), using the Lock-Crisp-West procedure [213, 214] to obtain the occupation density from which the occupied parts of the Brillouin zone could be inferred. The occupation density is shown in Fig. 4.5 (right) where black represents the lowest occupancy and white the highest.

A simple geometric simulation of such a Fermi surface is shown on the left of Fig. 4.5 and it, together with the experimental occupation density for the hydrated $Na_{0.35}CoO_2 \cdot 1.3D_2O$ (Fig. 4.5, right), is strongly suggestive of the presence of small hole pockets, which can be discerned close to the central hexagon; it is worth remarking that the a_{1g} sheet retains a strong hexagonal shape, whereas electronic structure calculations on the hydrated structure (although without the actual presence of water) predict something more circular [185]. The results suggest that the effects of hydration on the Fermi

surface are in fact rather modest and perhaps not as drastic as suggested by Xiao et al. [215]. The estimated area of the hexagonal a_{1g} sheet is 0.310, and (where appropriate) that of the six elliptical e'_g pockets, based on a comparison of simulations to the experimental data (with the total area constrained by the appropriate Na concentration), is 0.016. That the pockets appear rather close to the a_{1g} sheet is also noteworthy.

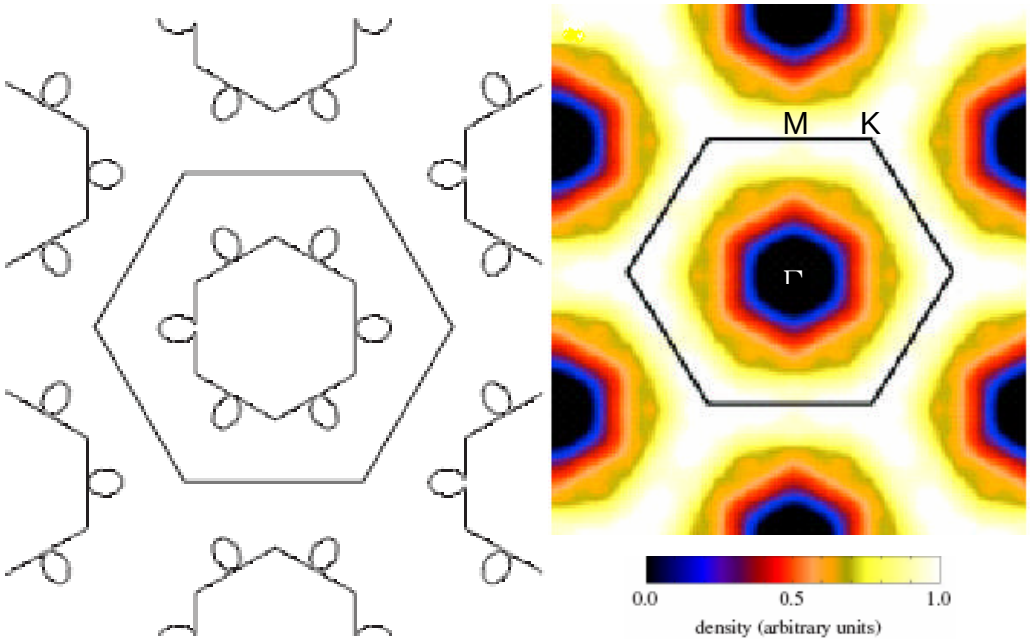

Fig. 4.5. A simulation of a Fermi surface comprising a central hexagonal sheet (representing the a_{1g} hole sheet) and six e'_g elliptical hole pockets (left) together with the experimental Fermi surface of $Na_{0.35}CoO_2 \cdot 1.3D_2O$ obtained from the reconstruction of five Compton profiles for each composition (right). The boundary of the first Brillouin zone is indicated.

4.4. Conclusion

In conclusion, the superconducting transition temperature of $Na_xCoO_2 \cdot 1.3H_2O$ ($x \approx 0.22–0.47$) is weakly influenced by the Na content. $T_c = 2.8–4.9$ K with $x \approx 0.28–0.42$, and the highest $T_c = 4.9$ K is found for $x \approx 0.42$. A revised superconducting ($Na_xCoO_2 \cdot 1.3H_2O$) and non-superconducting (Na_xCoO_2) phase diagram was presented.

The spin susceptibility in $Na_xCoO_2 \cdot 1.3H_2O$ measured by the Knight shift decreases below T_c and, at T = 1.7 K, follows a $\sqrt{H}$ dependence. Also, it has been reported that the spin-lattice relaxation rate $1/T_1$ follows a T^3 dependence below T_c, down to $T = T_c/6$. These results indicate that there are line nodes in the superconducting gap function and the Cooper pairs are in the spin-singlet form. These results strongly suggest that the Cooper pairing symmetry in $Na_xCoO_2 \cdot 1.3H_2O$ is of the *d*-wave type, as in the case of copper-oxide high-T_c superconductors. The antiferromagnetic fluctuations also resemble the behavior of the cuprates [178, 196] and may be responsible for the *d*-wave pairing.

We have presented the Fermi surface of $Na_{0.35}CoO_2 \cdot 1.3D_2O$, and the occupancy map shows the presence of small e'_g elliptical hole pockets. The observation of the pockets lends strong support to theories based on their special nesting properties in this family of compounds.

Chapter 5 Magnetic anisotropy of two-layer Na_xCoO_2 single crystals

5.1. Introduction

Layered cobaltite Na_xCoO_2 has received much attention because of its potential as a battery electrode material and in thermoelectric devices [216, 217]. The bulk superconductivity induced by water insertion in $Na_{0.33}CoO_2$ has increased the number of investigations into the physical properties of the Na_xCoO_2 compounds [6, 9, 96, 119], which have remained largely unexplored so far. One of the outstanding puzzles is the nature of the magnetic interactions. In the large-x region of Na_xCoO_2 ($x > 0.75$), the research has been hampered by difficulties in growing single crystals, as well as by phase separation effects, which appear above a threshold doping known as x_p [6]. So far, most studies have been carried out on polycrystalline samples or poor quality crystals. Studies using high quality single crystals will give more accurate results on the structure and physical properties of this frustrating material. In this work, I report on the anisotropic magnetic properties of large single crystals of Na_xCoO_2 with $x = 0.42$, 0.82, and 0.87.

5.2. Experiment

Crystals of $Na_{0.82}CoO_2$ and $Na_{0.87}CoO_2$ were prepared by the traveling solvent floating zone (TSFZ) method [70]. The $Na_{0.42}CoO_2$ sample was obtained by de-intercalation of $Na_{0.82}CoO_2$ as-grown single crystal, as previously described [40]. The composition of the samples for measurements was determined using energy dispersive X-ray (EDX) analysis. Single crystal X-ray diffraction (XRD) was carried out on mechanically cleaved faces of the crystals along the growth direction to examine the crystalline quality and orientation of the crystal growth. Cu K_α radiation was used as the X-ray source. The magnetic susceptibility measurements were carried out using a superconducting quantum interference device (SQUID) magnetometer (Quantum Design, model MPMS 7.0) over a wide range of temperatures from 2 to 300 K under a magnetic field of 1 T.

5.3. Results and discussion

Single crystals of Na_xCoO_2 were obtained with a growth rate of 1.5 mm/h in flowing oxygen atmosphere. The typical as-grown cylindrical crystal ingot size is 6.5 mm in diameter and 10 cm in length. When conditions were close to optimum, very clear facets appeared on opposite sides of the crystal rod. These facets were found to be perpendicular to the *c*-axis. The rest of the measurements were performed on crystal samples cleaved from the top ends of the crystal rods, which are normally of higher quality without any detectable Co_3O_4 impurity present.

Single crystal XRD measurements were made on crystal samples. Typical XRD patterns are shown in Fig. 5.1. All the peaks were indexed as the (00l) peaks of Na_xCoO_2. Using a fitting method based on the Nelson–Riley (N–R) function, the *c*-axis lattice constant is estimated to be 11.116 Å, 10.808 Å, and 10.806 Å for $Na_{0.42}CoO_2$, $Na_{0.82}CoO_2$, and $Na_{0.87}CoO_2$, respectively. The *c* parameter decreased as the Na content increased. No traces of impurities or inclusions were observed in my samples for magnetic measurements.

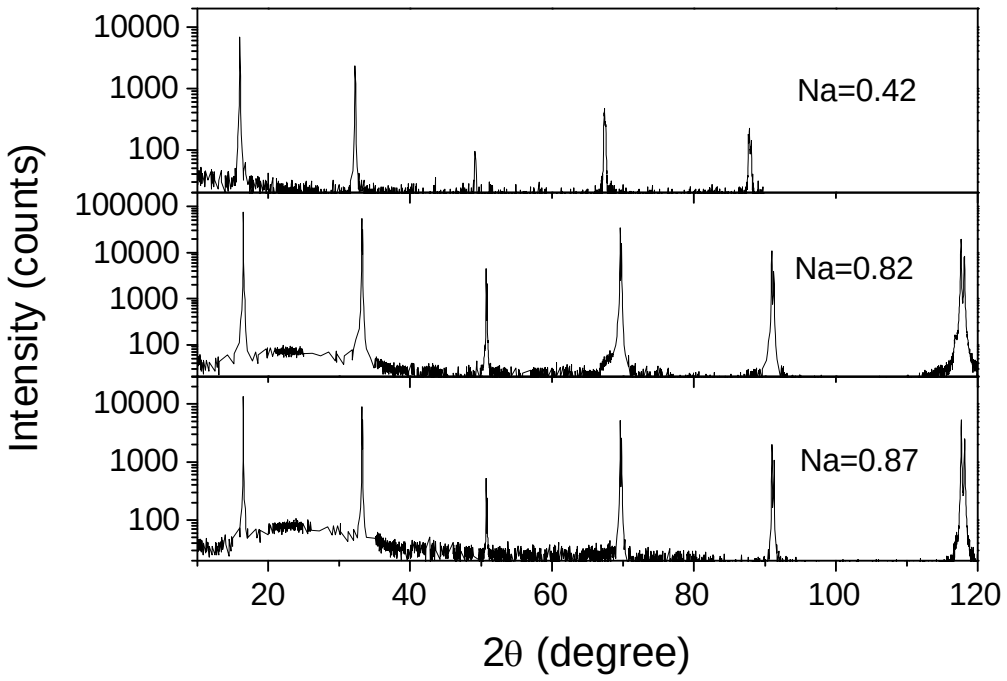

Fig. 5.1. X-ray diffraction patterns for Na_xCoO_2 single crystals cleaved along the growth direction. All the peaks can be attributed to the (00l) orientation.

The as-grown crystal quality was determined to be high, with the mosaic structure of the FWHM < 0.133^o. A typical X-ray (Mo K_α radiation) rocking curve measured on

$Na_{0.82}CoO_2$ crystal is presented in Fig. 5.2. The profiles of the (300) and (0010) Bragg reflections have FWHM values of 0.042 ^{o} and 0.133 ^{o}, respectively, indicating the excellent quality of the crystal.

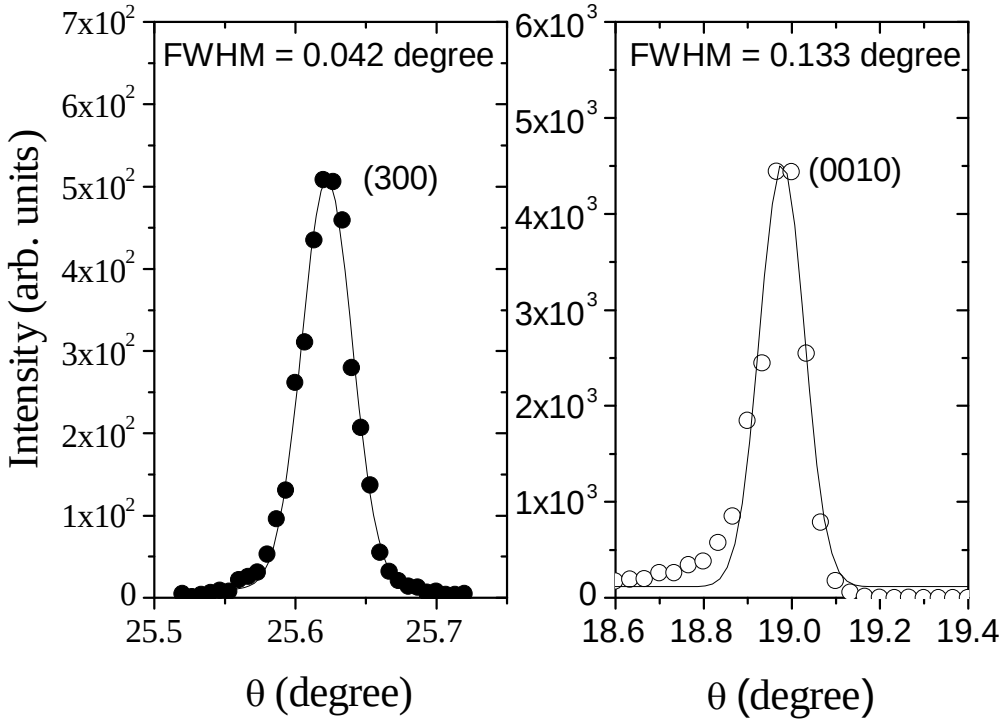

Fig. 5.2. X-ray rocking curves for the as-grown $Na_{0.82}CoO_2$ crystal (Mo K_α-radiation).

The temperature dependence of the susceptibility for the $Na_{0.82}CoO_2$ and $Na_{0.87}CoO_2$, measured in a field of 1 T oriented either along or perpendicular to the (001) direction, is shown in Fig. 5.3. Upon cooling, a broad peak appears around 21 K for the $Na_{0.82}CoO_2$ sample. Below 20 K, the susceptibility drops down sharply for H//*c*, but goes up for H//*ab*. Similar behaviors were observed for other single crystal samples

with sodium contents ranging from 0.78 to 0.85 [74, 128, 184]. The upturn of the curves below 14 K appears to be due to paramagnetic contributions from impurities; this upturn is suppressed in a field of 5 T [184].

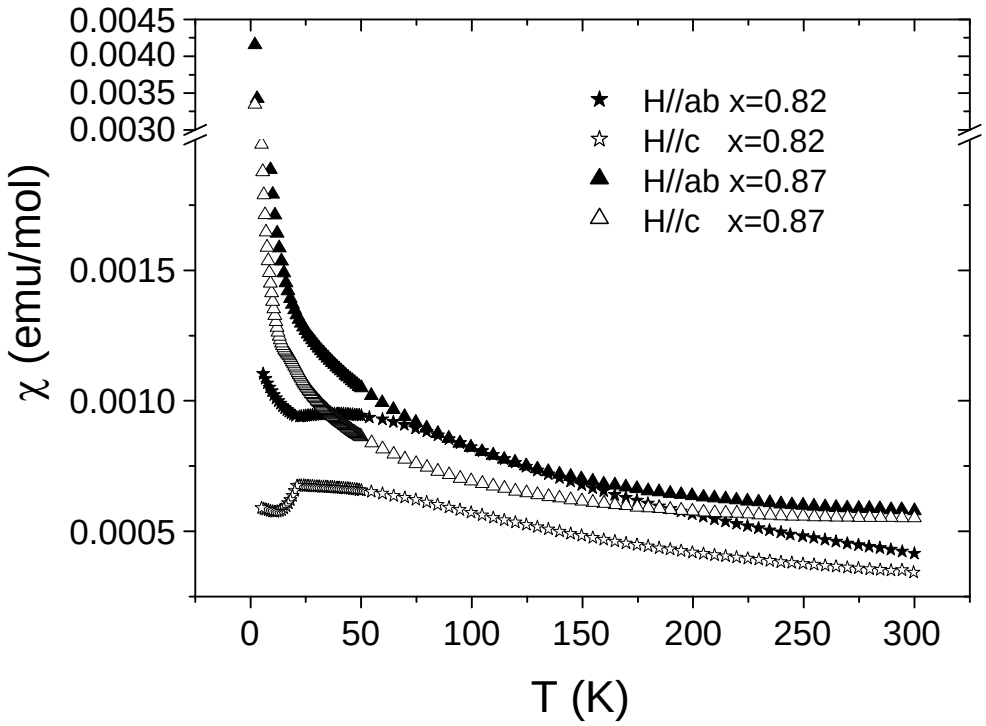

Fig. 5.3. Temperature dependence of the susceptibility of $Na_{0.82}CoO_2$ and $Na_{0.87}CoO_2$ measured in a field of 1 T. The open and closed symbols are for the magnetic field applied parallel and perpendicular to the (001) direction, respectively.

The broad maximum at ~40 K for H//*ab* is characteristic of low-dimensional short-range magnetic ordering.

The susceptibility of the $Na_{0.87}CoO_2$ sample shows paramagnetic behavior over a wide temperature range from 2 to 300 K. Two tiny kinks can be observed at about 19 K and 13 K in a field of 1 T parallel to (001), but are absent for the perpendicular direction.

The magnetization is very sensitive to the presence of Co_3O_4 and CoO, which are antiferromagnets with T_N = 35 and 292 K, respectively. No other transitions in the susceptibility have been found from 20 K to room temperature for any of the as-grown crystals, indicating high quality of the samples. This is consistent with the x-ray diffraction measurements, which exhibit no traces of impurities.

The magnetic susceptibility data for $Na_{0.42}CoO_2$ are shown in Fig. 5.4, where a magnetic field of 1 T was applied parallel to the *ab* plane and to the *c* direction. χ decreases from 300 to 86 K, and sharply increases again below 33 K. Two small anomalies develop at 51 and 86 K along the *c* direction. The susceptibility cusp at 51 K is isotropic, whereas the one near 86 K is anisotropic, which is consistent with the reports for $x \leq 0.5$ single crystals [10, 90]. I note that the 287 K anomaly does not exist in the parent x = 0.82 crystal sample. It is therefore tempting to assign the 287 K anomaly to the existence of CoO (T_N = 292 K) impurity which appears during the de-intercalation. It can be seen that the susceptibility increases as the sodium content x changes from 0.42 to 0.87.

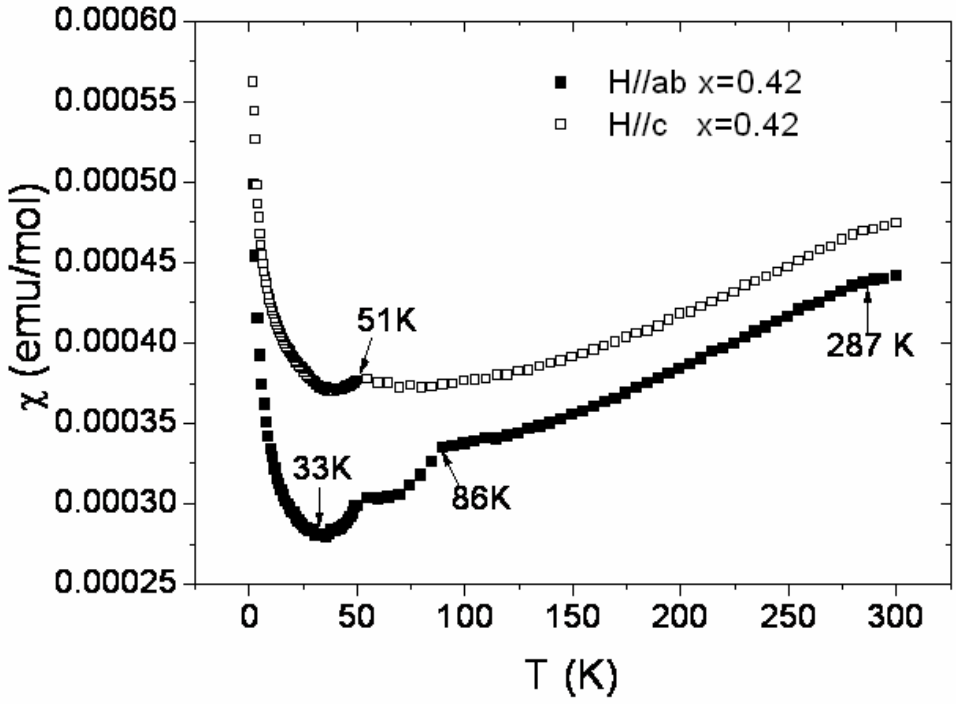

Fig. 5.4. Temperature dependence of the susceptibility for $Na_{0.42}CoO_2$ sample measured with the field parallel and perpendicular to the (001) direction.

In order to analyze the temperature dependence of the anisotropic susceptibility quantitatively, I plotted χ_{ab} (T) versus χ_c (T) with an implicit parameter T for the sample, as shown in Fig. 5.5. The analysis mentioned in ref. 12 leads to the relation between χ_{ab} (T) and χ_c (T):

$$\chi_{ab}(T) = (g_{ab}/g_c)2\,\chi_c(T) + (\chi^{ab}{}_0 - (g_{ab}/g_c)^2\,\chi^c{}_0)$$

where g_{ab} and g_c are the g-factors along the *ab*-plane and the *c* direction, respectively. The fitted slope of the data corresponds to the ratio $(g_{ab}/g_c)^2$. The samples with x =

0.42, 0.82, and 0.87 have $g_{ab}/g_c \approx 0.96$, 1.30, and 1.24, respectively. The sample with x = 0.82 has the largest anisotropy, whereas the sample with x = 0.42 is nearly isotropic. These results agree with the tendency reported by Chou et al [90].

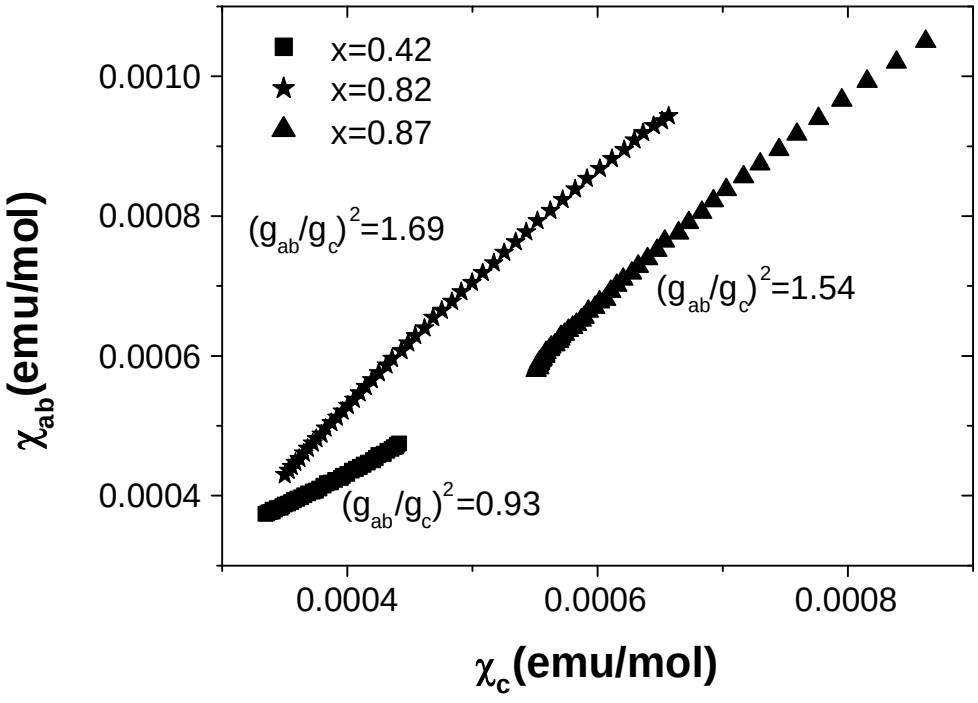

Fig. 5.5. χ_{ab} (T) versus χ_c (T) for single crystals of Na_xCoO_2 (x = 0.42, 0.82, and 0.87).

I fitted the temperature dependence of the susceptibility under a 1 T field for the x = 0.82 and 0.87 single crystals to a modified Curie-Weiss law, $\chi = \chi_o + C/(T-\theta)$, by a least-squares calculation, where χ_o, C, and θ are the temperature independent susceptibility, the Curie constant, and the asymptotic Curie temperature, respectively. The fitting parameters for both field orientations in the range T = 70-300 K are given in

Table 5.1. The fitted values for the powder average are also listed. As expected, I find that the Curie constants for H//*ab* and H//*c* are significantly different for these single crystal samples, which may arise from an anisotropic g-factor. The negative θ suggests antiferromagnetically interacting spins. The powder averaged Curie constant gives effective magnetic moments of μ_{exp} = 1.52 μ_B and 0.60 μ_B for the single crystal with x = 0.82 and 0.87, respectively, where μ_B is the Bohr magneton.

Table 5.1. Summary of magnetic data for $Na_{0.82}CoO_2$ and $Na_{0.87}CoO_2$.

Sample	Field orientation	C (cm^3K/mole)	θ (K)	χ_o (emu/mol_{Co}Oe)
$Na_{0.82}CoO_2$	//*ab*	0.36(2)	-243(10)	-0.00027(3)
	//*c*	0.135(7)	-159(8)	0.00004(1)
	powder	0.29(2)	-215(10)	-0.00019(3)
$Na_{0.87}CoO_2$	//*ab*	0.054 (2)	-33 (2)	0.00041(1)
	//*c*	0.0262(9)	-14(2)	0.00046(1)
	powder	0.045(2)	-27(2)	0.00043(1)

Since Na^+ is non-magnetic, the Curie-Weiss behavior of χ (T) is attributed to the distinct Co^{3+} and Co^{4+} ions arranged at the cobalt ion sites. In the localized spin approximation, there are three kinds of possible spin states for each cobalt ion, i.e., Co^{3+} : s = 0, 1, 2,

and Co^{4+} : s = 1/2, 3/2, 5/2, respectively. In this study, the effective magnetic moment was calculated using the formula,

$$\mu_{calc} = [x \times 4\,S\,(Co^{3+})\,(S\,(Co^{3+}) + 1) + (1\text{-}x) \times 4S\,(Co^{4+})\,(S(Co^{4+}) + 1)]^{1/2},$$

where the ratio $[Co^{3+}] : [Co^{4+}] = x : 1\text{-}x$, was assumed. The experimental value (0.60 μ_B) of x = 0.87 single crystal is close to the value of μ_{calc} = 0.62 μ_B, which is the spin-only value of Co^{4+} in S = 1/2. When assuming $S(Co^{3+}) = 0$ and $S(Co^{4+}) = 1/2$, the value obtained for x = 0.82 crystal is $\mu_{calc} = 0.73\mu_B$. The closest value obtained for x = 0.82 crystal is μ_{calc} = 1.64 μ_B, assuming $S(Co^{3+}) = 0$ and $S(Co^{4+}) = 3/2$. Another possible explanation for the larger experimental value for the x = 0.82 crystal is the spin state transition (SST) of the Co ions [72, 218], which implies that the actual mole fraction of the anisotropic spin sites in Na_xCoO_2 can be considerably larger than 1-x because of the presence of nearest-neighbor Co^{3+} ions. Further study is needed to understand the spin states of the mixed valence cobalt ions in the present compounds.

5.4. Conclusion

High quality single crystals of Na_xCoO_2 (x = 0.82 and x = 0.87) have been successfully prepared by the traveling solvent floating zone (TSFZ) method. A $Na_{0.42}CoO_2$ sample was obtained by de-intercalation of an as-grown single crystal. The magnetic susceptibility measurements revealed considerable anisotropy along H//*ab* and H//*c* for

the as-grown single crystals. The x = 0.82 sample had the largest derived anisotropic g-factor ratio of $g_{ab}/g_c \approx 1.30$, whereas the sample with x = 0.42 was nearly isotropic ($g_{ab}/g_c \approx 0.96$). The magnetic susceptibility for the as-grown crystals was fitted by a modified Curie-Weiss law, and the results were discussed.

Chapter 6 Studies of Single Crystal Growth and Anisotropic Magnetic Properties of Non-Stoichiometric Three-layer Sodium Cobalt Oxides

6.1. Introduction

Since the discovery of simultaneous surprisingly high thermoelectric power and low resistivity in Na_xCoO_2 ($x \leq 1$) [219, 220], and in particular, the discovery of superconductivity at temperatures below 5 K in $Na_{0.35}CoO_2 \cdot 1.3H_2O$, which is formed by the de-intercalation of Na from double layer γ-Na_xCoO_2 followed by a full hydration process [9], these materials have attracted considerable interest.

Early investigations on the sodium-cobalt-oxygen system have revealed that crystals with the formula Na_xCoO_2 ($x \leq 1$) are bronze type phases, consisting of sheets of octahedra $(CoO_2)_n$, between which are inserted sodium ions [21]. The unit cell of γ-Na_xCoO_2 has a P2 structure (prismatic, two layer), i.e., with two (2) sheets of edge shared CoO_2 in its unit cell, which are rotated by 60^o with respect to each other. The sodium ions, on two crystallographically distinct sites, are trigonal prismatic (P) in coordination to the oxygen atoms. α-Na_xCoO_2 has an O3 structure (octahedral, three layer), i.e., has three (3) sheets of edge shared CoO_2 per unit cell, displaced laterally from each other. The sodium ions are located only on one crystallographic site in an octahedron (O), with coordination to the oxygen atoms.

The transport and magnetic properties of two-layer Na_xCoO_2 are strongly dependent on the Na content. It has been found that as x increases from 0.3, the ground state of these compounds goes from a paramagnetic metal through a charge ordered insulator (at x = 0.5) to a 'Curie-Weiss metal' (around x = 0.70), and finally to a weak-moment magnetically ordered state (x > 0.75) [10]. Muon spin rotation (μSR) and NMR measurements have identified the stoichiometric three-layer Na_1CoO_2 phase to be a non-magnetic insulator [11, 12].

No superconductivity has been found in a new series of sodium cobalt oxyhydrates obtained from the parent compound β-$Na_{0.6}CoO_2$ [130], whereas the sodium cobalt oxyhydrates formed from α-$NaCoO_2$ show superconducting transitions at 4.3-4.6 K [221, 222]. Both parent materials have three CoO_2 layers per unit cell, in contrast to the first superconductor, $Na_xCoO_2 \cdot yH_2O$, which was obtained from a parent γ-Na_xCoO_2 containing only two CoO_2 layers per unit cell. This indicates that the geometrical shape of the site for the Na ions and the number of CoO_2 sheets play an important role in the resultant electronic and magnetic properties.

Single crystals are very desirable for experiments that require large volumes or areas of samples, such as neutron diffraction and anisotropic property measurements. Data obtained from the single crystal samples will shed light on the electronic and structural properties of this new type of superconductor. There has been much research on this family of materials. Single-crystalline whiskers with x = 0.5 have been grown by an

unconventional method from potassium-containing compositions. The maximum size of the whiskers is 1.6 mm in length, 15-40 μm in width, and 1.5-4.0 μm in thickness [223]. Using NaCl as a flux, plate-like single crystals of $NaCo_2O_4$ and $NaCoO_2$ have been prepared with typical sizes of 1.5 × 1.5 × 0.03 mm^3 and 0.5 × 0.5 × 0.02 mm^3, respectively [60, 63, 133, 219]. Compared to these methods, the traveling solvent floating zone (TSFZ) method is just as suitable for such single crystal growth. In principle, crystal growth can be performed continuously at one point on the temperature-composition phase diagram. Chou et al. succeeded in growing large single crystals of two-layer Na_xCoO_2 from a feed rod with x = 0.75, using an optical floating zone furnace under oxygen atmosphere [89]. Single crystals of Na_xCoO_2 with nominal Na content from 0.50 to 1.00 have also been grown successfully using the TSFZ method [70, 124, 142]. In this contribution, I present a detailed study on the crystal growth of large and high quality three-layer Na_xCoO_2 (x = 0.91, 0.92 and 0.93) single crystals by the floating zone method and demonstrate their structural behavior and anisotropic magnetic properties.

6.2. Experiment

The feed rods for the crystal growth were prepared by the conventional solid-state method. Powders of Na_2O_2（97 %） and Co_3O_4（99.998 %） were mixed in the molar ratios Na : Co = 1.00 : 1.00, 1.05 : 1.00, and 1.10 : 1.00 in an argon filled glove box. The temperature was slowly (150 °C/h) increased to 850 ℃, held constant for 24 hours

and finally slowly cooled down to room temperature in flowing oxygen. The polycrystalline powders were reground and formed into cylindrical rods 7 mm in diameter and 80 mm in length in an argon filled glove box. The rods were hydrostatically pressed under a pressure of ~70 MPa and then sintered at 900 °C for 24 h in flowing oxygen. After sintering, a 20 mm long rod was cut to serve as the first seed for crystal growth.

The crystal growth was performed in an infrared radiation furnace equipped with four 300 W halogen lamps. Prior to the crystal growth, a high density feed rod (~90 % of the crystal density) was obtained by pre-melting the rod at the rapid rate of 25 mm/h in flowing oxygen. A short polycrystalline pre-melted feed rod (~20 mm in length) was used as the seed rod in the crystal growth. Trials were made in which crystals were grown under different atmospheric compositions and pressures as follows: flowing oxygen, flowing argon, and low oxygen pressure (2 atm). The crystal growth speed also varied between 1 and 5 mm/h accompanied by a counter-rotation of the feed and seed rods at 30 rpm to ensure efficient mixing of the liquid and uniform temperature distribution in the molten zone.

Crystal wafers were cut perpendicular to the growth direction and polished to a mirror finish to allow us to examine them for the existence of macroscopic defects such as cracks, twins, grain boundaries, and inclusions under a polarized microscope. Compositional analysis of the as-grown crystals was obtained from inductively-coupled

plasma – atomic emission spectroscopy (ICP-AES). A Mo K_α X-ray source was used for powder XRD measurements to examine the phase purity and the crystal structure.

Single crystal X-ray diffraction (XRD) was carried out on mechanically cleaved faces of the crystals along the growth direction to examine the crystalline quality and orientation of the crystal growth. The measurements were conducted in a θ-2θ-scan mode in a 2θ range of 10-120^o for single crystal measurements. Cu K_α radiation was used as the X-ray source.

The magnetic susceptibility measurements were carried out using a superconducting quantum interference device (SQUID) magnetometer (Quantum Design, model MPMS 7.0) over the large temperature range of 2–350 K. Magnetic fields were perpendicular and parallel to the *c*-axis for cleaved as-grown crystals.

6.3. Results and discussion

6.3.1. Crystal growth

When preparing the polycrystalline Na_xCoO_2 by the solid state method, sintering the feed rods, pre-melting the feed rods, and growing the crystals at high temperatures, the sodium loss caused by high Na_2O vapor pressure has to be considered. Therefore, ceramic powders were synthesized using additional Na_2O_2 for compensation. Sintered powders were observed by X-ray powder diffraction (XRD) to consist of a main phase

of α-$NaCoO_2$ mixed with a small amount of Co_3O_4 impurity, due to the slow reaction in the core of the rod compared to the outside area; this is what normally happens in this series of compounds. Crystals grown using the impure feed rod did not contain any impurities, since Na has a large solubility range in the α-phase in this system, and the Na loss is corrected by homogeneous mixing in the following molten process.

Crystals grown under different conditions follow the aforementioned procedures. The quality of the pre-melted feed rods is one of the critical conditions of the TSFZ technique, because during the crystal growth the molten zone is sustained by the feed rod through surface tension. A straight, long, and equal-diameter feed rod is required to stabilize the molten zone over a long growth period. I found that it was very difficult to stabilize the molten zone during the atmospheric flow, due to the evaporation of Na, which can be observed as white Na_2O deposited on the inner wall of the quartz tube, with the molten zone collapse being the result of the composition change. Application of low-pressure oxygen (2 atm) during growth was found to greatly reduce the Na evaporation. Under these conditions, zone travel rates of 1.0, 2.0, 3.0 and 5.0 mm/h were employed. It was found that the zone travel rates in this range have no detectable influence on the crystal quality. However, it has been observed that the slower rate stabilized the molten zone. Considering the evaporation of Na ions during the growth, much slower rates were not applied.

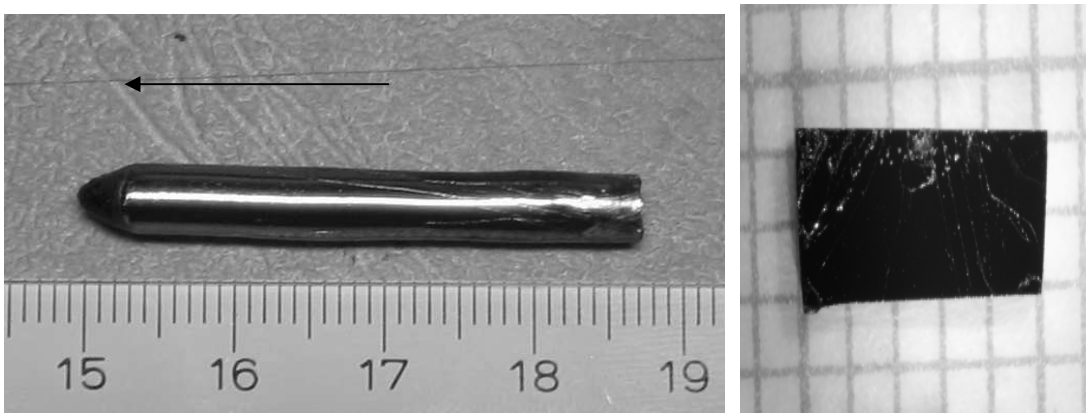

Fig. 6.1. As-grown single crystal of α-$NaCoO_2$ (left) and the cleaved crystal from the last grown part of the ingot (right).

Fig. 6.1 (left) presents a typical α-Na_xCoO_2 boule, which was grown at the moderate rate of 2mm/h under an oxygen pressure of 2 atm in an attempt to reduce the volatilization of Na and obtain large crystals. The boule was black with a metallic luster and was 5 mm in diameter and 37 mm in length. The arrow indicates the crystal growth direction. Due to the layer growth mechanism, the crystal grains were found to grow preferentially along the crystallographic *ab*-plane, parallel to the rod axis. It was found that the cleaved surface of the as-grown crystal was shiny, but unstable under atmospheric conditions, in contrast to γ-phase Na_xCoO_2 crystal. The cleaved surface became dull just 20 minutes after cleavage due to its reaction with moisture and CO_2 in the air. The crystal samples must be quickly removed after processing and stored in a clean and dry container to prevent the absorption of moisture.

The crystal wafers were cut from the last grown part and polished to a mirror face. Under a polarized light microscope, only a few separate grains were found in the

peripheral area. No inclusions, cracks, or grain boundaries were observed in the inner area of about 4mm diameter. Fig. 6.1 (right) displays a $5 \times 2 \times 1$ mm^3 crystal. This crystal was mechanically cleaved from the central region of the last grown part of the ingot using a sharp steel pin.

6.3.2. Composition and structure

There can be a concentration gradient of Na either along or across the crystal growth direction. In order to minimize this possibility, the crystal wafers were cut from the last grown part, in the range of 2 to 3 mm from the end. Three pieces of crystal were cut from the same crystal wafer, and all three pieces were analyzed by ICP-AES. I found that the Na concentrations of the three pieces of crystal are very close. The average values of Na determined from the three pieces of crystal are x = 0.91, 0.92, and 0.93 for the starting compositions of $Na_{1.00}CoO_2$ $Na_{1.05}CoO_2$, and $Na_{1.10}CoO_2$, respectively. Single crystal XRD measurements were made on both as-grown crystals. Plate-like crystals were cleaved along the growth direction. Typical XRD patterns are shown in Fig. 6.2. All the peaks were indexed to the (00l) peaks of α-$NaCoO_2$. Using a fitting method based on the Nelson–Riley (N–R) function, the *c*-axis lattice constant is estimated to be 15.597(2) Å for $Na_{0.92}CoO_2$, and 15.5928 (9) Å for $Na_{0.93}CoO_2$. No traces of impurities or inclusions were observed in my samples.

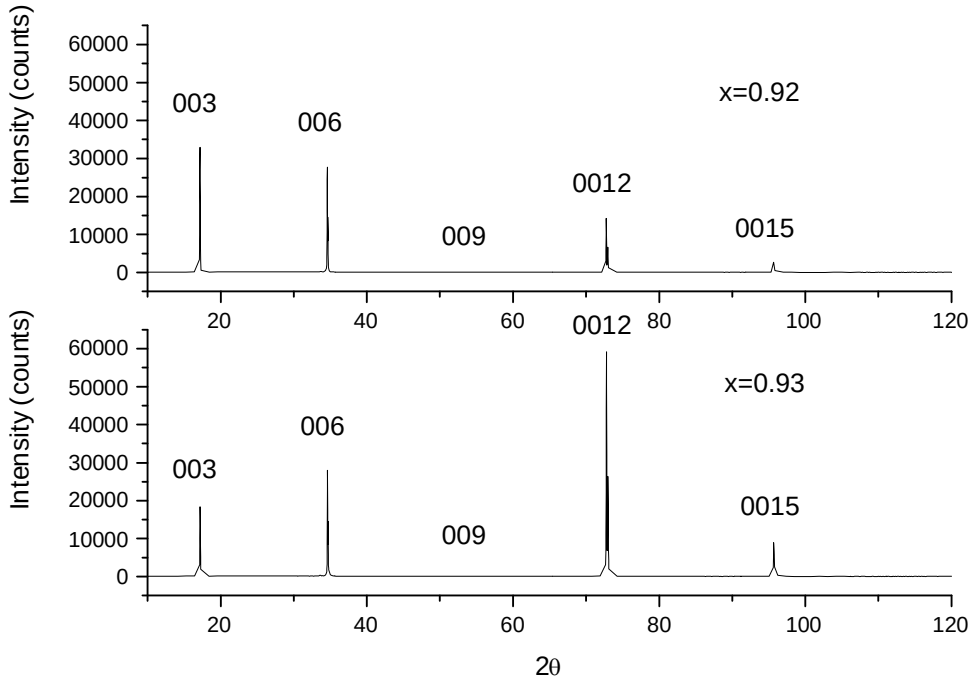

Fig. 6.2. X-ray diffraction patterns for α-$NaCoO_2$ single crystals cleaved along the growth direction. All the peaks can be attributed to (00l).

Table 6.1. Crystallographic data for $Na_{0.92}CoO_2$ in the space group R-3m.

Atom	*Wyckoff position*	*x*	*y*	*z*	*Occ*	*Biso(Å)* [a]
Na	3a	0	0	0	0.919(2)	0.98(9)
Co	3b	0	0	0.5	1	0.57(7)
O	6c	0	0	0.2308(3)	1	0.52(10)

[a]Isotropic temperature factor

The structure refinement of $Na_{0.92}CoO_2$ was performed using a Rietveld analysis program. I adopted the space group R-3m, and assumed that the sodium ions are on the (0, 0, 0) sites and are coordinated octahedrally to the oxygen from the CoO_2 layers. Table 6.1 lists the refined structure parameters, and Fig. 6.3 presents the refinement pattern of the $Na_{0.92}CoO_2$ single crystal. The final factors were quite low, decreasing to R_p = 8.50 %, R_{wp} = 10.89%, R_B = 1.83% and χ^2 = 1.01. The cell parameters are a = 2.88762(17) Å, c = 15.6020(8) Å. The lattice parameters of $Na_{0.93}CoO_2$ were determined by single-crystal x-ray diffraction along the (0, 0, l) and (h, k, 0) directions at room temperature, resulting in values of a = 2.8878(7) Å and c = 15.596(2) Å: these values agree with the reported crystal data for α-$NaCoO_2$ [96, 133].

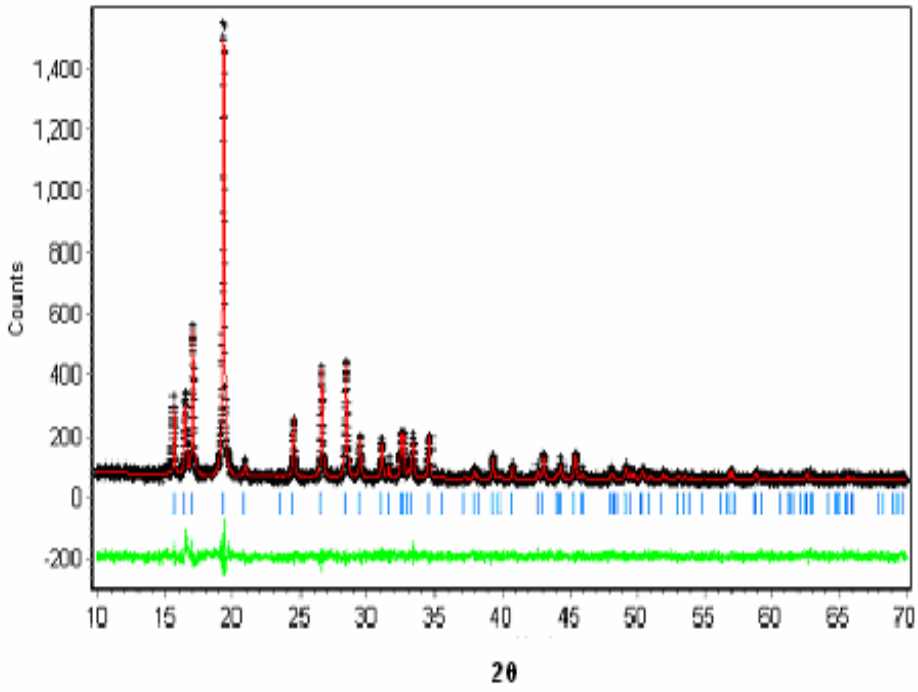

Fig. 6.3. Rietveld refinement pattern for the as-grown α-$Na_{0.92}CoO_2$ crystal. The observed diffraction intensities and the calculated patterns are represented by the plus signs and the solid lines, respectively. The pattern at the bottom represents the

difference. Short bars below the observed and calculated patterns indicate the positions of allowed Bragg reflections.

6.3.3. Magnetic anisotropy

The temperature dependence of the susceptibility for the $Na_{0.92}CoO_2$ sample, as measured in a field of 1 T oriented either along or perpendicular to the (001) direction, is shown in Fig. 6.4. Upon cooling, a peak develops around 20.5 K, which is sharper than that observed in two layer $Na_{0.82}CoO_2$ single crystal [184]. The following sharp decrease of the (001) direction susceptibility around 19.6 K heralds an antiferromagnetic transition with ordered moments along *c*. The inset in Fig. 6.4 shows that the transition is only weakly affected by the field. The upturn of the curves below 14 K appears to be due to paramagnetic contributions from impurities; this upturn is suppressed in a field of 5 T.

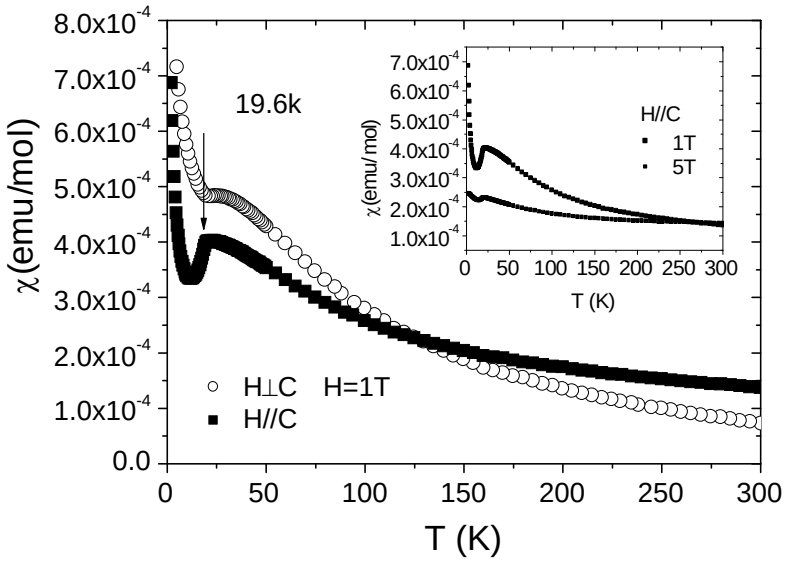

Fig. 6.4. Temperature dependence of the susceptibility for $Na_{0.92}CoO_2$ sample measured with field parallel and perpendicular to the (001) direction. Inset shows the data measured in 1 and 5 T with field parallel to (001).

The magnetization is very sensitive to the presence of Co_3O_4 and CoO, which are antiferromagnets with T_N = 35 and 292 K, respectively. No other transitions in the susceptibility have been found from 20.5 K to room temperature for any of the single crystal samples, indicating high quality. This is consistent with the x-ray diffraction measurements, which exhibit no traces of impurities.

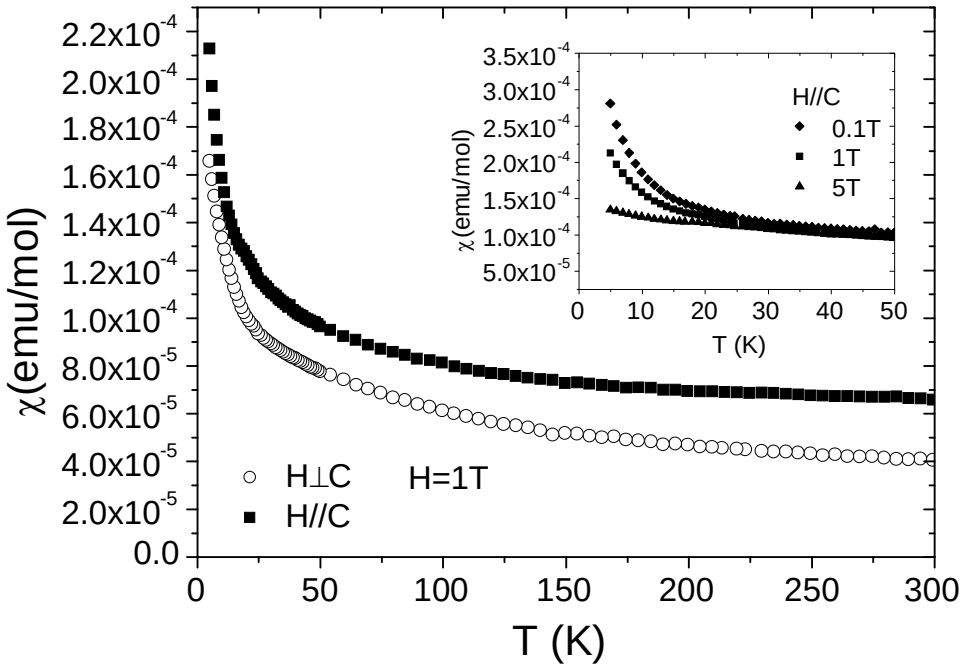

Fig. 6.5. Temperature dependence of the susceptibility for $Na_{0.93}CoO_2$ sample measured in a field of 1 T. The open and closed symbols are for the magnetic field applied perpendicular and parallel to the (001) direction, respectively. Inset shows low temperature results at different parallel magnetic fields.

The temperature dependence of the susceptibility for the $Na_{0.93}CoO_2$ sample measured in a field of 1 T parallel and perpendicular to the (001) direction is shown in Fig. 6.5. It can be seen that the antiferromagnetic transition at 19.6 K seen in the $Na_{0.92}CoO_2$ sample is absent for the $Na_{0.93}CoO_2$ sample. Furthermore, χ gradually increases with decreasing temperature, showing typical paramagnetic behavior. The inset figure shows the separation below $T_C \approx 20$ K, where the susceptibility decreased as the applied magnetic field increased below this temperature.

As to why such a little difference in the composition could cause such a big difference in the magnetic properties of the α-Na_xCoO_2 single crystals, I believe that the compositions of x = 0.92 and 0.93 are located right at a boundary (in the magnetic phase diagram) that separates two different regions with different magnetic phases, antiferromagnetic and paramagnetic. Considering the fact that the alpha phase only forms for x = 0.9 up to x = 1.0 [21], the compounds with x = 0.90 and 0.92 are antiferromagnetic, as has been observed in crystals grown by the flux method [90] and in the crystals presented in this work. For x > 0.92, samples are paramagnetic (as in the case of my x = 0.93 crystals) and eventually become non-magnetic for x = 1 [11].

In order to analyze the T dependence of the anisotropic susceptibility quantitatively, I plotted $\chi_{ab}(T)$ versus $\chi_c(T)$ with an implicit parameter T for both single crystals (Fig. 6.6). The analysis mentioned in ref. 23 leads to the relation between $\chi_{ab}(T)$ and $\chi_c(T)$:

$$\chi_{ab}(T)=(g_{ab}/g_c)^2\,\chi_c(T)+[\,\chi^{ab}{}_o-(g_{ab}/g_c)^2\,\chi^{c}{}_0]$$

The fitted slope of the data in Fig. 6.6 corresponds to the ratio $(g_{ab}/g_c)^2$. The samples with x = 0.91, 0.92, and 0.93 have $g_{ab}/g_c \approx 1.40$, 1.29, and 1.12, respectively. These results indicate that the derived anisotropic g-factor ratios (g_{ab}/g_c) decrease significantly with a small change in the sodium concentration, indicating that the physical properties of the three-layer Na_xCoO_2 should be very sensitive to the Na contents.

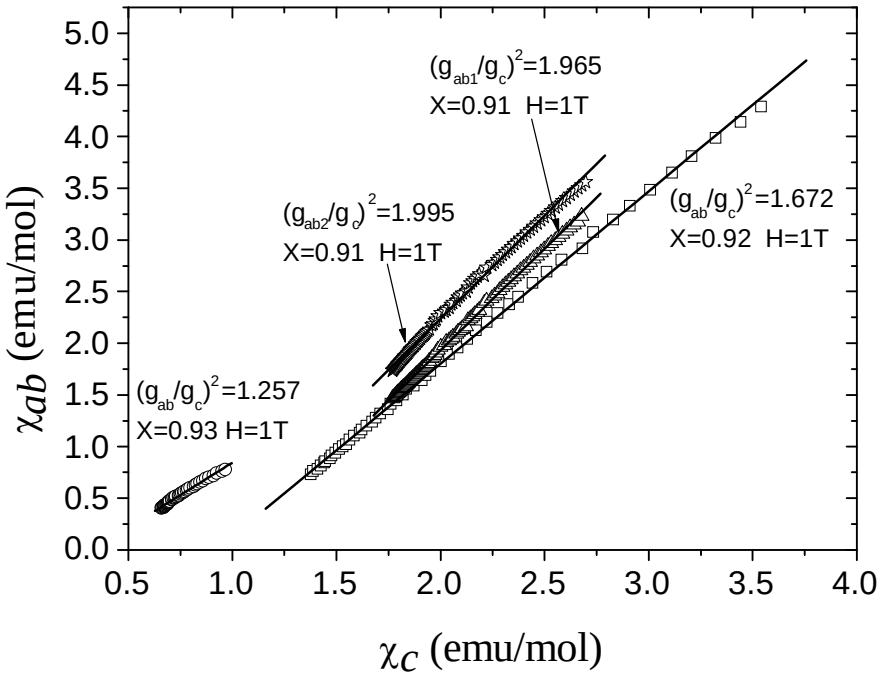

Fig. 6.6. χ_{ab} versus χ_c for α-Na_xCoO_2 with x = 0.91, 0.92, and 0.93.

I fit the temperature dependence of the susceptibility under a 1 T field for the x = 0.91, 0.92, and 0.93 single crystals to a modified Curie-Weiss law, $\chi = \chi_o + C/(T-\theta)$, by a least-squares calculation, where χ_o, C, and θ are the temperature independent susceptibility, the Curie constant, and the asymptotic Curie temperature, respectively. The fitting parameters for both field orientations in the range T = 50-300 K are given in Table 6.2. The fitted values for the powder average are also listed. As expected, it has been found that the Curie constants for H//*ab* and H//*c* are significantly different for these single crystal samples, which may arise from an anisotropic g-factor. The negative θ suggests antiferromagnetically interacting spins.

Table 6.2. Summary of magnetic data for three-layer Na_xCoO_2.

NA_XCOO_2	FIELD ORIENTATIONS	C (CM^3K/MOLE)	θ (K)	X_O ($EMU/MOLE_{CO}OE$)
X = 0.91	//AB1	0.0370(6)	-64(2)	-0.00001(2E-6)
	//AB2	0.0491(7)	-85(2)	0.00002(2E-6)
	//C	0.0144(3)	-38(2)	0.00012(9E-7)
X = 0.92	//AB	0.0633（14）	-68(2)	-0.0001(3E-6)
	//C	0.0328(6)	-55(2)	0.00004(2E-6)
X = 0.93	//AB	0.0056(1)	-53(2)	0.00002(4E-7)
	//C	0.00263(9)	-15(2)	0.00006(3E-7)
X = 0.91 (POWDER)		0.0334（7）	-63(2)	0.00005（1E-6）
X = 0.92 (POWDER)		0.053(1)	-65(2)	-0.00005 (3E-6)
X = 0.93 (POWDER)		0.0047(1)	-34(2)	0.00005(3E-7)

The three layer Na_xCoO_2 has a hexagonal crystal structure with in-plane and out of plane parameters a = 2.887 Å and c = 15.60 Å with space group R-3m. It is obvious that the crystal structure is highly anisotropic. Therefore, the difference in the in-plane and

the out-of-plane magnetic properties is expected, and it has been indeed observed in my crystal samples. However, the occurrence of in-plane anisotropy seems hard to predict. Nevertheless, I have noticed that in-plane anisotropy in two layer Na_xCoO_2 compounds has just recently been observed using the neutron diffraction technique [224]. Therefore, there could be a possibility of in-plane anisotropy in three-layer Na_xCoO_2 crystals.

Although the determination of the *a* direction in the *ab*-plane is very difficult for the Na_xCoO_2 crystals, it still can be determined how the magnetization changes when the magnetic field is rotated in the *ab*-plane. Therefore, the *ab* in-plane magnetic anisotropy was measured by the following procedures for the crystals: I first measured the sample with the field along one direction in the *ab* plane (the *ab*1 direction as indicated in the inset of Fig. 6.7), and then measured it again by rotating the sample 90^o in the *ab*-plane as indicated by the *ab*2 direction in the same inset. A large crystal ($4 \times 4 \times 1$ mm^3) with x = 0.91 was chosen for the in-plane anisotropy study, and its out-of-plane anisotropy was also measured.

The temperature dependence of the susceptibility (χ-T) for the x = 0.91 sample measured in a field of 1 T is shown in Fig. 6.7. It can be seen that although the susceptibilities measured along the two in-plane directions show the same trend with temperature, they show about a 10-18 % difference in magnitude over a wide range of temperatures. The two in-plane susceptibilities are very different from that along the *c* direction. A cross-over is clearly seen at 120 K or 180 K, respectively, which is also

seen in the x = 0.92 sample at 120 K, as shown in Fig. 6.4. The above results indicate that in-plane anisotropy exists in the α phase Na_xCoO_2 crystals. The in-plane and out-of-plane Curie constants are calculated by fitting to the modified Curie-Weiss law, and their values are given in Table 6.2. It can be seen that the *C* values for the *ab*1 and *ab*2 in-plane directions are very close (0.037 and 0.049 cm^3 K·mole).

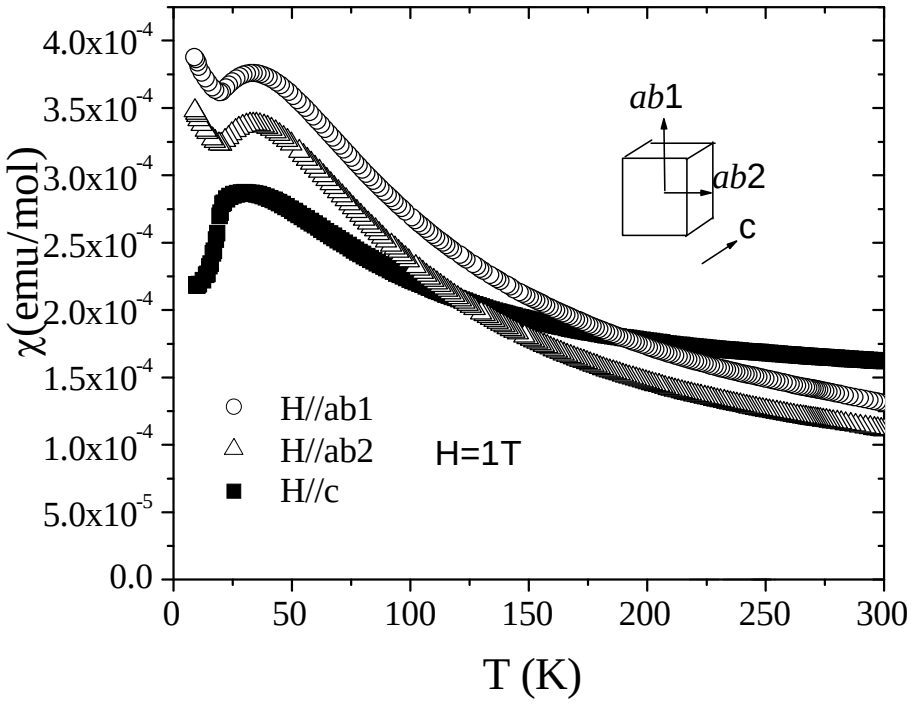

Fig. 6.7. Temperature dependence of the susceptibility for $Na_{0.91}CoO_2$ sample measured with three different magnetic field directions.

However, the difference between the in-plane and out-of-plane values is big, which is similar to what has been found for the x = 0.92 and 0.93 crystals. The difference in the in-plane Curie constants is apparently due to the in-plane anisotropy of the three-layer α phase Na_xCoO_2 crystals. my observations on the in-plane anisotropy in the α-$NaCoO_2$

single crystal samples are in agreement with what has been reported for two-layer γ Na_xCoO_2 phase. However, I should point out that it is very hard to align the crystal perfectly in the *ab*-plane for each measurement. Therefore, less accuracy in the alignment of the *ab*-plane could also contribute to the different susceptibility values in the *ab*-plane. Further work is needed on an in-plane anisotropy measurement with very accurate alignment in the *ab*-plane.

6.4. Conclusion

In summary, large, non-stoichiometric α-Na_xCoO_2 in the form of high quality single crystals can be grown using the traveling solvent floating zone (TSFZ) method under oxygen atmosphere. As-grown single crystals are more sensitive under ambient conditions compared with two-layer crystals. The structure derived from the single crystals agrees with the reported powder samples. Lattice parameter *c* decreases with increasing Na content, while *a* remains constant. The compound was found to be antiferromagnetic at $T_N \approx 20$ K for x = 0.91 and 0.92, and paramagnetic for x = 0.93. In-plane and out-of-plane anisotropy were observed for the x = 0.91 crystals. The anisotropic g-factor ratios (g_{ab}/g_c) along H//*ab* and H//*c* decrease significantly as the sodium composition is slightly increased.

Chapter 7 Transport anisotropy in $Na_{0.91}CoO_2$ single crystals: variable range hopping, small-polaron metallic conduction, and spin-wave scattering

7.1. Introduction

The conducting layered cobaltite Na_xCoO_2 has received much attention because of its potential for thermoelectric applications, such as battery electrode material and Peltier refrigerators [57, 59, 216]. The discovery of the bulk superconductivity at $T_c \approx 5$ K induced by water insertion into $Na_{0.33}CoO_2$ has stimulated investigations into the physical properties of the Na_xCoO_2 compounds [6, 9, 96, 119]. The recent report on the electrochemically reversible modification of surface conductivity in Na_xCoO_2 (x = 0.79) has attracted further interest in these compounds, because it indicates the potential of this material to be used in nanoscale rewritable media [41]. The richness in the sodium cobaltate phases, physics, and chemistry, which had remained largely unexplored until recently, is now being revealed by theoretical and experimental studies [10, 21, 40, 70, 83, 84, 152, 165, 170, 225].

One of the outstanding puzzles is the nature of the electronic properties. In the sodium cobalt oxide series, the essential structural elements are layers of edge sharing CoO_6 octahedra, which are separated by a variety of intermediate structures. The triangular in-plane layers of CoO_2 favor the geometrical frustration of interactions. Their layered crystal structure gives rise to relatively strong anisotropic electronic correlations [59].

The structures between the CoO_2 layers can be modified in a variety of ways in order to change their dimensionalities [162, 226, 227], ionic states [9, 228], carrier doping in the CoO_2 planes [51], and relevant interaction strengths. The transport and magnetic properties of Na_xCoO_2 are strongly dependent on the Na content. Recent neutron diffraction measurements performed on single crystals have revealed that the Na^+ ion patterning also has a decisive role in the transport and magnetic properties [111]. It has been found that as x increases from 0.3, the ground state of these compounds goes from a paramagnetic metal through a charge ordered insulator (at x = 0.5) to a 'Curie-Weiss metal' (around x = 0.70), and finally to a weak-moment magnetically ordered state (x > 0.75) [10]. Muon spin rotation (μSR) and nuclear magnetic resonance (NMR) measurements have identified the stoichiometric three-layer Na_1CoO_2 phase to be a non-magnetic insulator [11, 12].

Because of the richness in crystal phases with various Na contents and the sensitivity of Na order and spin order to small variations in x, contributions from the interactions of polarons, spin, and charge to the electrical properties are expected. Up to now, there has been no unified description of the temperature dependence of the resistivity for this family of sodium cobaltates. Information directly obtained from anisotropic transport measurements on heavily Na doped Na_xCoO_2 single crystals will be significantly helpful for a full understanding of the electronic properties in the system.

Very little transport anisotropy has so far been reported on non-hydrated cobaltates. Here I investigate the transport properties in the large x region of α-Na_xCoO_2 (x > 0.90). Research has been hampered due to the difficulties in growing single crystals, as well as the phase separation effects, which appear above a threshold doping known as x_p (x ≈ 0.85) [6]. A single-crystal α-$Na_{0.9}CoO_2$ sample grown by the flux method was found to be metallic in the temperature interval 20K < T < 300 K, with an anomalous increase below 20 K for in-plane resistivity [63]. However, a polycrystalline α-$Na_{0.99}CoO_2$ sample was a semiconductor, with a remarkable increase in resistance at low temperatures [132]. Surprisingly, the curves of the in-plane resistivity versus T in highly doped cobaltate (x ≈ 0.89, 0.96, 0.97, 0.99, 1.0) retain a 'metallic' profile down to the low temperature of 4 K [6], even for x = 1, which should be an insulator. Studies using high quality single crystals will give more accurate results on the structures and physical properties of this frustrating material.

In this work, I report the results on the temperature dependence of both the in-plane and out-of-plane resistivity of high quality three-layer $Na_{0.91}CoO_2$ single crystals. To the best of my knowledge, this is the first systematic transport anisotropy study of high quality single crystal. The data clearly indicate that the resistivity, both perpendicular and parallel to the *c*-axis, shows metallic behavior down to 20 K, and its temperature dependence becomes insulating in the magnetically ordered state, with large magnitude and strong temperature dependence of the anisotropy ρ_c/ρ_{ab} (ρ_c/ρ_{ab} = 52 at 300 K). The

dominant mechanism for both directions is discussed in combination with the magnetic results.

7.2. Experiment

$Na_{0.91}CoO_2$ single crystals were grown by the traveling solvent floating zone (TSFZ) method, as described previously [143]. The average value of the Na content determined from the three pieces of crystal by inductively-coupled plasma atomic emission spectroscopy (ICP-AES) was x = 0.91. X-ray diffraction (XRD) pattern results on the lattice parameters agree with the reported crystal data on α-Na_xCoO_2 [63, 96], and no traces of impurities or secondary phase were observed in my samples, from either the single crystal X-ray diffraction results or the magnetic measurements. The crystal quality was determined to be high, with the full width at half maximum (FWHM) < 0.05º, as shown in Fig. 7.1.

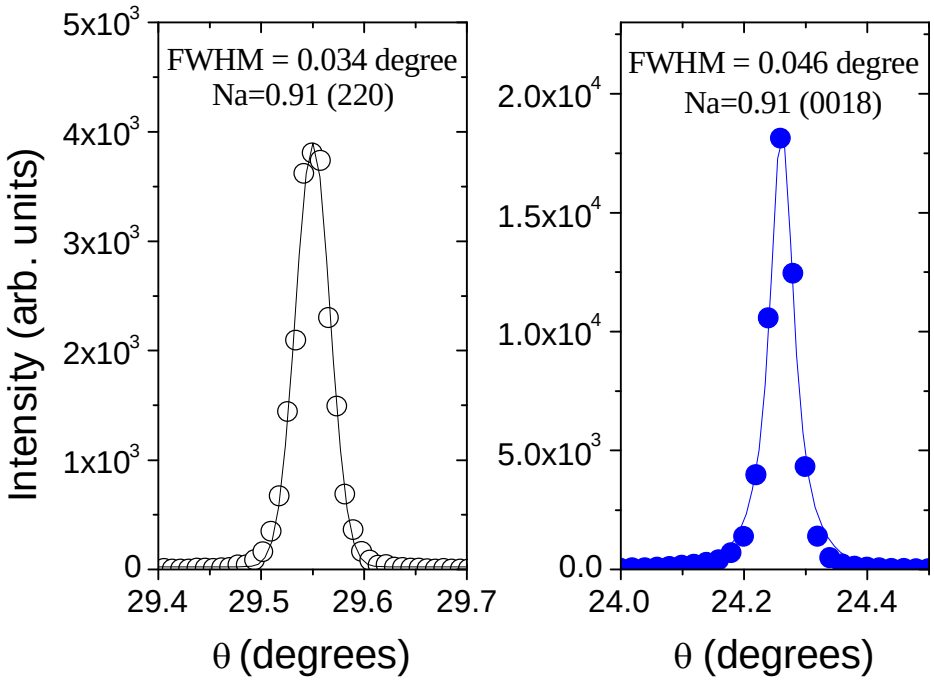

Fig. 7.1. X-ray rocking curves for the as-grown $Na_{0.91}CoO_2$ crystal (Mo K_α-radiation).

The magnetic susceptibility measurements were carried out using a superconducting quantum interference device magnetometer (Quantum Design, model MPMS 7.0) over the large temperature range of 2–350 K. Magnetic fields were perpendicular and parallel to the *c*-axis for cleaved as-grown crystals. The samples for the resistivity measurements were shaped into platelets with typical dimensions of 6.0 × 2.0 × 0.7 mm^3, with the wide faces exactly parallel to the *ab*-plane. The uncertainty in the absolute values of ρ_{ab} and ρ_c is minimized by using relatively long samples (at least 5 mm long) and by painting narrow contact pads with a width less than 0.2 mm.

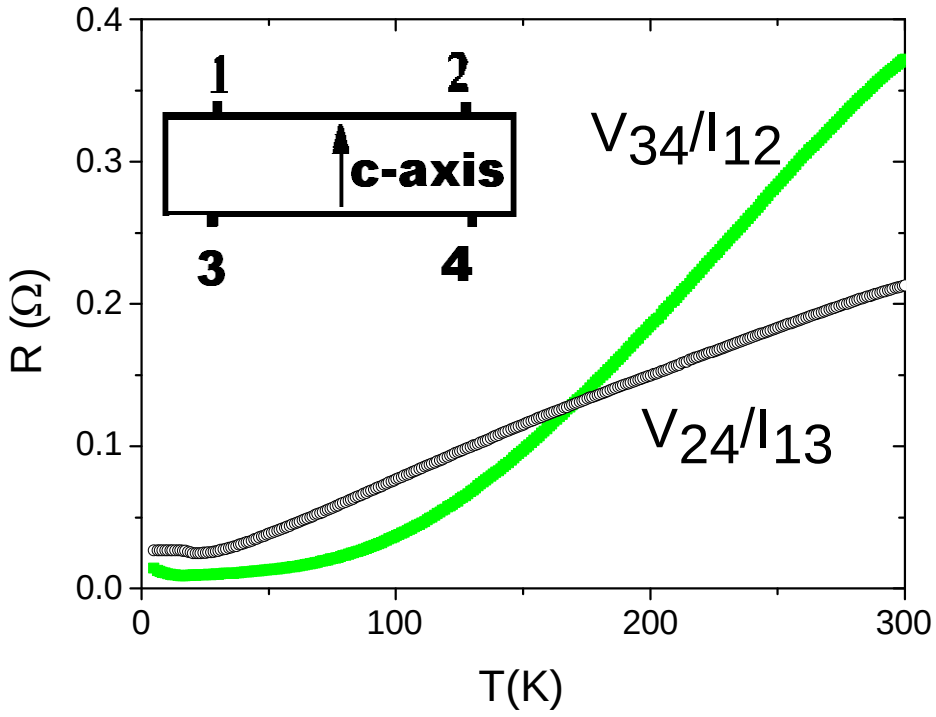

Fig. 7.2. The raw resistance vs. temperature data for the sample. Inset: Definition of contact arrangement.

Electrical contacts with resistance less than 2 Ω were made from silver epoxy on the freshly cleaved surface; a contact configuration with two contacts on the *ab*-planes of a crystal was used, as shown in the inset of Fig. 7.2. ρ_{ab} and ρ_c were obtained from Montgomery-type (MT) analysis using a Quantum Design physical properties measurement system (PPMS) in the 5-300 K temperature range.

7.3. Results and discussion

The transport anisotropic behavior of the $Na_{0.91}CoO_2$ single crystal is presented in Fig. 7.3. Fig. 7.2 is based on raw data obtained from the two sets of measurements. Due to the combined effects of the contact configuration, crystal geometry, and resistivity anisotropy, the values of V_{34}/I_{12} and V_{24}/I_{13} are rather different. I use MT analysis to extract values of ρ_{ab} and ρ_c, with the finite contact size taken into account.

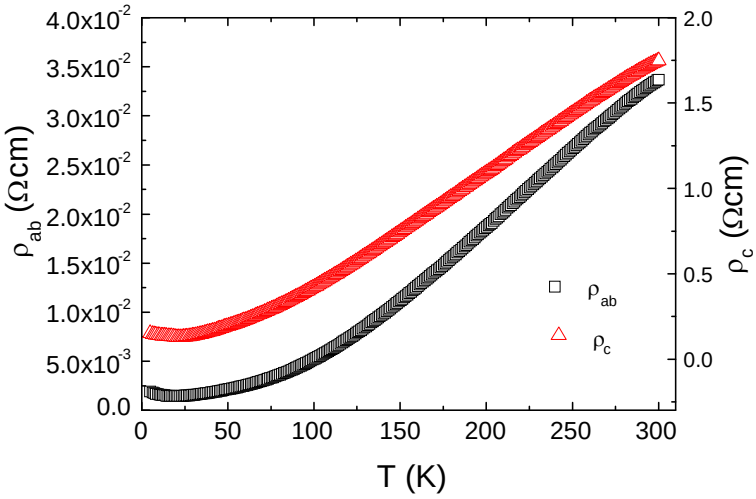

Fig. 7.3. The temperature dependence of the in- and out-of-plane resistivity of $Na_{0.91}CoO_2$ single crystals deduced from Montgomery-type analysis.

The temperature dependence of the electrical resistivity of the $Na_{0.91}CoO_2$ crystals is shown in Fig. 7.3. The resistivity is anisotropic, with the anisotropy having a magnitude of 52-92 from 5 up to 300 K, as expected from the layered structure characteristics. The in- and out-of-plane room temperature resistivity is 33.7 mΩ cm and 1.75 Ω cm, respectively. The in-plane resistivity at room temperature agrees well with previous reports [6, 63, 140]. The magnitude of the resistivity for both directions is much larger than for lower Na doping samples, indicating that the difference in the magnitude of ρ is

to be mainly attributed to the sodium content x rather than the crystal structure, which shows a reduced distance between the adjacent CoO_2 planes and an increase in the in-plane Co-Co separation when x increases. The data clearly indicate that the resistivity, both perpendicular and parallel to the *c*-axis, shows metallic behavior and exhibits complicated non-linear temperature dependence down to 20 K, with the temperature dependence becoming insulating below this temperature. (The 20 K anomaly is pronounced in the logarithm of the resistivity, as shown in Fig. 7.4.) Since the magnetic susceptibilities of the $Na_{0.91}CoO_2$ single crystals have a clear cusp at the same temperature (inset of Fig. 7.4), the increase in ρ_{ab} and ρ_c below 20 K may be related to a notable magnetically ordered state which has been well documented in previous works [12, 74, 225]. The magnetization is very sensitive to the presence of Co_3O_4 and CoO, which are antiferromagnets, with T_N = 35 and 292 K, respectively. No other transitions in the susceptibility have been found from 20 K to room temperature in as-grown crystals, again indicating the high quality of the samples. This is consistent with x-ray diffraction measurements showing no traces of impurities.

The resistivity values also show an inflexion at 270 – 285 K, which may be related to the Na rearrangement at 285 K that was observed in Ref. 111.

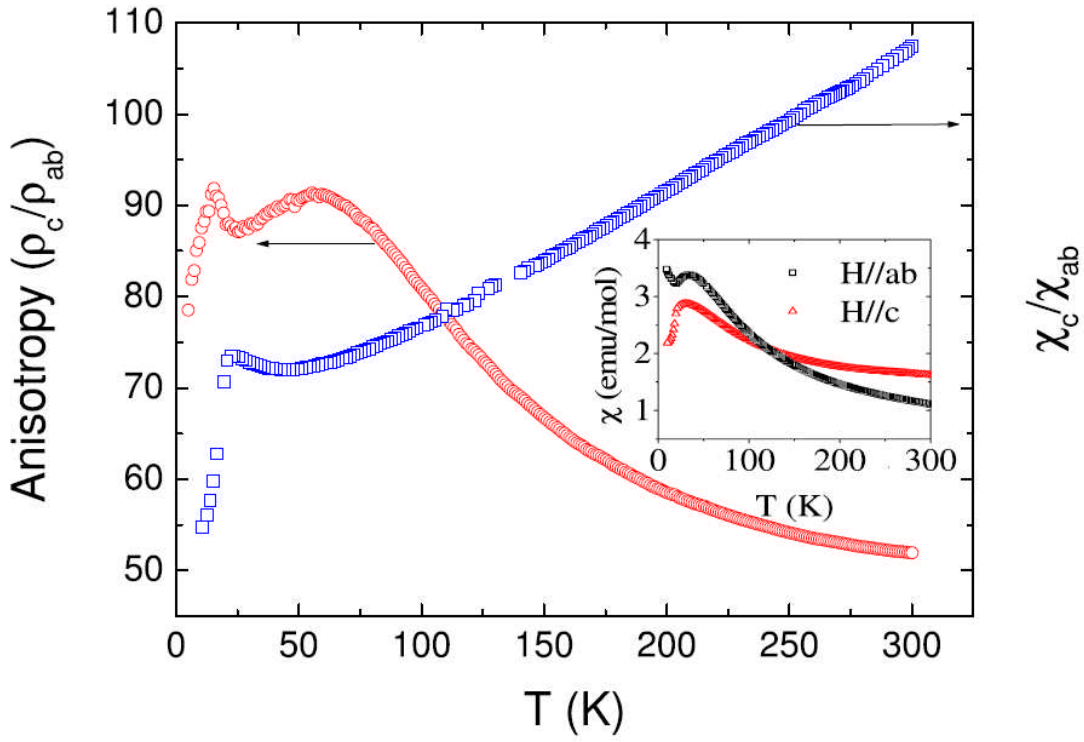

Fig. 7.4. Resistivity ratio ρ_c/ρ_{ab} and susceptibility ratio χ_c/χ_{ab} for $Na_{091}CoO_2$ crystal measured with the field parallel and perpendicular to the (001) direction. Inset: Temperature dependence of the susceptibility for the same sample.

The details in the variation of the anisotropy as a function of temperature can be clearly seen by plotting ρ_c/ρ_{ab} versus temperature. From Fig. 7.4 we can see a pronounced anisotropy in the resistivity for the $Na_{0.91}CoO_2$ single crystal. Upon cooling, the resistivity ratio increases, and a broad peak develops at 54 K. The magnetic susceptibility ratio also starts to turn up around this temperature. Since both α- and β-Na_xCoO_2 samples with $0.4 < x < 0.5$ have clearly revealed a transition at 53 K [132], I propose that this peak is associated with a magnetic ordering and a metal-to-insulator transition developing from this temperature. When the magnetic ordering reaches a

significant level, the metal-to insulator transition takes place at about 20 K, revealing itself as the sharp upturn in the resistivity ratio. The peak in the susceptibility ratio also occurs at the same temperature. The unpredicted resistivity ratio peak at 15.5 K may relate to another magnetic transition which has been observed very recently in the 'fast cooled' state of $Na_{0.85}CoO_2$ single crystal [229]. Below the peak temperature, ρ_c/ρ_{ab} decreases dramatically with decreasing T, suggesting that the system is heading towards an anisotropic three-dimensional (3D) state as $T \rightarrow 0$. This crystal has the smallest resistivity ratio ($\rho_c/\rho_{ab} = 52$ at 300 K) compared with other phases of sodium cobaltate [127, 131, 230]. This can be explained from the point of view of the geometric structure, which has the smallest lattice anisotropic ratio $c/a(b) = 1.799$ for this α phase.

In order to elucidate the transport mechanism over the whole measured temperature range and illuminate the intrinsic properties of this compound, attempts were made to fit the ρ-T curves according to several models suggested by previous reports [52, 65, 138]. For example, fits were attempted to models of electron-electron scattering (proportional to T^2 or to $T^2 + bT^5$), of unconventional T-dependence ($T^{1.5}$) for the scattering of the conduction electrons by locally cooperative band length fluctuations in a matrix of vibronic and Fermi-liquid electrons, and of a power-law, $\rho(T) = \rho_0 + FT^n$. All the fits are quite bad. Other possible models, such as of electron-phonon interaction, hopping motion of small polarons, and variable range hopping were also tried. As shown in Fig. 7.5, the best fit by a standard Bloch-Grüneisen (BG) expression [231] deviates

substantially below 110 K and 140 K from the in- and out-of-plane data, respectively. This fit is given by

$$\rho = \rho_0 + C^*(4\pi)^2 (2T/\Theta_D)^5 \int_0^{\Theta_D/2T} x^5/\sinh^2(x)dx , \qquad (1)$$

where ρ_0 is the residual resistivity, C is a T-independent proportionality constant, and Θ_D is the Debye temperature. Although the Debye temperature (Θ = 585 K) deduced from the in-plane fitting is in good agreement with the result obtained from the equation [31] $\Theta = 373 + 232x$ (Θ = 584 K), where x is the Na content, the deduced out-of-plane Debye temperature (Θ = 538 K) is not consistent with the in-plane value. These results indicate that the BG expression is not valid for this material.

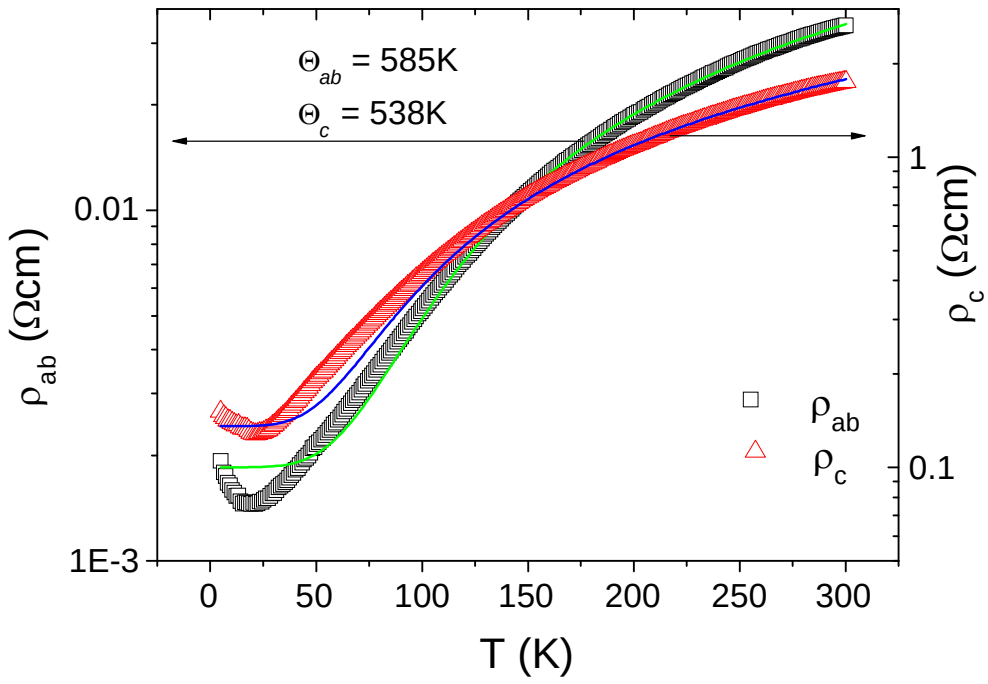

Fig. 7.5. Temperature dependence of the electrical resistivity for $Na_{091}CoO_2$ crystal. The solid lines are fits to the experimental data using Eq. (1).

The resistivity data for both directions below 20 K are well described by the variable-range hopping (VRH) model, assuming the view of carrier localization of Mott and Davis [232], and Shklovskii and Efros [233], that is,

$$\rho(T) = \rho_0 \exp [(T_0/T)^{\nu}]. \qquad (2)$$

Here ρ_0 is a constant which depends on the assumptions made on the electron-phonon interaction, T_0 is a constant proportional to the density of states at the Fermi level and the localization length in 3D, and $\nu = (n+1) / (n+d+1)$, with d being the dimensionality of the hopping process, while n describes the energy dependence of the density of states (DOS) in the vicinity of the Fermi energy, $N(E_F)$. As shown in the inset of Fig. 7.6 (open circles), a $T^{-0.25}$ regime is clearly observed for both directions, showing 3D VRH behavior for the low temperature resistivity. However, within one decade of T, one cannot reliably distinguish between $\nu = 1/4$, 1/3, or 1/2. (Semi-log plots of ρ_{ab} and ρ_c vs. $T^{-1/4}$, $T^{-1/3}$, or $T^{-1/2}$ also appear to be linear for the 15.5 K to 5 K range.) Moreover, the parameter T_0, determined by fitting the data in Fig. 7.6 with Eq. (2), is twice as large for ρ_c as for ρ_{ab}.

I cannot definitely determine whether $\nu = 1/4$, 1/3, or 1/2 is more valid, due to the limited temperature range. However, a value of 1/4 seems to fit the data better than 1/2 or 1/3, although my data spans only a decade in the resistivity values. I assume that a 3D-like VRH occurs in this three-layer crystal. The parameter T_0 extracted from the low

T data is 8 K or 4 K parallel and perpendicular to the *ab*-plane, respectively. The source of the T_0 anisotropy is not clear at this stage. VRH behavior with $\nu = 1/4$ has been found in a two-layer $Na_{0.5}CoO_2$ sample [227] very recently.

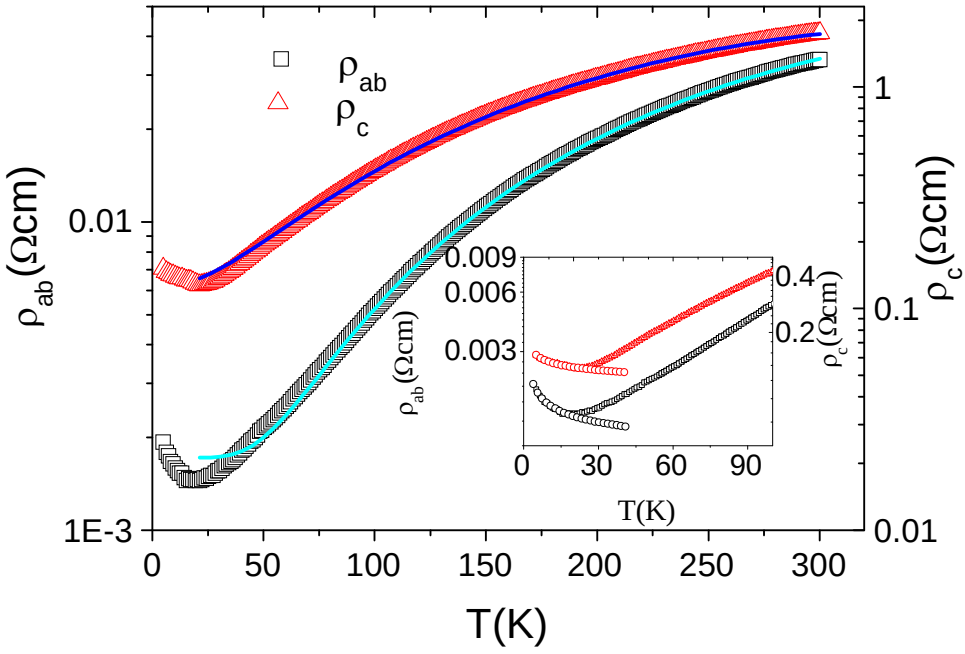

Fig. 7.6. Temperature dependence of the electrical resistivity for a $Na_{091}CoO_2$ crystal. The solid lines are fits to the experimental data using Eq. (3). The inset shows a plot of log (ρ) vs. $T^{-0.25}$ below 20 K.

The resistivity over a wide temperature range from 20 to 300 K can be fitted by a model of small-polaron and spin-wave scattering [234]. The classical expression for the resistivity in this temperature region is given by

$$\rho(T) = \rho_0 + A\omega_s/\sinh^2(\hbar\omega_s/2k_BT) + BT^{7/2}, \qquad (3)$$

where ρ_0 is the residual resistivity due to various temperature independent scattering mechanisms, A is a constant that is proportional to the effective mass of the polarons, ω_s is the average frequency of the softest optical mode, and B is a fitting coefficient. The excellent fitting of the data by Eq. (3) (solid curves in Fig. 7.6) above 54 K (where the magnetic ordering begins, as mentioned above), suggests that the terms $A\omega_s/\sinh^2(\hbar\omega_s/2k_BT)$ and $BT^{7/2}$ capture the basic physics responsible for the charge carrier scattering in this temperature region, which can be attributed to the small polaron [235, 236] and spin-wave [237] scattering, respectively. A model based on a Bardeen, Cooper and Schrieffer (BCS)-approach has demonstrated that unusual spin-polaron behavior can exist in heavily Na doped Na_xCoO_2 [238], and a spin-wave model has been suggested to account for the three-dimensional spin fluctuation in this material [114].

7.5. Conclusion

In summary, I investigated the temperature dependence of the resistivity for both in-plane and out-of-plane directions in high quality three-layer $Na_{0.91}CoO_2$ single crystals. The data clearly indicate that the resistivity, both perpendicular and parallel to the *c*-axis, shows metallic behavior down to 20 K, and the temperature dependences become insulating in the magnetically ordered state below this temperature. Although the resistivity is strongly anisotropic, nevertheless it is 3D (in the sense that the

temperature dependence of the resistivity is dominated by the same mode in all directions) in the low temperature range, where the resistivity is described by a variable-range hopping model in the insulating state, and by a small-polaron and spin-wave scattering model above 54 K. Present results provide compelling evidence for the existence of small polaron and spin-wave scattering metallic conduction in heavily Na doped α-phase sodium cobaltate. I propose that small polaron and spin-wave scattering are needed to explain the basic physics of other phases of Na_xCoO_2, because most of them are as substantially anisotropic as α-Na_xCoO_2.

Chapter 8 Conclusions

Growing a series of two-layer Na_xCoO_2 single crystals with varying Na content for investigation was performed by the optical floating zone technique. A high quality compound was formed at x = 0.75, i.e. ά-phase, while other phases with lower sodium content of x < 0.70 (β-phase with x = 0.55 and 0.60, and γ-phase with x = 0.65 and 0.70, respectively) are observed always to contain Na_2O, Co_3O_4, and Na-poor phases, with the pure phase only formed in the tail part of the ingot. The availability of these Na_xCoO_2 crystals has provided the opportunity for a more accurate characterization with respect to various aspects: structure, thermoelectric and electric behavior, and superconductivity.

Using TG-DTA I found that Na_xCoO_2 is an incongruently melting compound. Both non-hydrated and fully hydrated crystals are exceptionally sensitive under ambient conditions. XRD and TG studies indicated that the semi-hydrated phase $Na_xCoO_2{\cdot}0.6H_2O$ is more stable than the other compositions under ambient conditions. The hydrated compound is strongly unstable in terms of its chemical, structural, and electrical properties. The data show that the water intercalation/ de-intercalation processes in $Na_{0.3}CoO_2 \cdot$ yH2O single crystals are essentially different. The intercalation process from immersing the crystals in water takes place in such a way that two water molecules are inserted initially in the Na-plane followed by two more to make up a group of four, which forms a hydrated cluster of $Na(H_2O)_4$ in a formula unit. In the

water de-intercalation process monitored by TG measurements, the water molecules are removed from the hydrated cluster of $Na(H_2O)_4$ one by one at elevated temperatures, starting from 50 °C. The intercalation/de-intercalation dynamics in different hydrates may lead to complex non-equilibrium states in the bulk, especially on the surfaces of single crystals. There are indications of multiphase formation and the coexistence of multiple phases in $Na_{0.3}CoO_2 \cdot yH_2O$. Their effect on the electronic and superconducting properties remains unclear. However, depending on the reaction conditions, transition-like phenomena mark phase boundaries between quasi-equilibrium states with y = 0 (n = 0), 0.3 (n = 1), 0.6 (n = 2), 0.9 (n = 3), 1.3 (n = 4), and 1.8 (n = 6). This signals that, presuming a careful control of hydration conditions, it is possible to study the cobaltates under quasi-equilibrium conditions. I therefore proposed to carefully reinvestigate the recently claimed evidence for unconventional superconductivity in single crystals.

The superconducting transition temperature of $Na_xCoO_2 \cdot 1.3H_2O$ ($x \approx 0.22–0.47$) is weakly influenced by the Na content. T_c = 2.8–4.9 K with $x \approx 0.28–0.42$ is observed, and the highest T_c = 4.9 K is found for $x \approx 0.42$. A revised superconducting ($Na_xCoO_2 \cdot 1.3H_2O$) and non-superconducting (Na_xCoO_2) phase diagram was obtained.

The spin susceptibility in $Na_xCoO_2 \cdot 1.3H_2O$ measured by the Knight shift decreases below T_c and, at T = 1.7 K, follows a $\sqrt{H}$ variation. Also, it has been reported that the spin-lattice relaxation rate $1/T_1$ follows a T^3 dependence below T_c, down to $T = T_c/6$.

These results indicate that line nodes exist in the superconducting gap function and the Cooper pairs are in the spin-singlet form. The data strongly suggest that the Cooper pairing symmetry in $Na_xCoO_2 \cdot 1.3H_2O$ is of the *d*-wave type, as in the case of copper-oxide high-T_c superconductors. The antiferromagnetic fluctuations also resemble what is seen in the cuprates [178, 196], and they may be responsible for the *d*-wave pairing.

We have presented the Fermi surface of $Na_{0.35}CoO_2 \cdot 1.3D_2O$, where the occupancy map shows the presence of small e'_g elliptical hole pockets. The observation of the pockets lends strong support to theories based on their special nesting properties in this family of compounds.

For the high quality single crystals of two-layer Na_xCoO_2 (x = 0.42, 0.82, and 0.87), the magnetic susceptibility measurements revealed considerable anisotropy for H//*ab* and H//*c* in the as-grown single crystals. The x = 0.82 sample had the largest derived anisotropic g-factor ratio of $g_{ab}/g_c \approx 1.30$, whereas the sample with x = 0.42 was nearly isotropic ($g_{ab}/g_c \approx 0.96$). The magnetic susceptibility of the as-grown crystals was fitted by a modified Curie-Weiss law, and the results were discussed.

Large, non-stoichiometric three-layerα-Na_xCoO_2 single crystals can be grown using the travelling solvent floating zone (TSFZ) method under oxygen atmosphere. As-grown single crystals are more sensitive under ambient conditions compared with two-layer

crystals. The structure derived from the single crystals agrees with the reported powder samples. The lattice parameter *c* decreases with increasing Na content, while *a* remains constant. The compound was found to be antiferromagnetic at $T_N \approx 20$ K for x = 0.91 and 0.92, and paramagnetic for x = 0.93. In-plane and out-of-plane anisotropy were observed for the x = 0.91 crystals. The anisotropic g-factor ratios (g_{ab}/g_c) for H//*ab* and H//*c* decrease significantly as the sodium composition is slightly increased.

I also investigated the temperature dependence of the resistivity for both in-plane and out-of-plane directions in high quality three-layer $Na_{0.91}CoO_2$ single crystals. The data clearly indicate that the resistivity, both perpendicular and parallel to the *c*-axis, shows metallic behaviour down to 20 K, and its temperature dependences become insulating in the magnetically ordered state below this temperature. Although the resistivity is strongly anisotropic, nevertheless it is 3D (in the sense that the temperature dependence of the resistivity is dominated by the same mode in all directions) in the low temperature range, where the resistivity is described by a variable-range hopping model in the insulating state, and by a small-polaron and spin-wave scattering model above 54 K. Present results provide compelling evidence for the existence of small polaron and spin-wave scattering metallic conduction in heavily Na doped α-phase sodium cobaltate. I propose that small polaron and spin-wave scattering are needed to explain the basic physics of other phases of Na_xCoO_2, because most of them are as substantially anisotropic as α-Na_xCoO_2.

References

1. J. G. Bednorz and K. A. Müller, *Z. Phys. B* 64, 189 (1986).
2. For example, in "3*d* transition-metal oxides," M. Hase, I. Terasaki, and K. Uchinokura, *Phys. Rev. Lett.* 70, 3651 (1993); M. Azuma *et al.*, *Phys. Rev. Lett.* 73, 3463 (1994); Y. Tomioka *et al.*, *Phys. Rev. Lett.* 74, 5108 (1995); M. Uehara *et al.*, *J. Phys. Soc. Jpn.* 65, 2764 (1996).
3. J. Orenstein, and A. J. Millis, *Science* 288, 468–474 (2000).
4. J. Molenda, Solid State Ionics 21, 263 (1986).
5. I. Terasaki, Y. Sasago, and K. Uchinokura, *Phys. Rev. B* 56, R12685 (1997); M. Imada, A. Fujimori, and Y. Tokura: *Rev. Mod. Phys.* 70, 1039 (1998); Y. Wang, N. S. Rogado, R. J. Cava, and N. P. Ong, *Nature* (London) 423, 425 (2003); J. Sugiyama, *et al.*, *Phys. Rev. Lett.* 92, 017602 (2005).
6. P. Minhyea Lee, Liliana Viciu, Lu Li, Yayu Wang, M. L. Foo, S. Watauchi, and R. A. Pascal Jr., R. J. Cava, and N. P. Ong, *Nature Materials* 5, 537 (2006).
7. M. Von Jansen and R. Hoppe, *Z. Anorg. Allg. Chem.* 408, 104 (1974).
8. T. Tanaka, S. Nakamura, and S. Iida, Jpn. *J. Appl. Phys.* 33, 581 (1994).
9. K. Takada, H. Sakurai, E. Takayama-Muromachi, F. Izumi, R. Dilanian, and T. Sasaki, *Nature* 422, 53 (2003).
10. M. L. Foo, Y. Wang, S. Watauchi, H. W. Zandbergen, T. He, R. J. Cava, and N. P. Ong, *Phys. Rev. Lett.* 92, 247001 (2004).

11. G. Lang, J. Bobroff, H. Alloul, P. Mandels, N. Blanchard, and G. Collin, *Phys. Rev. B* 72, 094404 (2005).

12. C. de Vaulx, M.-H. Julien, C. Berthier, M. Horvatic, P. Bordet, V. Simonet, D. P. Chen, and C. T. Lin, *Phys. Rev. Lett.* 95, 186405 (2005).

13. K. Takada, K. Fukuda, M. Osada, I. Nakai, F. Izumi, R. A. Dilanian, K. Kato, M. Takata, H. Sakurai, E. Takayama-Muromachi, and T. Sasaki, *J. Mater. Chem.* 14, 1448 (2004).

14. C. J. Milne, D. N. Argyriou, A. Chemseddine, N. Aliouane, J. Veira, S. Landsgesell, and D. Alber, *Phys. Rev. Lett.* 93, 247007 (2004).

15. M. Karppinen, I. Asako, T. Motohashi, and H. Yamauchi, *Chem. Mater.* 16, 1693 (2004).

16. G. Gašparović, R. A. Ott, J.-H. Cho, F. C. Chou, Y. Chu, J. W. Lynn, and Y. S. Lee, *Phys. Rev. Lett.* 96, 046403 (2006).

17. M. Murakami, *Superconductor Sci. Technol.* 5, 185 (1992).

18. L. F. Schennmeyer in *Processing and Properties of High* T_c *Superconductor*s, (S. Jin ed.), World Scientific, Singapore (1993).

19. A. Revcolevschi and J. Jegoudez, *Progress in Materials Science* 42, 321 (1997).

20. J. C. Brice, *The Growth of Crystals from the Melt*, (E. P. Wohlfarth ed.), P. 156, North-Holland Publishing Company, Amsterdam (1965).

21. Claude Fouassier, Guy Matejka, Jean-Maurice Reau, Paul Hagenmuller, *J. Solid State Chem.* 6, 532 (1973).

22. Q. Huang, M. L. Foo, R.A. Pascal Jr., J. W. Lynn, B. H. Toby, T. He, H.W. Zandbergen, R. J. Cava, *Phys. Rev B* 70, 184110 (2004).
23. I. Terasaki, Y. Sasago, and K. Uchinokura, *Phys. Rev. B* 56, R12 685 (1997).
24. Yayu Wang, N. S. Rogado, R. J. Cava, and N. P. Ong, *Nature* 423, 425 (2003).
25. C. Delmas, C. Fouassier, and P. Hagenmuller, *Physica B & C* 99, 81 (1980).
26. C. Delmas, J.-J. Braconnier, C. Fouassier, and P. Hagenmuller, *Solid State Ionics* 3/4, 165 (1981).
27. T. Motohashi, E. Naujalis, R. Ueda, K. Isawa, M. Karppinen, and H. Yamauchi, *Appl. Phys. Lett.* 79, 1480 (2001).
28. J.W. Lynn, Q. Huang, C.M. Brown, V.L. Miller, M.L. Foo, R.E. Schaak, C.Y. Jones, E.A. Mackey, R.J. Cava, *Phys. Rev. B* 68 214516 (2003).
29. H. W. Zandbergen, M. Foo, Q. Xu, V. Kumar, and R. J. Cava, *Phys. Rev. B* 70, 024101 (2004).
30. H. Sakurai, S. Takenouchi, N. Tsujii and E. Takayama-Muromachi, *Journal of the Physical Society of Japan* 73, 2081 (2004).
31. H. Sakurai, N. Tsujii, and E. Takayama-Muromachi, *Journal of the Physical Society of Japan* 73, 2393 (2004).
32. I. R. Mukhamedshin, H. Alloul, G. Collin, and N. Blanchardet, *Phys. Rev. Lett*. 93, 167601 (2004).
33. L. Cui, Y. G. Zhao, G. M. Zhang, W. Y. Zhang, Z. P. Guo, W. Ren, X. P. Zhang and M. H. Zhu, *J. Alloys and Compounds* 426, 72 (2006).

34. S. Miyazaki, S. Kikkawa, and M. Koizumi, *Synth. Met.* 6, 211 (1983); R. Gupta and A. Manthiram, *J. Solid State Chem.* 121, 483 (1996).

35. A. R. Wizansky, P. E. Rauch, and F. J. Disalvo, *J. Solid State Chem.* 81, 203 (1989).

36. T. Wu, D. F. Fang, G. Y. Wang, L. Zhao, G. Wu, X. G. Luo, C. H. Wang, and X. H. Chen, *Phys. Rev. B* 76, 024403 (2007).

37. M. Karppinen, I. Asako, E. Motohashi, and H. Yamauchi, *Phys. Rev. B* 71, 092105 (2005).

38. J. Molenda, C. Delmas, P. Dordor, *Solid State Ionics* 12, 473 (1989).

39. F. C. Chou, E. T. Abel, J. H. Cho, and Y. S. Lee, arXiv: cond-mat/0405158 (2004).

40. C. T. Lin, D. P. Chen, P. Lemmens, X. N. Zhang, A. Maljuk, P. X. Zhang, *J. Crystal Growth* 275, 606 (2005).

41. O. Schneegans, A. Moradpour, O. Dragos, S. Franger, N. Dragoe, L. Pinsard-Gaudart, P. Chrétien, and A. Revcolevschi, *J. Am. Chem. Soc.* 129, 7482 (2007).

42. Y. Ando, N. Miyamoto K. Segawa T. Kawata and I. Terasaki, *Phys. Rev. B* 60, 10580 (1999).

43. K. Takahata, Y. Iguchi, D. Tanaka, and T. Itoh, and I. Terasaki, *Phys. Rev. B* 61, 12551 (2000).

44. H. Yakabe, K. Fujita, K. Nakamura, and K. Kikuchi, in *Proceedings of the 17th International Conference on Thermoelectricity* (ICT ’98), Nagoya, Japan,, 1998 (The Institute of Electrical and Electronics Engineers, Piscataway, 1998), p. 551.

45. A. Mrotzek, E. Mueller, J. Plewa, and H. Altenberg, in *Proceedings of the 22th International Conference on Thermoelectricity* (ICT ’03), (The Institute of Electrical and Electronics Engineers, Piscataway, 2003), p. 219.
46. I. Terasaki, I. Tsukada, and Y. Iguchi, *Phys. Rev. B* 65, 195106 (2002).
47. I. Terasaki, *Physica B* 328, 63 (2003).
48. M. Yokoi, H. Watanabe, Y. Mori, T. Moyoshi, Y. Kobatashi, and M. Saito, *J. Phys. Soc. Jpn.* 73, 1297 (2004).
49. W. Y. Zhang, H. C. Yu, Y. G. Zhao, X. P. Zhang, Y. G. Shi, Z. H. Cheng, and J. Q. Li, *J. Phys.: Condens. Matter* 16, 4935 (2004).
50. W. Y. Zhang, Y. G. Zhao, Z. P. Guo, P. T. Qiao, L. Cui, L. B. Luo, X. P. Zhang, H. C. Yu, Y. G. Shi, S. Y. Zhang, T. Y. Zhao, and J. Q. Li, *Solid State Commun.* 135, 480 (2005).
51. Z. P. Guo, Y. G. Zhao, W. Y. Zhang, L. Cui, and L. B. Luo, *J. Phys.: Condens. Matter* 18, 4381 (2006).
52. L. B. Luo, Y. G. Zhao, G. M. Zhang, S. M. Guo and L. Cui, *Phys. Rev. B* 73, 245113 (2006).
53. H. Ohta, S.-W. Kim, S. Ohta, K. Koumoto, M. Hirano, and H. Hosono, *Cryst. Growth Des.* 5, 25 (2005).
54. W. J. Chang, C. C. Hsieh, T. Y. Chung, S. Y. Hsu, K. H. Wu, and T. M. Uen, et al. *Appl. Phys. Lett.* 90, 061917(2007).

55. W. J. Chang, J.-Y. Lin, T. Y. Chung, J.M. Chen, C.-H. Hsu, S.Y. Hsu, T.M. Uen, K.H. Wu, Y.S. Goua, J.Y. Juang, *Journal of Magnetism and Magnetic Materials* 310, e335 (2007).
56. X. P. Zhang, Y. S. Xiao, H. Zhou, B. T. Xie, C. X. Yang, Y. G. Zhao, *Materials Science Forum* 475, 3807 (2005).
57. Y. Ishida, H. Ohta, A. Fujimori, and H. Hosono, *J. Phys. Soc. Jpn.* 76, 103709 (2007).
58. J. Y. Son, Bog G. Kim, and J. H. Cho, *Appl. Phys. Lett.* 86, 221918 (2005).
59. I. Terasaki, Y. Sasago, and K. Uchinokura, *Phys. Rev. B* 56 R12685 (1997).
60. K. Fujita, T. Mochida, and K. Nakamura, *Jpn. J. Appl. Phys.* 40, 4644 (2001).
61. K. Fujita, T. Mochida, and K. Nakamura, in *Proceedings of the 20th International Conference on Thermoelectricity* (ICT ’01), 2001 (The Institute of Electrical and Electronics Engineers, Piscataway, 2001), p. 168.
62. Hongtao Wang, Zhangzhang Chen and Qingli Jin, *Materials Letters* 59, 3917 (2005).
63. M. Mikami, M. Yoshimura, Y. Mori, and T. Sasaki, *Jpn. J. Appl. Phys.* 42, 7383 (2003).
64. N. L. Wang, P. Zheng, D. Wu, Y. C. Ma, T. Xiang, R. Y. Jin, and D. Mandrus, *Phys. Rev. Lett*. 93, 237007 (2004).
65. S. Y. Li, L. Taillefer, D. G. Hawthorn, M. A. Tanatar, J. Paglione, M. Sutherland, R. W. Hill, C. H. Wang, and X. H. Chen, *Phys. Rev. Lett.* 93, 056401 (2004).
66. R. Jin, B. C. Sales, S. Li, and D. Mandrus, *Phys. Rev. B* 72, 060512(R) (2005).

67. M. Mikami, et al., in *Proceedings of the 20th International Conference on Thermoelectricity* (ICT ’01), 2001 (The Institute of Electrical and Electronics Engineers, Piscataway, 2001), p. 195.

68. M. N. Iliev, A. P. Litvinchuk, R. L. Meng, Y. Y. Sun, J. Cmaidalka, and C. W. Chu, *Physica C* 40, 239 (2004).

69. S. Bayrakci, C. Bernhard, D. P. Chen, B. Keimer, P. Lemmens, C. T. Lin, C. Niedermayer, and J. Strempfer, *Phys. Rev. B* 69, 100410 (2004).

70. D. P. Chen, H. C. Chen, A. Maljuk, A. Kulakov, H. Zhang, P. Lemmens, and C. T. Lin, *Phys. Rev. B* 70, 024506 (2004).

71. P. Lemmens, V. Gnezdilov, N. N. Kovaleva, K. Y. Choi, H. Sakurai, E. Takayama-Muromachi, K. Takada, T. Sasaki, D. P. Chen, F. C. Chou, C. T. Lin, and B. Keimer, *J. Phys.: Condens. Matter* 16, S857 (2004).

72. C Bernhard., A.V. Boris, N.N. Kovaleva, G. Khaliullin, A. Pimenov, L. Yu, D.P. Chen, C.T. Lin, and B. Keimer, *Phys. Rev. Lett.* 93,167003 (2004).

73. S. P. Bayrakci, I. Mirebeau, P. Bourges, Y. Sidis, M. Enderle, J. Mesot, D. P. Chen, C. T. Lin, and B. Keimer, *Phys. Rev. Lett.* 94, 157205 (2005).

74. J. L. Luo, N. L. Wang, G. T. Liu, D. Wu, X. N. Jing, F. Hu, and T. Xiang, *Phys. Rev. Lett.* 93, 187203 (2004).

75. J. Wooldridge, D. McK. Paul, G. Balakrishnan, and M. R. Lees, *J. Phys.: Condens. Matter* 17, 707 (2005).

76. C. A. M. dos Santos, J. J. Neumeier, Yi-Kuo Yu, R. K. Bollinger, R. Jin, D. Mandrus, and B. C. Sales, *Phys. Rev. B* 74, 132402 (2006).

77. T. F. Schulze, P. S. Häfliger, C. Niedermayer, K. Mattenberger, S. Bubenhofer, and B. Batlogg, cond-mat, arXiv:0707. 1630vl (2007).

78. D. J. Singh, *Phys. Rev. B* 68, 020503(R) (2003).

79. D. J. Singh and D. Kasinathan, *Phys. Rev. Lett.* 97, 016404 (2006).

80. S. Zhou, M. Gao, H. Ding, P. A. Lee, and Z. Wang, *Phys. Rev. Lett.* 94, 206401 (2005).

81. W. B. Wu, D. J. Huang, J. Okamoto, A. Tanaka, H.-J. Lin, F. C. Chou, A. Fujimori, and C. T. Chen, *Phys. Rev. Lett.* 94, 146402 (2005).

82. K. Kuroki, S. Ohkubo, T, Nojima, R. Arita, S. Onari, and Y. Tanaka, *Phys. Rev. Lett.* 98, 136401 (2007).

83. C. A. Marianetti and G. Kotliar, *Phys. Rev. Lett.* 98, 176405 (2007).

84. D. J. Singh, *Phys. Rev. B* 61, 13397 (2000).

85. M. D. Johammes, I. I. Mazin, and D. J. Singh, *Phys. Rev. B* 71, 205103 (2005).

86. K.-W. Lee and W. E. Pickett, *J. Appl. Phys.* 99, 08P702 (2006).

87. Q. Huang, M. L. Foo, J. W. Lynn, H. W. Zandbergen, G. Lawes, Y. Wang, B. H. Toby, A. P. Ramirez, N. P. Ong, and R. J. Cava, *J. Phys.: Condens. Matter* 16, 5803 (2004).

88. Q. Huang, M. L. Foo, R. A. Pascal, Jr., J. W. Lynn, B. H. Toby, T. He, H. W. Zandbergen, and R. J. Cava, *Phys. Rev. B* 70, 184110 (2004).

89. F. C. Chou, J. H. Cho, P. A. Lee, E. T. Abel, K. Matan, and Y. S. Lee, *Phys. Rev. Lett.* 92, 157004 (2004).

90. F. C. Chou, J. H. Cho, and Y. S. Lee, *Phys. Rev. B* 70, 144526 (2004).

91. L. Balicas, M. Abdel-Jawad, N. E. Hussey, F. C. Chou, and P. A. Lee, *Phys. Rev. Lett.* 94, 236402 (2005).

92. F. C. Chou, E. T. Abel, J. H. Cho, and Y. S. Lee, *J. Phys. Chem. Solids* 66, 155 (2005).

93. M. Yokoi, T. Moyoshi, Y. Kobayashi, M. Soda, Y. Yasui, and M. Sato, *J. Phys. Soc. Jpn.* 74, 3046 (2005).

94. X. N. Zhang, P. Lemmens, V. Gnezdilov, K. Y. Choi, B. Keimer, D. P. Chen, C. T. Lin, and F. C. Chou, *Physica B* 359-361, 424 (2005).

95. G. Garbarino, M. Monteverde, M. Núñez-Regueiro, C. Acha, M.L. Foo, and R.J. Cava, arXiv: 0710. 4341 (2007).

96. L. Viciu, J. W. Bos, H. W. Zandbergen, Q. Huang, M. L. Foo, S. Ishiwata, A. P. Ramirez, M. Lee, N. P. Ong, and R. J. Cava, *Phys. Rev. B* 73, 174104 (2006).

97. C. H. Wang, X. H. Chen, G. Wu, T. Wu, H. T. Zhang, J. L. Luo, G. T. Liu, and N. L. Wang, *Phys. Rev. B* 74, 172507 (2006).

98. K.-W. Lee, J. Kunes, P. Novak, and W. E. Pickett, *Phys. Rev. Lett.* 94, 026403 (2005).

99. T. Sugibayashi, D.S. Hirashima, *Solid State Communications* 132， 43 (2004).

100. Ting-Pong Choy, Dimitrios Galanakis, and Philip Phillips, *Phys. Rev. B* 75, 073103 （2007）.

101. D. N. Argyriou, O. Prokhnenko, K. Kiefer, and C. J. Milne, *Phys. Rev. B* 76, 134506 (2007).

102. J Y Son, *J. Phys. D: Appl. Phys.* 41, 095405 (2008).

103.H.X. Yang, C.J. Nie, Y.G. Shi, H.C. Yu, S. Ding, Y.L. Liu, D. Wu, N.L. Wang, J.Q. Li, *Solid State Communications* 134, 403 (2005).

104.N. L.Wang, D. Wu, G. Li, X. H. Chen, C. H. Wang, and X.G. Luo, *Phys. Rev. Lett.* 93, 147403 (2004).

105.T. Arakane, T. Satoa, , T. Takahashia, H. Ding, T. Fujii, and A. Asamitsu, *Physica B* 403, 1086 (2008).

106.Y. Xia, D. Qian, D. Hsieh, L. Wray, L. Viciu, R.J. Cava, and M.Z. Hasan, *Physica* B 403, 1007 (2008).

107.R. Ray, A. Ghoshray, and K. Ghoshray, and S. Nakamura, *Phys. Rev. B* 59, 9454 (1999).

108.F. L. Ning, S. M. Golin, K. Ahilan, T. Imai1, G.J. Shu, and F. C. Chou, arXiv: 0711.4341 (2008).

109.M.Z. Hasan, Y.-D. Chuang, D. Qian, Y.W. Li, Y. Kong, A. Kuprin, A.V. Fedorov, R. Kimmerling, E. Rotenberg, K. Rossnagel, Z. Hussain, H. Koh, N.S. Rogado, M.L. Foo, and R.J. Cava, *Phys. Rev. Lett.* 92，246402 (2004).

110.H.-B. Yang, S.-C. Wang, A.K.P. Sekharan, H. Matsui, S. Souma, T. Sato, T. Takahashi, T. Takeuchi, J.C. Campuzano, R. Jin, B.C. Sales, D. Madrus, Z. Wang, H. Ding, *Phys. Rev. Lett.* 95，146401 (2005).

111.M. Roger, D. J. P. Morris, D. A. Tennant, M. J. Gutmann, J. P. Goff, J. U. Hoffmann, R. Feyerherm, E. Dudzik, D. Prabhakaran, A. T. Boothroyd, N. Shannon, B. Lake, and P. P. Deen, *Nature* 445, 631 (2007).

112.J. Geck, M. V. Zimmermann, H. Berger, S.V. Borisenko, H. Eschrig, K. Koepernik, M. Knupfer, and B. Büchner, *Phys. Rev. Lett.* 97, 106403 (2006).

113.M.-H. Julien, C. de Vaulx, H. Mayaffre, C. Berthier, M. Horvatic, V. Simonet, J.Wooldridge, G. Balakrishnan, M. R. Lees, D. P. Chen, C. T. Lin, and P. Lejay, *Phys. Rev. Lett.* 100, 096405 (2008).

114.L. M. Helme, A. T. Boothroyd, R. Coldea, D. Prabhakaran, D. A. Tennant, A. Hiess, and J. Kulda, *Phys. Rev. Lett.* 94, 157206 (2005).

115.L. M. Helme, A. T. Boothroyd, R. Coldea, and D. Prabhakaran, *Phys. Rev. B* 73, 054405 (2006).

116.M. D. Johannes, I. I. Mazin, and D. J. Singh, *Phys. Rev. B* 71, 214410 (2005).

117. A. T. Boothroyd, R. Coldea, D. A.Temmant, D. Prabhakaran, L. M. Helme, and C. D. Frost, *Phys. Rev. Lett.* 92, 197201 (2004).

118.Pusheng Liu, Gang Chen, Ying Cui, Hongjie Zhang, Feng Xiao, Lin Wang, and Hiromi Nakano, *Solid State Ionics,* 179, 2308 (2008).

119.T. Motohashi, R. Ueda, E. Naujalis, T. Tojo, I. Terasaki, T. Atake, M. Karppinen, and H. Yamauchi, *Phys. Rev. B* 67, 064406 (2003).

120.J. Sugiyama and H. Itahara, *Phys. Rev. B* 67, 214420 (2003).

121.Hirotaka Okabe, Jun Akimitsu, Takashi Kubodera, Masanori Matoba, Toru Kyomen and Mitsuru Itoh, *Physica B: Condensed Matter*, 378-380, 863 (2006).

122.J. Sugiyama, J. H. Brewer, E. J. Ansaldo, H. Itahara, T. Tani, M. Mikami, Y. Mori, T. Sasaki, S. Hebert, and A. Maignan, *Phys. Rev. Lett.* 92, 017602 (2004).

123. Y. G. Shi, Y. L. Lin, H. X. Yang, C. J. Nie, R. Jin, and J. Q. Li, *Phys. Rev. B* 70, 052502 (2004).

124. D. Prabhakaran, A. T. Boothroyd, R. Coldea, N. R. Charnley, *J. Cryst. Growth* 271, 74 (2004).

125. K. Miyoshi, E. Morikuni, K. Fujiwara, J. Takeuchi, and T. Hamasaki, *Phys. Rev. B* 69, 132412 (2004).

126. J. B. Peng, and C. T. Lin, *Journal of Crystal Growth* Article in Press, (2008).

127. B. C. Sales, R. Jin, K. A. Affholter, P. Khalifah, G. M. Veith, and D. Mandrus, *Phys. Rev. B* 70, 174419 (2004).

128. M.-H. Whangbo and D. Dai, *Inor. Chem.* 45, 5989 (2006).

129. D. Qian, L. Wray, D. Hsieh, L. Viciu, R. J. Cava, J. L. Luo, D. Wu, N. L. Wang, and M. Z. Hasan, *Phys. Rev. Lett.* 97, 186405 (2006).

130. Sundip Mistry, Donna C. Arnold, Chris J. Nuttall, Alexandros Lappas and Mark A. Green, *Chem. Commun.* 2440 (2004).

131. R. Jin, B. C. Sales, P. Khalifah, and D. Mandrus, *Phys. Rev. Lett.* 91, 217001 (2003).

132. Y. G. Shi, H. X. Yang, H, Huang, X. Liu, and J. Q. Li, *Phys. Rev. B* 73, 094505 (2006).

133. Y. Takahashi, Y.Gotoh, and J. Akimoto, *J. Solid State Chem.* 172, 22 (2003).

134. J. D. Jorgensen, M. Avdeev, D. G. Hinks, J. C. Burley, and S. Short, *Phys. Rev. B* 68, 214517 (2003).

135. Y. Ono, R. Ishikawa, Y. Miyazaki, Y. Ishii, Y. Morii, and T. Kajitani, *J. Solid State Chem.* 166, 177 (2002).

136. R. Siegel. J. Hirschinger, D. Carlier, M. Menetrier, and C. Demas, *Solid State Nucl. Magn. Reson.* 23, 243 (2003).

137. C. Bernhard, Ch. Niedermayer, A. Drew, G. Khaliullin, S. Bayrakci, J. Strempfer, R.K. Kremer, D.P. Chen, C.T. Lin, and B. Keimer, *Europhysics Letters* 80, 27005 (2007).

138. F. Rivadulla, J.-S. Zhou, and J. B. Goodenough, *Phys. Rev. B* 68, 075108 (2003).

139. C. Thinaharan, D. K. Aswal, A. Singh, S. Bhattacharya, N. Joshi, S. K. Gupta, and J. V. Yakhmi, *Cryst. Res. Technol.* 39, 572 (2004).

140. J. Sugiyama, J. H. Brewer, E. J. Ansaldo, B. Hitti, M. Mikami, Y. Mori, and T. Sasaki, *Phys. Rev. B* 69, 214423 (2004).

141. M. Mikami, M. Yoshimura, Y. Mori, T. Sasaki, R. Funahashi, and M. Shikano, in *Proceedings of 21st International Conference on Thermoelectrics, Long Beach, 2002* (Institute of Electrical and Electronics Engineers, Piscataway, 2002), pp. 223–225.

142. Lin, C.T., D. P. Chen, A. Maljuk, and P. Lemmens, *Journal of Crystal Growth*, 292, 422 (2006).

143. D. P. Chen, Xiaolin Wang, C. T. Lin, and S. X. Dou, *Phys. Rev. B* 76, 134511 (2007).

144. P. K. Jha, A. Troper, I. Lima, M. Talati, and S. P. Sanyal, *Physica B* 366, 153 (2005).

145. J. Meena Devi, N. Gayathri, A. Bharathi, and K. Ramachandran, *Bulletin of Materials Science* 30, 345 (2007).

146. Y. Krockenberger, I. Fritsch, G. Cristiani, A. Matveev, L. Alff , H.-U. Habermeiera, and B. Keimer, *Thin Solid Films* 486, 170 (2005).

147. L. Yu, Y. Krockenberger, Ingo Fritsch, and H.-U. Habermeier, *Progress in Solid State Chemistry* 35 (2007) 545e551.

148. J. W. Lynn, Q. Huang, C. M. Brown, V. L. Miller, M. L. Foo, R. E. Schaak, C. Y. Jones, E. A. Mackey, and R. J. Cava, *Phys. Rev. B* 68, 214516 (2003).

149. K. Takada, K. Fukud, M. Osada, I. Nakai, F. Izumi, Ruben A. Dilanian, K. Kato, M. Takata, H.Sakurai, Eiji Takayama-Muromachid, and T. Sasakia, *J. Mater. Chem.* 14, 1448 (2004).

150. K. Takada, H. Sakurai, T.-M. Eiji, F. Izumi, R. A. Dilamian, and T. Sasaki, *Adv. Mater.* 16, 1901 (2004).

151. K. Takada, M. Osada, F. Izumi, H. Sakurai, T.-M. Eiji, and T. Sasaki, *Chem. Mater.* 17, 2040 (2005)

152. R. E. Schaak, T. Klimczuk, M. L. Foo, and R. J. Cava, *Nature* 424, 527 (2003).

153. A. J. Leadbetter, R. C. Ward, J. W. Clark, P. A. Tucker, T. Matsuo, and H. Suga, *J. Chem. Phys.* 82, 424 (1985).

154. M.L. Foo, T. Klimczuka, Lu Li, N.P. Ong, and R.J. Cava, *Solid State Communications* 133, 407 (2005).

155. P. W. Barnes, M. Avdeev, J. D. Jorgensen, D. G. Hinks, H. Claus, and S. Short, *Phys. Rev. B* 72, 134515 (2005).

156. M.L. Foo, R.E. Schaak, V.L. Miller, T. Klimczuk, N.S. Rogadoa Y. Wangc, G.C. Lau, C. Craley, H.W. Zandbergen, N.P. Ong, and R.J. Cava, *Solid State Communications* 127, 33 (2003).

157. H. Ohta, C. Michioka, Y. Itoh, and K. Yoshimura, *J. Phys. Soc. Jpn.* 74, 3147 (2005).

158. A. I. Kolesnikov, H. X. Yang, Y. G. Shi, J. Q. Li, R. I. Walton, and J. C. Li, *Phys. Rev. B* 76, 092302 (2007).

159. Y. Krockenberger, I. Fritsch, G. Christiani, H.-U. Habermeier, Li Yu, C. Bernhard, and B. Keimer, and L. Alff, *Appl. Phys. Lett.* 88, 162501 (2006).

160. Y. Ihara, K. Ishida, C. Michioka, M. Kato, K. Yoshimura, K. Takada, T. Sasaki, H. Sakurai, and E. Takayama-Muromachi, *Journal of the Physical Society of Japan* 73, 2069 (2004).

161. E. Kusano, S. Kawasaki, K. Matano, Guo-qing Zheng, R. L. Meng, J. Cmaidalka, and C. W. Chu, *Phys. Rev. B* 76, 100506(R) (2007).

162. B. Lorenz, J. Cmaidalk, R. L. Meng, and C. W. Chu, *Phys. Rev. B* 68, 132504 (2003).

163. I. R. Mukhamedshin, H. Alloul, G. Collin, and N. Blanchard, *Phys. Rev. Lett.* 94, 247602 (2005).

164. C. Michioka, Y. Itoh, H. Ohta, M. Kato and K. Yoshimura, *J. Phys. Chem. Solids* 68, 2115 (2007).

165. G.-Q. Zheng, K. Matano, D. P. Chen, and C. T. Lin, *Phys. Rev. B* 73, 180503(R) (2006).

166. J. Laverock, S. B. Dugdale, J. A. Duffy, J. Wooldridge, G. Balakrishnan, M. R. Lees, G.-Q. Zheng, D. Chen, C. T. Lin, A. Andrejczuk, M. Itou, and Y. Sakurai, *Phys. Rev. B* 76, 052509 (2007).

167. P. Lemmens, K.Y. Choi, V. Gnezdilov, E. Ya. Sherman, D. P. Chen, C. T. Lin, F. C. Chou, and B. Keimer, *Phys. Rev. Lett.* 96, 167204 (2006).

168. P. Lemmens, P. Scheib, Y. Krockenberger, L. Alff, F. C. Chou, C. T. Lin, H.-U. Habermeier, and B. Keimer, *Phys. Rev. B* 75, 106501 (2007).

169. Akihiro Tanaka and Xiao Hu, *Phys. Rev. Lett.* 91, 257006 (2003).

170. Brijesh Kumar and B. Sriram Shastry, *Phys. Rev. B* 68, 104508 (2003).

171. C. A. Marianetti, G. Kotliar, and G. Ceder, *Phys. Rev. Lett.* 92, 196405 (2004).

172. Q.-H.Wang, D.-H.Lee, and P. A. Lee, *Phys. Rev. B* 69, 092504 (2004).

173. A. Foussats, A. Greco, M. Bejas, and A. Muramatsu, *Phys. Rev. B* 72, 020504(R) (2005).

174. K. Kuroki, Y. Tanaka, and R. Arita, *Phys. Rev. B* 71, 024506 (2005).

175. K. Kuroki, Y. Tanaka, and R. Arita, *Journal of Physics and Chemistry of Solids* 67, 542 (2006).

176. G. Baskaran, *Phys. Rev. Lett.* 91, 097003 (2003).

177. I. I. Mazin and M. D. Johannes, *Nature Physics* 1, 91 (2005).

178. T. Fujimoto, G.-Qing Zheng, Y. Kitaoka, R. L. Meng, J. Cmaidalka, and C.W. Chu, *Phys. Rev. Lett.* 92, 047004 (2004).

179. Y.-J. Chen, C.-J. Liu, J.-S. Wang, J.-Y. Lin, C. P. Sun, S. W. Huang, J. M. Lee, J. M. Chen, J. F. Lee, D. G. Liu, and H. D. Yang, *Phys. Rev. B* 76, 092501 (2007).

180.K. Matano, G.-Q. Zheng, D.P. Chen, C.T. Lin, J. Cmaidalka, R.L. Meng, C.W. Chu, *Journal of Magnetism and Magnetic Materials* 310, 687 (2007).

181.K. Matano, Guo-Qing Zheng, D.P. Chen, and C.T. Lin, *Physica B* 403, 1107 (2008)
.

182.J. Cmaidalka, A. Baikalov, Y.Y. Xue, R.L. Meng, C.W. Chu, *Physica C* 403, 125 (2004).

183.H. Sakurai, K. Takada, S. Yoshii, T. Sasaki, K. Kindo, E. Takayama-Muromachi, *Phys. Rev. B* 68, 132507 (2003).

184.S. Bayrakci, C. Bernhard, D.P. Chen, B. Keimer, R.K. Kremer, P. Lemmens, C.T. Lin, C. Niedermayer, J. Strempfer, *Phys. Rev. B* 69, 100410(R) (2004).

185.M.D. Johannes, D.J. Singh, *Phys. Rev. B* 70, 014507 (2004).

186.M. Chen, B. Hallstedt, and L. J. Gauckler, *J. Phase Equilib.* 24, 212 (2003).

187.H. A. Wriedt, *Bull. Alloy Phase Diagrams* 8, 234 (1987).

188.C. Fouassier, G. Matejka, J.-M. Reau, P. Hagenmuller, *J. of Solid State Chemistry* 6, 532. (1973).

189.Y. Tanaka, Y. Yanase, and M. Ogata, *J. Phys. Soc. Jpn.* 73, 319 (2004).

190.O. I. Motrunich and P. A. Lee, *Phys. Rev. B* 70, 024514 (2004).

191.H. Ikeda, Y. Nishikawa, and K. Yamada, *J. Phys. Soc. Jpn.* 73, 17 (2004).

192.K. Kuroki, Y. Tanaka, and R. Arita, *Phys. Rev. Lett*. 93, 077001 (2004).

193.M. D. Johannes, I. I. Mazin, D. J. Singh, and D. A. Papaconstantopoulos, *Phys. Rev. Lett.* 93, 097005 (2004).

194.Y. Bang, A. Balatsky, *Phys. Rev. B* 68, 212504 (2004).

195. Q.H. Wang, Z.D. Wang, *Phys. Rev. B* 69, 092502 (2004).

196. G.-Q. Zheng, K. Matano, R.L. Meng, J. Cmaidalka, C.W. Chu, *J. Phys.: Condens. Matter* 18, L63 (2006).

197. E. Kusano, S. Kawasaki, K. Matano, G.-Q. Zheng, R.L. Meng, J. Cmaidalka, C.W. Chu, *Phys. Rev. B* 76, 100506 (2007).

198. M. Mochizuki, Y. Yanase, and M. Ogata, *Phys. Rev. Lett.* 94, 147005 (2005).

199. M. Z. Hasan, Y. D. Chuang, D. Qian, Y. W. Li, Y. Kong, A. P. Kuprin, A. V. Fedorov, R. Kimmerling, E. Rotenberg, K. Rossnagel, Z. Hussain, H. Koh, N. S. Rogado, M. L. Foo, and R. J. Cava, *Phys. Rev. Lett.* 92, 246402 (2004).

200. H. B. Yang, S. C. Wang, A. K. P. Sekharan, H. Matsui, S. Souma, T. Sato, T. Takahashi, T. Takeuchi, J. C. Campuzano, R. Jin, B. C. Sales, D. Mandrus, Z. Wang, and H. Ding, *Phys. Rev. Lett.* 92, 246403 (2004).

201. H. B. Yang, Z. H. Pan, A. K. P. Sekharan, T. Sato, S. Souma, T. Takahashi, R. Jin, B. C. Sales, D. Mandrus, A. V. Fedorov, Z. Wang, and H. Ding, *Phys. Rev. Lett.* 95, 146401 (2005).

202. D. Qian, L. Wray, D. Hsieh, D. Wu, J. L. Luo, N. L. Wang, A. Kuprin, A. Fedorov, R. J. Cava, L. Viciu, and M. Z. Hasan, *Phys. Rev. Lett.* 96, 046407 (2006).

203. D. Qian, D. Hsieh, L. Wray, Y. D. Chuang, A. Fedorov, D. Wu, J. L. Luo, N. L. Wang, M. Viciu, R. J. Cava, and M. Z. Hasan, *Phys. Rev. Lett.* 96, 216405 (2006).

204. J.L. Gavilano, D. Rau, B. Pedrini, J. Hinderer, H.R. Ott, S.M. Kazakov, J. Karpinski, *Phys. Rev. B* 69, 100404 (2004).

205. Y. Kobayashi, et al., J. Phys. Soc. Japan 72, 2453 (2003).

206.C. Caroli, P.G. de Gennes, J. Matricon, *Phys. Lett.* 75, 2754 (1964).

207.G.E. Volovik, *JETP Lett.* 58, 469 (1993).

208.G.-Q. Zheng, et al., *Phys. Rev. Lett.* 88, 077003 (2002).

209.M. Ogata, *J. Phys. Soc. Japan* 72, 1839 (2003).

210.N. Hiraoka, M. Itou, T. Ohata, M. Mizumaki, Y. Sakurai, and N. Sakai, J. *Synchrotron Radiat.* 8, 26 (2001).

211.Y. Sakurai and M. Itou, *J. Phys. Chem. Solids* 65, 2061 (2004).

212.G. Kontrym-Sznajd, *Phys. Status Solidi* A 117, 227 (1990).

213.Z. S. Major, S. B. Dugdale, R. J. Watts, G. Santi, M. A. Alam, S. M. Hayden, J. A. Duffy, J. W. Taylor, T. Jarlborg, E. Bruno, D. Benea, and H. Ebert, *Phys. Rev. Lett.* 92, 107003 (2004).

214.S. B. Dugdale, R. J. Watts, J. Laverock, Z S. Major, M. A. Alam, M. Samsel-Czekała, G. Kontrym-Sznajd, Y. Sakurai, and M. Itou, D. Fort, *Phys. Rev. Lett.* 96, 046406 (2006).

215.R. J. Xiao, H. X. Yang, and J. Q. Li, *Phys. Rev. B* 73, 092517 (2006).

216.M. M. Doeff, S. J. Visco, Y. Ma, M. Peng, L. Ding, and L. C. De Jonghe, *Electrochim. Acta* 40, 2205 (1995).

217.I. Terasaki, Y. Sasago, and K. Uchinokura, *Phys. Rev. B* 56, R12685 (1997).

218.G. Khaliullin, *Prog. Theor. Phys. Suppl.* 160, 155 (2005).

219.I. Terasaki, Y. Sasago, and K. Uchinokura, *Phys. Rev. B* 56, 12685 (1997).

220.T. Motohashi, M. Karppinen, and H. Uamauchi, *Proceedings of 2002 Materials Research Society Fall Meeting*, Dec. 2-6, 2002, Boston, Massachusetts, USA.

221. K. Takada , H. Sakurai, E. Takayama-Muromacki, F. Izumi, R. A. Dilanian, and T. Sasaki, *Adv. Mater.* 16(21), 1901 (2004).

222. M. L. Foo, T. Klimczuk, Lu Li, N. P. Ong, and R. J. Cava, *Solid State Communications*, 133(6), 407 (2005).

223. G. Peleckis, T. Motohashi, M. Karppinen, and H. Yamauchi, *Appl. Phys. Lett.* 83, 5416 (2003).

224. L.M. Helme, A.T. Boothroyd, R. Coldea, and D. Prabhakaran, *Phys. Rev. B* 73 054405 (2006).

225. C. Bernhard, A.V. Boris, N. N. Kovaleva, G. Khaliullin, A. Pimenov, L. Yu, D. P. Chen, C. T. Lin, and B. Keimer, *Phys. Rev. Lett.* 93, 167003 (2004).

226. J. Wooldridge, D. M^{c}K. Paul, G .Balakrishnan, and M. R. Lees, *J. Phys.: Condens. Matter* 18, 4731 (2006).

227. G. Garbarino, M. Monteverde, M. Núñez-Regueiro, C. Acha, M. L. Foo and R. J. Cava, *cond-mat/*0717.4341.

228. T. Kawata, Y. Iguchi, T. Itoh, K. Takahata, and I. Terasaki, *Phys. Rev. B* 60, 10584 (1999).

229. T. F. Schulze, P. S. Haefliger, Ch. Niedermayer, K. Mattenberger, S. Bubenhofer, and B. Batlogg, *cond-mat*/0707.1630vl.

230. T. Valla, P. D. Johnson, Z. Yusof, B. Wells, Q. Li, S. M. Loureiro, R. J. Cava, M. Mikami, Y. Mori, M. Yoshimura, and T. Sasaki, *Nature* 417, 627 (2002).

231. Y. Kong, O. V. Dolgov, O. Jepsen, and O. K. Andersen, *Phys. Rev. B* 64, 020501 (2001).

232. N. F. Mott and E. A. Davis, *Electronic Processes in Non-Crystalline Materials* (Clarendon Press, Oxford, 1979).

233. B. I. Shklovskii, A. L. Efros, *Electronic Properties of Doped Semiconductors*, (Springer-Verlag, Berlin, 1984).

234. X. J. Chen, H.-U. Habermeier, C. L. Zhang, H. Zhang, and C. C. Almasan, *Phys. Rev. B* 67, 134405 (2003).

235. I. G. Lang and Yu. A. Firsov, Sov. Phys. JETP 16, 1301 (1963).

236. V. N. Bogomolov, E. K. Kudinov, and Yu. A. Firsov, *Sov. Phys. Solid State* 9, 2502 (1968).

237. F. J. Dyson, *Phys. Rev.* 102, 1217 (1956).

238. Giniyat Khaliullin and Jiri Chaloupka, *The origin of strong correlations and superconductivity in* Na_xCoO_2, preprint.

Publications

1. **D. P. Chen**, Xiaolin Wang, C. T. Lin, S. X. Dou, *Magnetic anisotropy of Na_xCoO_2 single crystals,* **J. Appl. Phys.** 103, 07C702 (2008)

2. R. Amin , J. Maier , P. Balaya , **D.P. Chen** , C.T. Lin, *Ionic and electronic transport in single crystalline $LiFePO_4$ grown by optical floating zone technique*， **Solid State Ionics** 179, 1683 (2008)

3. M. H. Julien, C. de Vaulx, H. Mayaffre, C. Berthier, M. Horvatic, V. Simonet, J. Wooldridge, G. Balakrishnan, M. R. Lees, **D. P. Chen**, C. T. Lin, and P. Lejay, *Electronic texture of the thermoelectric oxide $Na_{0.75}CoO_2$* , **Phys. Rev. Lett**. 100, 096405 (2008).

4. K. Matano, Guo-Qing Zheng, **D.P. Chen** and C.T. Lin *Evidence for d-wave pairing in the cobalt oxide superconductor $Na_xCoO_2{\cdot}1.3H_2O$*, **Physica B** 403, 1107 (2008).

5. **D. P. Chen**, Xiaolin Wang, C. T. Lin, and S. X. Dou *Single-crystal growth and anisotropic magnetic properties of non-stoichiometric three-layer sodium cobalt oxides,* **Phys. Rev. B** 76, 134511 (2007)

6. J. Laverock, S. B. Dugdale, J. A. Duffy, J. Wooldridge, G. Balakrishnan, M. R. Lees, G.-Q. Zheng, **D. Chen,** C. T. Lin, A. Andrejczuk, M. Itou, Y. Sakurai, et al., *Elliptical hole pockets in the Fermi surfaces of unhydrated and hydrated sodium cobalt oxides* Phys. Rev. B 76, 052509 (2007).

7. **D. P. Chen**, Xiaolin Wang, Y. S. Hu, C. T. Lin, S. X. Dou, and R. Nigam, *Magnetic anisotropy in doped and undoped $LiFePO_4$ single crystals,* **J. Appl. Phys.** 101, 09N512 (2007).

8. K. Matanoa, G.-Q. Zheng, **D.P. Chen**, C.T. Lin, J. Cmaidalka, R.L. Meng, and C.W. Chu, *NMR and NQR studies of the pairing symmetry in the superconducting state of $NaxCoO_2 \cdot 1{:}3H_2O$,* **Journal of Magnetism and Magnetic Materials** 310, 687 (2007).

9. C.T. Lin, **D.P. Chen**, J.B. Peng and P.X. Zhang, *Growth and characterization of high quality single crystals of Na_xCoO_2,* **Physica C**, 460-462, 471 (2007).

10. V. Hinkov, P. Bourges, S. Pailhès, Y. Sidis, A. Ivanov, C. D. Frost, T. G. Perring, C. T. Lin, **D. P. Chen,** and B. Keimer, *Spin dynamics in the pseudogap state of a high-temperature superconductor*, **Nature Physics** 3, 780 (2007).

11. C. Bernhard, Ch. Niedermayer, A. Drew, G. Khaliullin, S. Bayrakci, J. Strempfer; R.K. Kremer, **D.P. Chen**, C.T. Lin, and B. Keimer, *Muon-spin-rotation study of magnetism in Na_xCoO_2 single crystals with $0.78 \leq x \leq 0.97$*, **Europhysics Letters** 80, 27005 (2007).

12. C. T. Lin, **D. P. Chen,** A. Maljuk, and P. Lemmens, Sodium cobaltates: *Crystal growth, structure, thermoelectricity, and superconductivity,* **Journal of Crystal Growth**, 292, 422 (2006).

13. Guo-qing Zheng, Kazuaki Matano, **D. P. Chen**, and C. T. Lin, *Spin singlet pairing in the superconducting state of* $Na_xCoO_2{\cdot}1.3H_2O$*: Evidence from a* ^{59}Co *Knight shift in a single crystal,* **Phys. Rev. B** 73, 180503(R) (2006)

14. P. Lemmens, K.Y. Choi, V. Gnezdilov, E. Ya. Sherman, **D.P. Chen,** C.T. Lin, F.C. Chou, B. Keimer, *Anomalous electronic Raman scattering in $Na_xCoO_2 \cdot yH_2O$,* **Phys. Rev. Lett**. 96, 167204 (2006).